Dissemination of ultra-stable optical frequencies over commercial fiber networks

Von der Fakultät für Mathematik und Physik der
Gottfried Wilhelm Leibniz Universität Hannover
zur Erlangung des Grades

Doktor der Naturwissenschaften
Dr. rer. nat.
genehmigte Dissertation
von

M.Sc. Osama Terra
geboren am 27.11.1975
in Kairo (Ägypten)

December 1, 2010

Referent: Prof. Dr. Wolfgang Ertmer

Korreferent: Prof. Dr. Piet Schmidt

Tag der Promotion: 30. November 2010

Contents

Abstract

The development of optical frequency standards has a strong impact on metrology, astronomy and on fundamental physics. Todays optical frequency standards reach a relative uncertainty below 10^{-16} and a relative instability of $10^{-15}/(\tau^{1/2}/\mathrm{s})$. For the dissemination of such a stable frequency, an optical fiber link provides a promising technique to avoid degradation of frequency stability and accuracy when used with a technique that compensates phase noise due to temperature fluctuations and acoustic perturbations of the optical fiber.

In this thesis, an all-in-fiber interferometer to detect and compensate the phase noise introduced by the fiber link has been developed. In order to measure the lowest attainable phase noise after compensation, the interferometer is stabilized after being connected to a short fiber. The interferometer reaches a relative instability of $\sigma_y(\tau) = 2\times10^{-17}/(\tau/\mathrm{s})$ that drops below 10^{-20} after about one hour. Even for the free-running interferometer the relative instability reaches a flicker floor of 1×10^{-18} after a few minutes. This extremely low noise floor is attributed to the careful design of the interferometer.

This interferometer has been used to investigate the performance of a 146 km telecommunication fiber to transfer ultrastable optical frequencies. The 146 km long fiber consists of two 73 km fibers connecting the Physikalisch-Technischen Bundesanstalt (PTB) in Braunschweig to the Leibniz University of Hanover (LUH). The phase noise introduced by the fiber is compensated with a compensation bandwidth limited by the time delay introduced by the fiber link. The frequency transfer is performed over the 146 km fiber link with a relative instability of $\sigma_y(\tau) = 3.3\times10^{-15}/(\tau/\mathrm{s})$ and a relative uncertainty below 1×10^{-19}.

As an application, the frequency of the Mg frequency standard at the Institute of Quantum Optics (IQ) in LUH has been remotely measured against that of optical

frequency standards at PTB using the frequency stabilized 73 km fiber link. A frequency comb has been used to transfer the stability of the frequency standard at PTB to a fiber laser at λ=1542 nm. At IQ, a second femtosecond frequency comb is used to compare the transmitted light frequency with that of Mg frequency standard at λ=914 nm (which is then frequency doubled to meet the clock transition of Mg at λ=457 nm). The ratio between the frequencies of the transfered light from PTB and the Mg laser showed a relative short term instability of about $\sigma_y = 4 \times 10^{-15}$ at 0.1 s limited by the instability of the Mg interrogation laser.

Currently, this technique described in this thesis is implemented to enable frequency comparison over a fiber link of about 900 km between PTB and the Max-Planck institute of Quantum Optics (MPQ) in Garching. Here the transmitted signal has to be amplified several times to maintain the required power level and signal to noise ratio (SNR). Eight bidirectional erbium-doped fiber amplifier (BEDFA) stations are used to amplify the signal about every 100 km. All stations are controlled remotely using a wavelength of 1.3 μm and a built-in microcontroller with specially designed software.

The performance of a fiber Brillouin amplifier (FBA) instead of BEDFA has been additionally studied in order to bridge larger spans in a single step. Unlike BEDFA, a FBA enables bidirectional amplification without suffering from lasing effects or saturation in the gain medium. The FBA amplification can reach about 50 dB down to an input signal power of several nW's. This allows to bridge distances of about 250 km in a single step. We have tested this technique over a 480 km fiber link using only one intermediate amplification station, together with amplifiers at the remote and the local ends. The relative instability of the frequency transfer is $\sigma_y(\tau)$=$2\times10^{-14}/(\tau/\mathrm{s})$ and reaches 2×10^{-18} after about two hours. The mean value of the transmitted frequency is shifted from that of the reference laser by 64 μHz with a statistical uncertainty of 54 μHz. This shift corresponds to fractional frequency deviation of 3×10^{-19}. This result demonstrates for the first time worldwide that, telecommunication fibers with lengths up to about 500 km are suitable to remotely compare the best available optical clocks within a few seconds.

Keywords: Frequency transfer over optical fiber, fiber phase noise, optical amplification, All-in-fiber interferometer, comparison of frequency standards.

Zusammenfassung

Optische Frequenznormale haben großes Anwendungspotenzial in der Metrologie, Astronomie, und für fundamentale Fragen der Physik. Heutige optische Frequenznormale erreichen relative Unsicherheit von 10^{-17} und eine relative Instabilität von $10^{-15}/(\tau^{0.5}/\mathrm{s})$. Um dieses Potenzial voll auszuschöpfen, ist es erforderlich, auch Frequenznormale an unterschiedlichen Standorten direkt miteinander zu vergleichen. Ein solcher Vergleich kann durch die Übertragung optischer Frequenzen über eine Telekommunikationsglasfaser erfolgen. Diese Verfahren wird in dieser Arbeit untersucht.

In dieser Arbeit wurde ein Faserinterferometer aufgebaut, um das Phasenrauschen der Glasfaser aufgrund von akustischen und thermischen Schwankung hochempfindlich zu detektieren und zu kompensieren. Schließt man den Messarm des Interferometers mit einem kurzen Stück Faser ab, lässt sich das Eigenrauschen des Interferometers und damit seine Nachweisgrenze für Phasenfluktuationen bestimmen. Als Folge eines sorgfältigen Aufbaus, bei dem insbesondere die Länge unkompensierter Faser minimiert wurde, erreicht das stabilisierte Interferometer eine relative Instabilität von $\sigma_y(\tau) = 2{\times}10^{-17}/(\tau/\mathrm{s})$; nach einer Stunde beträgt die relative Instabilität bereits weniger als 10^{-20}. Selbst für das unstabilisierte Interferometer konnte bereits nach eine paar Minuten eine relative Instabilität von $1{\times}10^{-18}$ erreicht werden.

Die Eignung dieses Interferometers, eine optische Frequenz über eine 146 km lange, kommerzielle Glasfaserstrecke hochstabil zu übertragen, wurde untersucht. Die 146 km lange Teststrecke besteht aus zwei 73 km langen Fasern, die die Physikalisch-Technischen Bundesanstalt (PTB) in Braunschweig mit der Leibniz Universität Hannover (LUH) verbinden. Auf dieser Übertragungsstrecke wurde eine relative Instabilität von $\sigma_y(\tau) = 3.3{\times}10^{-15}/(\tau/\mathrm{s})$ und ein relative Genauigkeit von $1{\times}10^{-19}$ erreicht. Dabei wird die erreichbare Instabilität durch das Phasenrauschen der unstabilisierten Faser und durch die Laufzeit des Lichts in der Faser bestimmt.

Eine der beiden 73 km Fasern wurde zur Messung der Frequenz des Uhrenübergangs eines Mg-Frequenznormals am Institut für Quantenoptik (IQ) der LUH benutzt. Dazu wurde die Stabilität eines optischen Frequenznormals der PTB mittels Frequenzkamm einem Faserlaser bei λ=1542 nm aufgeprägt, dessen Frequenz über die Faserstrecke zum IQ übertragen wurde. Am IQ wird mit einem zweiten Frequenzkamm das Frequenzverhältnis des Mg stabilisierten Lasers bei 914 nm und der übertragenen Frequenz des Faserlasers bestimmt. Das Frequenzverhältnis beider Laser zeigte eine Kurzzeitstabilität von $\sigma_y = 4 \times 10^{-15}$ bei 0.1 s, die durch die Instabilität des Mg-Lasers limitiert war.

Zur Zeit wird dieses Verfahren auf einer 900 km langen Übertragungstrecke von der PTB zum Max-Planck Institut für Quantenoptik (MPQ) in Garching eingesetzt. Hierbei muss das Lichtsignal allerdings mehrfach verstärkt werden um das erforderliche Signal-zu-Rausch-Verhältnis (SNR) aufrecht zu erhalten. Acht bidirektionale Erbium-dotierte Faserverstärker (BEDFA) Stationen wurde aufgebaut, um das Lichtsignal etwa alle 100 km zu verstärken. Diese Verstärkerstationen lassen sich über einen Kommunikationskanal bei λ=1.3 μm fernsteuern.

Um längere Strecken in einem Schritt zu überbrücken, wurde ein neuartiger Faser Brillouin Verstärker (FBA) entwickelt und charakterisiert. Im Gegensatz zu den bis verwendeten BEDFA, ermöglicht ein FBA bidirektional Verstärkung ohne Begrenzungen durch Sättigung oder Einsetzen von Laseraktivität. Der im Rahmen dieser Arbeit entwickelte FBA kann ein Lichtsignal mit einer Leistung von einige nW um bis zu 50 dB verstärken und erlaubt es, eine Strecke von etwa 250 km auf einmal zu überbrücken. Dieser Verstärker wurde auf einer 480 km langen kommerziellen Telekommunikationsglasfaserverbindung eingesetzt. Neben Verstärkern am Eingang und am entfernten Ende wurde nur ein FBA in nur einer Zwischenstation für eine phasenkohärenten Frequenzübertragung benötigt. Für die relative Instabilität der Frequenzübertragung wurde eine Allan Abweichung von $\sigma_y(\tau)$=$2\times10^{-14}/(\tau/\mathrm{s})$ erreicht. Nach zwei Stunden betrug der Wert der Allan Abweichung 2×10^{-18}. Die gemittelte Abweichung der übertragenen Frequenz vom Sollwert betrug 64 μHz mit einer statistischen Unsicherheit von 54 μHz. Das entspricht einer relativen Frequenzverschiebung von 3×10^{-19}. Damit wurde zum ersten mal weltweit eine optische Frequenz über eine Länge von ca. 500 km auf einer kommerziellen Telekommunikationsfaser mit einer Instabilität übertragen, die ein Vergleich optischer Frequenznormale innerhalb weniger Sekunden ermöglicht.

Stichworte: Frequenzübertragung über Glasfasern, Phasenrauschen optischer Glasfasern, optische Verstärkung, Faserinterferometer, Vergleich zwischen Frequenznormalen.

Chapter 1

Introduction

"Never measure anything but frequency" T. W. Hänsch cited A. Schawlow in his Nobel prize lecture [1]. Indeed, the advent of frequency standards based on atomic transitions makes frequency the most accurately measured physical quantity [2]. Consequently, the number of applications using precise frequency standards are increasing. The following applications are some of these:

- *In metrology*, the definition of the "second" is directly related to the hyperfine-transition frequency in ^{133}Cs atom, therefore, the duration of the second is the most accurately measured quantity in the international system of units. Many other important physical quantities are defined or measured in terms of the second. For example, the meter is defined as the distance light travels in vacuum in a time interval of 1/299792458 of a second. As a result, lasers of a known and fixed frequency have become the practical standards for length metrology. Another example is the practical realization of the volt, which can be obtained via Josephson effect in terms of the product of a physical constant and the frequency [3]. Currently there are even efforts to link the kilogram, the only remaining artifact standard, to the second [4].

- *In the Global Positioning System (GPS)*, a frequency standard (clock) is installed in each of the 24 GPS satellites. A receiver on earth is equipped with a low accuracy clock. The time lag, between the received signal from the satellite and the receiver's own clock, determines its distance to the satellite. The receiver uses three satellites to determine its longitude, latitude, and altitude, and a fourth satellite to calibrate its own clock. A network of reference stations

distributed over the globe are equipped with high stability frequency standards in order to monitor the installed frequency standards in the satellites.

- *In radio astronomy* for the observation of distant cosmic objects, the size of a radio telescope limits its resolution. However, by phase-coherently collecting data from different radio telescopes, the angular resolution improves with increasing the distance between these telescopes. To synchronize the data collection in the so called very long baseline interferometry (VLBI), active hydrogen masers are used at each telescope [5]. VLBI is also used to study the orientation of the earth to an inertial reference frame and the motion of tectonic plates which allows the prediction of earthquakes [6, 7, 8].

- Predictions of *General relativity* (time dilation due to gravity) and *special relativity* (time dilation due to high speed) have been verified by comparing a frequency standard on earth with one installed in a spacecraft (hydrogen maser). *General relativity* is verified by performing the comparison along it's track to an altitude of 10,000 km and back to earth. *Special relativity* is verified by performing the comparison while the spacecraft is in motion [9, 10].

- The search for the possible *time variation of fundamental constants*, such as the fine structure constant (α), allows the test of fundamental theories. In order to search for the variation in α, two different atomic transitions with different sensitivity to the change in α are chosen. For example, a comparison has been made between the hyperfine frequencies of ^{133}Cs and ^{87}Rb atomic fountains over five years. This comparison sets an upper bound to the possible fractional time variation of the fine structure constant of (-0.4$\pm$16)$\times$ 10^{-16}/year [11].

Therefore, many fields would benefit from the increased stability and accuracy of the frequency standards. The relative instability of a frequency standard, which has a transition linewidth of $\Delta\nu$, can be expressed as $\sigma_y(\tau) \approx \frac{\Delta\nu}{\nu_o}\frac{1}{SNR}\frac{1}{\sqrt{\tau/s}}$. Assuming that the linewidth of the reference transition and the detection signal to noise ratio (SNR) are similar for all transitions, then the higher the operating frequency ν_o, the better the stability of the frequency standard.

Therefore, optical frequencies which are four orders of magnitude larger than microwave frequencies, should be theoretically four orders of magnitude more stable. Recently, Rosenband et al. presented ion frequency standards based on the

optical transitions in $^{27}Al^{+}$ and $^{199}Hg^{+}$. They surpassed the performance of the best microwave frequency standards and have a relative uncertainty of 5.2×10^{-17} together with a short-term relative frequency instability of $3.9 \times 10^{-15}\ \tau^{-1/2}$ [2]. Optical neutral-atom lattice frequency standards are expected to reach a level of accuracy comparable to the ion systems, with significantly improved stability due to the large number of atoms involved in the measurement. Recently, Boyd et al. reported a relative uncertainty of 2.5×10^{-15} of an optical transition in ^{87}Sr lattice [12].

Such frequency standards can accelerate and improve the search for variation in the fundamental constants [2], and allow the test of general relativity on earth [13]. They are also considered for a possible redefinition of the second. However, a prerequisite for these applications is the ability to *compare* optical frequencies at the level of uncertainty and stability of the optical frequency standards.

Within the same laboratory, this problem was essentially solved with the advent of femtosecond frequency combs. Frequency combs allow the comparison between different optical frequency standards operating at different wavelengths. They also enable the comparison between microwave and optical frequencies.

However, comparison between frequency standards which are not located in the same laboratory is not possible, since todays optical frequency standards are not yet portable due to their complex setup. Traditional methods for transferring and comparing frequency and time standards around the world are the common-view and the two-way time transfer using the global positioning system (GPS) [14]. However, these techniques require long averaging times to reach the stability of the optical frequency standards. It requires about 30 hours of averaging time to reach an uncertainty in the order of 10^{-15} [15]. Therefore, this technique is not suitable for comparison of optical frequency standards with a stability in the order of 10^{-15} in one second [2], see black line in fig. (1.1).

A promising alternative is the transmission of a reference frequency over optical fibers. Optical fibers are environmentally isolated more than free-space paths, immune against electromagnetic effects and offer low loss for optical signals at the communication wavelength of 1.5 μm. Moreover, a worldwide fiber network infrastructure already exists.

However, there are still refractive index changes caused by thermal and acoustic fluctuations on the optical fiber. This leads to phase fluctuations of the transmitted frequency that has to be compensated in order to provide a stable and accurate frequency at the remote end. Using phase noise compensated fibers starts in 1994, when Ma et al. transfer a stable optical frequency over only 25 m of phase noise compensated fiber at the National Institute of Standards and Technology (NIST) [16]. However, it was not before 2005 as Daussy et al. used a phase noise compensated "relatively" long fiber link (86 km) to transfer stable frequencies [17]. As the fiber length increases, many limitations need to be considered. For example, increasing the fiber length increases the Brillouin scattering and hence limits the input power, increases the overall attenuation, limits the phase noise compensation bandwidth, and as a result increases the fiber induced phase noise.

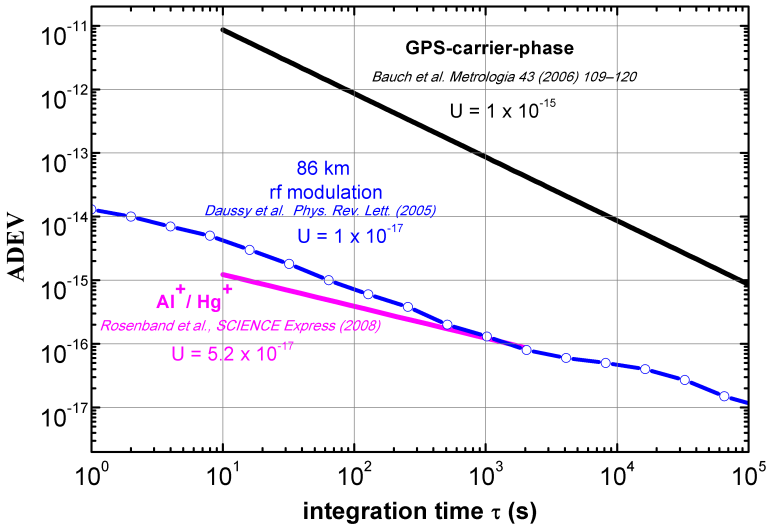

Figure 1.1: Today's best optical frequency standards comparison is made between Hg^+ and Al^+ (pink line) [2], GPS transfer stability (black line) [15], and frequency transfer over phase noise compensated fiber using rf modulated light (blue open circles) [17].

The stability of the 86 km fiber link mensioned above was already much better than that of the GPS transfer. However, it requires improvement in order to compare todays optical frequency standards such as Hg^+ and Al^+, see fig. (1.1). The instability of the compensated 86 km fiber link is shown as blue open circles. The instability of a local comparison between Hg^+ and Al^+ is shown as a pink line. Therefore, we [18, 19, 20, 21] as well as others [22, 23, 24, 25] started investigating

the use of phase noise compensated fiber links to perform comparison of frequency standards.

There are several methods to transfer frequencies over optical fibers [22]. Among all of them, the use of an amplitude-modulated (AM) carrier frequency [22, 23] and the direct transfer of a highly stable optical carrier [19, 20, 21, 24, 25], are the most promising methods for long-haul frequency dissemination based on existing telecommunication fiber networks at λ=1.5 μm. The optical carrier frequency transfer offers several advantages over the AM-modulated carrier. The optical carrier gives much higher resolution for measuring the phase fluctuations of the fiber link. Moreover, it allows larger distances to be bridged, since it allows to detect small signals by means of a heterodyne beat with a local optical oscillator. Furthermore, it puts less stringent requirements on the SNR needed to achieve a certain instability.

In this thesis, the first transmission of a highly stable carrier frequency over a commercial optical fiber network in Germany is presented. A typical remote optical frequency comparison over an optical fiber link between frequency standards (A, B) is shown in fig. (1.2). A laser at a wavelength of 1.5 μm is used as a transfer laser between site A and B. At each site, a femtosecond frequency comb is used to compare the stability of the frequency standard to that of the transfer laser.

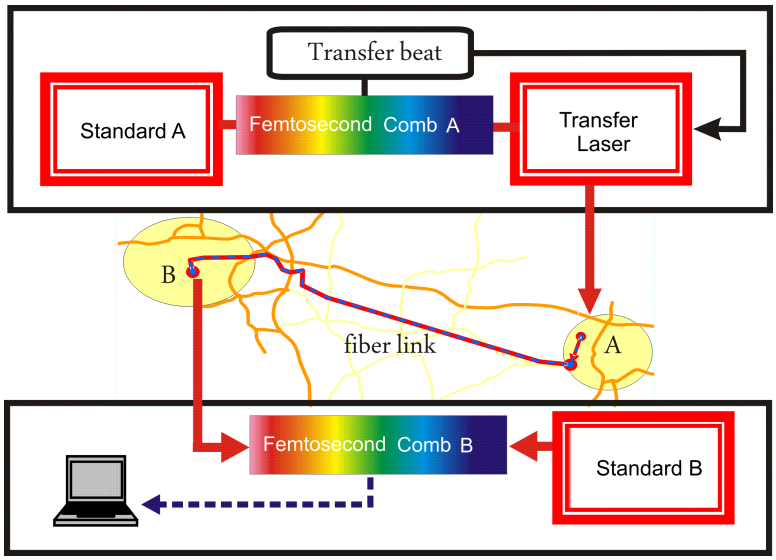

Figure 1.2: Typical remote frequency comparison over optical fiber between a frequency standard at site A and one at site B. A transfer laser at 1.5 μm is used to transfer a stable frequency from one site to the other.

An interferometer based on all-in-fiber components has been constructed to detect and compensate the phase noise introduced by the fiber link. The interferometer is based on a Michelson interferometer with the fiber link forming one interferometer arm. The light crosses the fiber twice in the forward and in the return direction to beat with the reference light.

As fiber length is increased, attenuation increases. In order to overcome this, optical amplifiers are used. For a fiber length of about 120 km, only one bi-directional Erbium-doped fiber amplifier (BEDFA) is necessary to amplify light in the forward and in the return direction. For longer distances, a chain of BEDFA is required to transfer the optical signal with minimized loss. However, saturation of the gain medium and lasing effects are observed; in consequence the gain of the bi-directional EDFA has to be kept below 25 dB. The fiber Brillouin amplifier (FBA) is introduced as an alternative to the BEDFA for long distances. The FBA enables the amplification of a very small input signal (a few nano Watt) by more than 50 dB in a single gain step and allows to bridge larger distances in one step. This technique has been implemented to demonstrate an ultrastable frequency transfer over a 480 km fiber link with only one intermediate amplifier station, and additional amplifiers at the remote, and the local ends [21]. This technique paves the road to envisaged European fiber network for remote frequency standards comparison.

This thesis is organized as follows:

- *In the first chapter*, a short overview about the frequency standards used in this work is given. The technique used to compare frequency standards using a femtosecond frequency comb is described. The possibility of using optical fibers to remotely compare frequency standards and the problems that have to be considered are discussed.

- *In the second chapter*, different methods for the measurement of phase noise in the frequency and time domains are described. A technique is given to identify different phase noise sources. A phase noise detection and compensation system is constructed, and the transfer function of this system is modelled. Different phase noise contributions to the system are discussed and the performance of this system is characterized.

- *In the third chapter*, the noise sources affecting the detected signal amplitude are described and their measurements are presented. Two methods to

bi-directionally compensate the attenuation of long-haul fiber systems are presented: BEDFA and FBA. The operation of the routinely used EDFA is described. The new technique for bi-directional optical amplification based on FBA is developed. A comparison between both amplifiers has been performed.

- *In the fourth chapter*, a transfer of an ultrastable frequency over an installed 146 km fiber is made. The effect of laser phase noise on the frequency transfer is studied. The overall performance of the frequency transfer is characterized.

- *In the fifth chapter*, a 74 km fiber link between the Physikalisch-Technische Bundesanstalt (PTB) in Braunschweig and the Institute of Quantum Optics (IQ) in Hanover is used to compare optical and microwave frequency standards in both institutes. It is used to measure the stability of the cavity stabilized lasers in IQ against that of PTB. The stability of an optical frequency standard based on ^{24}Mg atom at IQ is measured against hydrogen maser at PTB.

- *In the sixth chapter*, the world-wide first ultrastable frequency transfer over a distance of 480 km fiber link has been demonstrated. Here, with the new bi-directional FBA technique, only one intermediate amplification station was necessary. The frequency transfer over the 480 km fiber link is then characterized.

- *In the seventh chapter*, the preparation for the 900 km fiber link between PTB and the Max-Planck Institute of Quantum Optics (MPQ) in Garching is shortly described. The current status of this link is mentioned. The possibility of establishing an European network to link between European laboratories that host optical frequency standards is discussed.

Chapter 2

Comparison of frequency standards

The advent of femtosecond frequency combs allows comparisons between optical frequency standards or even optical and microwave frequency standards. Furthermore, optical fibers enable the comparison between frequency standards in the same building, different buildings or even in different institutes. In this chapter, a short description of several frequency standards used in this work is given. Afterwards, the frequency comparison using a femtosecond frequency comb is described. Finally, some properties of optical fibers that are relavant for transmission of an ultra-stable frequency are discussed.

2.1 Frequency standards

In this section, a short description of the frequency standards used in this work, with respect to instability and uncertainty, is given. To characterize individual frequency standards, the Allan deviation (ADEV) is used as a measure of the frequency instability.

1. *Cavity stabilized laser at PTB (CSL-PTB)*: The laser CSL-PTB is operated at 657 nm and stabilized to an optical high finese cavity using the Pound-Drever-Hall technique [26]. The laser exhibits a linewidth of about 2 Hz and reaches a relative frequency stability of 2×10^{-15} [27], as shown as red squares in fig. (2.1).

2. *Cavity stabilized laser at IQ (CSL1-IQ, CSL2-IQ)*: CSL1-IQ, CSL2-IQ are cavity stabilized lasers using also the Pound-Drever-Hall technique. Both lasers are operated at 914 nm. CSL2-IQ uses a horizontal resonator (finesse F = 600,000) mounted near the symmetry plane for reduced vibrational sensitivity, similar to a design used in [28]. An instability measurement of both lasers against each other and against CSL-PTB will be shown later in this work in chapter (6).

3. *Mg stabilized laser at IQ (Mg-laser)*: The phrase "Mg-laser" referes to one of the cavity stabilized lasers (CSL1-IQ or CSL2-IQ), which is frequency doubled and locked to the clock transition ($^1S_0 - ^3P_1$) at 457 nm in Magnesium (^{24}Mg). A previous stability measurement for Mg-standard against a passive hydrogen maser (H7) is shown as blue circles [29].

4. *Cesium fountain (CSF1) at PTB*: CSF1 is one of the primary frequency standard at PTB. CSF1 has a relative frequency instability of $2.5 \times 10^{-13}\ (\tau/\mathrm{s})^{-1/2}$ (as shown in fig. (2.1)) and uncertainty of 8×10^{-16} [30].

5. *Hydrogen maser (H5) at PTB*: H5 is an active Hydrogen maser which has a short term instability of about 2×10^{-13} at 1 second, and a flicker floor of 1×10^{-15} after about 1 hour. Fig. (2.1) shows the measured instability (black dots) for the Hydrogen maser H5 against (CSL-PTB). The measurement gives the instability of H5 since the short term stability of CSL-PTB (red squares) is much better than that of H5.

6. *Hydrogen maser (H7) at IQ*: H7 is a transportable passive Hydrogen maser with short term instability of about 6×10^{-13} and a flicker floor of about 2×10^{-14} after about 1 hour. H7 was calibrated at PTB against H5. At IQ, it served as a local reference for the frequency comb. Fig. (2.1) shows an instability measurement of H7 against CSL1-IQ. Since the short term stability of CSL1-IQ (see chapter (6)) is much better than H7, the measurement gives the instability of H7.

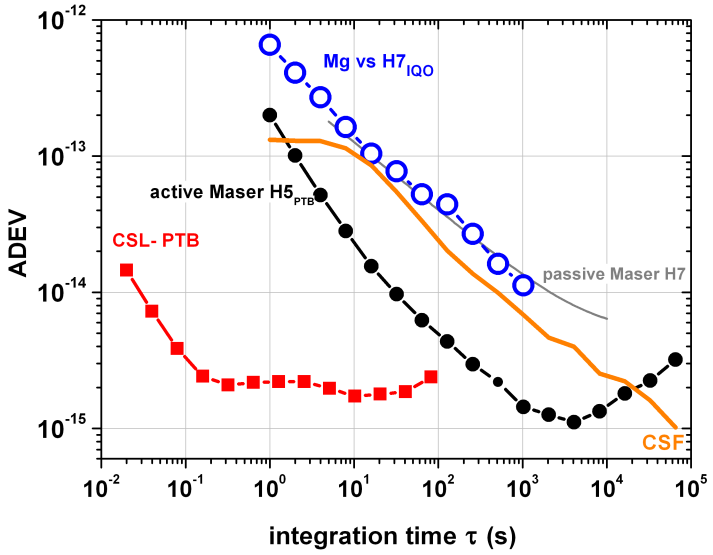

Figure 2.1: Instability (ADEV) of the frequency standards used in this work.

2.2 Femtosecond frequency comb as a transfer oscillator

The advent of the femtosecond frequency comb systems (FFCS) revolutionized optical frequency metrology and synthesis [1]. It is now possible to measure optical frequencies (10^{14} Hz) with reference to microwave frequencies (10^{9} Hz) without the need to establish a frequency chain between both frequencies as demonstrated in [31].

In this section a brief introduction to FFCS in the time and frequency domain is given. Afterwards, a method to compare two different frequencies using a FFCS without introducing noise from the FFCS is discussed.

2.2.1 Basics of femtosecond frequency combs

The frequency comb system consists mainly of a mode-locked laser. The mode-locking process establishes a fixed phase relation between the cavity oscillating modes across a broad spectrum of frequencies, and thus generates a train of "ultrashort" optical pulses (down to 5 femtoseconds) in the time domain [32]. This train of ultrashort pulses in time domain corresponds to discrete, regularly spaced lines in the frequency domain, called an optical frequency comb, see fig.'s (2.2, 2.3). The

frequency spacing between the comb lines is called the repetition rate (f_{rep}). It is inversely proportional to the time delay between pulses.

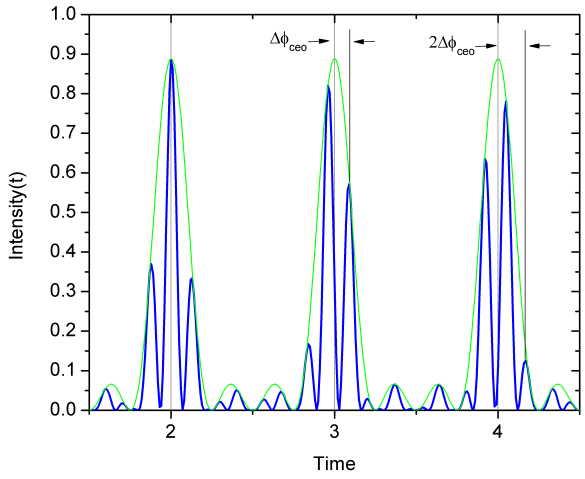

Figure 2.2: Time domain representation of frequency comb. $\Delta\phi_{ceo}$ is the offset phase between two consecutive pulses.

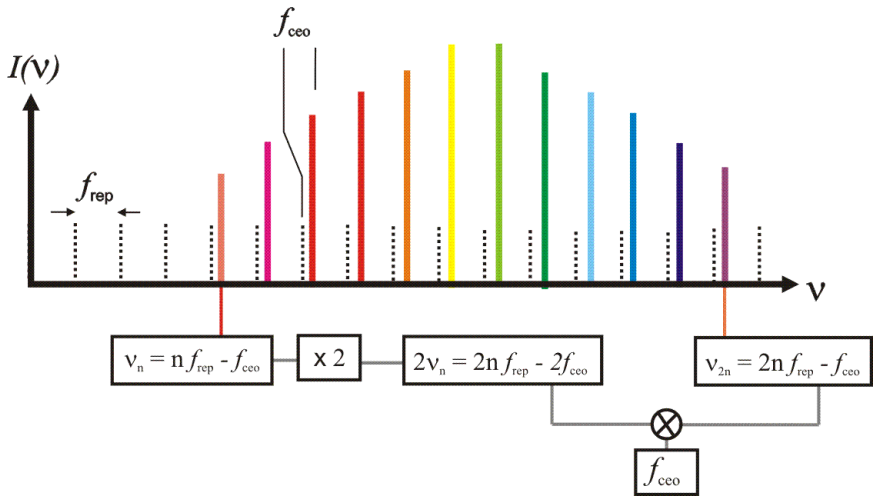

Figure 2.3: Frequency domain representation of frequency comb together with a scheme to detect the carrier offset frequency f_{ceo}.

When a wide spectrum of short pulse propagates in dispersive medium with normal dispersion, longer wavelengths propagate faster than shorter wavelengths. Therefore, the pulse propagates with the group velocity (envelop velocity), while the center wavelength (carrier) propagates with the phase velocity. Due to the difference in velocities, the phase of the carrier evolves in time with respect to the maximum of the envelope, see fig. (2.2). This phase shift ($\Delta\phi_{ceo}$) in time domain

corresponds to a frequency shift (f_{ceo}) in the frequency domain. This frequency shift is given by:

$$f_{ceo} = \frac{f_{rep}\ \Delta\phi_{ceo}}{2\pi}$$

The frequency of a single mode ν_n with mode number n in a frequency comb can then be expressed as:

$$\nu_n = n\ f_{rep} + f_{ceo} \tag{2.1}$$

Therefore, for the absolute measurement of the frequency ν_n, the two RF frequencies f_{rep}, f_{ceo} must be measured. The measurement of f_{rep} is done simply by detecting the pulse train with fast photodiode. On the other hand, the measurement of f_{ceo} requires an interferometric technique. For this so called self-referencing, the spectrum must span an octave in frequency to contain ν_n as well as ν_{2n}. The broadening of the spectrum can be done in photonic crystal fiber or highly nonlinear fiber [33]. The comb frequency ν_n is doubled with nonlinear crystal. The doubled frequency is then heterodyned with the corresponding comb frequency ν_{2n} to produce the offset frequency f_{ceo}, see fig. (2.3).

In order to measure an optical frequency ν_{fs}, both (f_{rep}, f_{ceo}) are usually stabilized to a microwave frequency standard (example: hydrogen maser). The absolute value of the measured optical frequency ν_{fs} can be calculated from:

$$\nu_{fs} = n\ f_{rep} + f_{ceo} + \Delta_{fs} \tag{2.2}$$

where Δ_{fs} is the beat between the optical frequency and the nearest comb mode with number n. The accuracy and the stability of the measurement will be limited by the microwave frequency standard. An example for this measurement is given in section (2.2.3).

For the comparison between optical frequency standards, the ratio between both frequencies is measured using what is called the *transfer oscillator* concept. By using this concept, the frequency noise of the comb is eliminated. Further details to this concept are given in section (2.2.3).

2.2.2 Fiber based frequency combs

Recently, frequency comb systems based on Er-doped fiber lasers attracted a lot of attention [34]. Unlike systems based on Ti:Sapphire femtosecond lasers, they are compact, easy to use, capable to operate continuously over weeks, and cost-effective. Therefore, they are excellent candidates for long-term metrology and comparison of permanently running optical frequency standards. The operation wavelength around 1.55 μm makes them also highly suitable to transfer the stability of optical frequency standards to telecommunication lasers, which will be used later in this work. The frequency of these lasers is then broadcasted via fiber networks to other remote optical frequency standards.

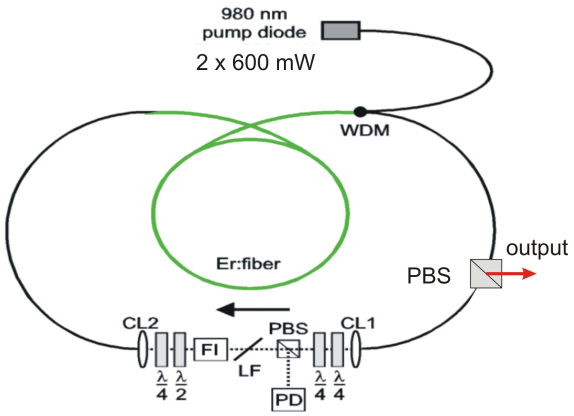

Figure 2.4: Principle setup for the nonlinear the polarization rotation and the polarization control used to achieve the pulsed operation [35]. WDM: Wavelength devision multiplexer, PBS: polarizating beam splitter, $\lambda/4$: quarter-wave plate, $\lambda/2$: half-wave plate, PD: photodetector, CL: fiber-to-free-space coupling lenses, LF: Lyot filter.

In this work, an Er-doped fiber-based system from Menlo Systems (FC-1500) with a repetition rate of $f_{rep} \approx 100$ MHz is used. The FC-1500 comprises a mode-locked Er-doped fiber laser, a frequency doubling unit for the measurement in the visible spectrum, an offset frequency detection unit, and detection and control electronics. To our knowledge, the mode-locked fiber laser implements nonlinear polarization rotation (NPR) to achieve mode-locking. The NPR is a passive-mode locking technique that relies on the Kerr effect in a length of optical fiber in conjunction with polarizers to cause artificial saturable absorber action [36]. A quarter-wave plate polarizes the light elliptically. The light passes then through an Er^{+3} doped

fiber, where additional elliptical rotation occurs. The Kerr effect in the optical fiber rotates the peak of the pulse more than the pulse wings. At the output of the fiber, a half-wave plate orients the pulse so that the peak of the pulse passes through the polarizer while the wings of the pulse are extinguished, thus achieving pulsed operation, see fig. (2.4). As reported by Menlo System, the achieved pulse length is $<$ 90 fs. The output spectrum from the Er-doped mode-locked laser has a bandwidth of about 100 nm centered at 1560 nm.

In order to detect f_{ceo}, an octave spanning spectrum typically (1050 nm to 2200 nm) is obtained using highly nonlinear fiber. The output is frequency doubled by a PPLN (periodically poled Lithium Niobate) crystal. The frequency doubled spectrum is superimposed on the original spectrum, propagates through interference filter at 1064 nm to a photodetector to detect f_{ceo} frequency. The detected signal is then used to stabilize the f_{ceo} frequency by changing the pump power of the femtosecond fiber laser.

The stabilization of the repetation rate is more demanding, since phase noise at this frequency enters an optical frequency measurement with a large multiplication factor. Thus, phase noise of the electronics becomes a critical issue. In order to avoid this, the 114 harmonic of the pluse repetation frequency is detected using a fast photodiode. This microwave signal is down converted, filtered and frequency multiplied by 128 using a harmonic tracking filter, see fig. (2.5). Due to the large multiplication factor, the resolution of the counting process is enhanced by $114 \times 128 = 14952$ and digitization errors are reduced. The down-converted signal is used to slowly control the repetition frequency of the laser using the built-in piezo-electric transducer that controls the cavity length.

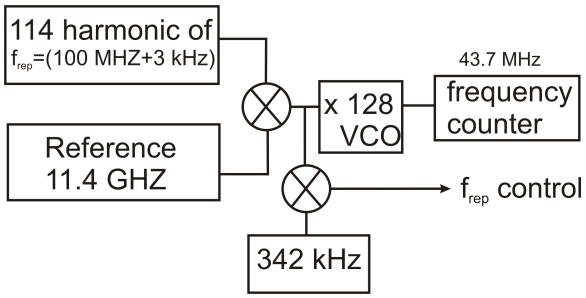

Figure 2.5: Harmonic detection of the repetition rate (f_{rep}).

2.2.3 Transferring the stability of a cavity stabilized laser to a fiber laser

As discussed in the previous section, femtosecond frequency combs based on Er-doped fiber lasers are better suited for our application than Ti:Sapphire lasers. However, they still exhibiting significantly more high frequency phase noise than Ti:Sapphire lasers [37, 35]. The stability and the accuracy of the fiber combs can be enhanced by stabilizing both degrees of freedom (f_{rep}, f_{ceo}) to a microwave frequency standard (like H5). However, the measurement of frequency standards will be ultimately limited by the frequency instability and accuracy of the microwave reference [38, 39]. As the stability of the optical frequency standards outperform that of their microwave counterparts [40], the *transfer oscillator* concept is introduced to perform comparisons between optical frequency standards without contributions from phase noise of the frequency comb [41]. A measurement of the frequency ratio between the fundamental frequency at 1064 nm and its second harmonic at 532 nm of a Nd:YAG laser using the *transfer oscillator* concept showed an uncertainty below 10^{-18} [42]. Using this method, a single beat frequency called "transfer beat" is derived that represents the relative stability of both optical frequencies and is free from the noise of the femtosecond comb. Thus, a transfer beat between two optical frequencies can be used to stabilize one of them relative to the other. As an example, the frequency stability of a cavity stabilized laser is transfered to a telecommunication laser at 1543 nm with stability below 2×10^{-15} (1 s) and 5×10^{-18} (8000 s) [38].

Fig. 2.6 illustrates the *transfer oscillator* concept. The stability of CSL-PTB is transfered to a fiber laser (NIR-PTB) using the transfer beat $\Delta_{transfer}$ to generate an error signal. NIR-PTB is a commercially available near-infrared fiber laser at PTB. It is a single-frequency distributed-feedback laser operating at a wavelength of $\lambda = 1542$ nm ($\nu = 194$ THz) with a free-running linewidth of about 5 kHz. Its frequency can be tuned using a piezo-electric transducer (PZT) with tuning range of about 100 pm.

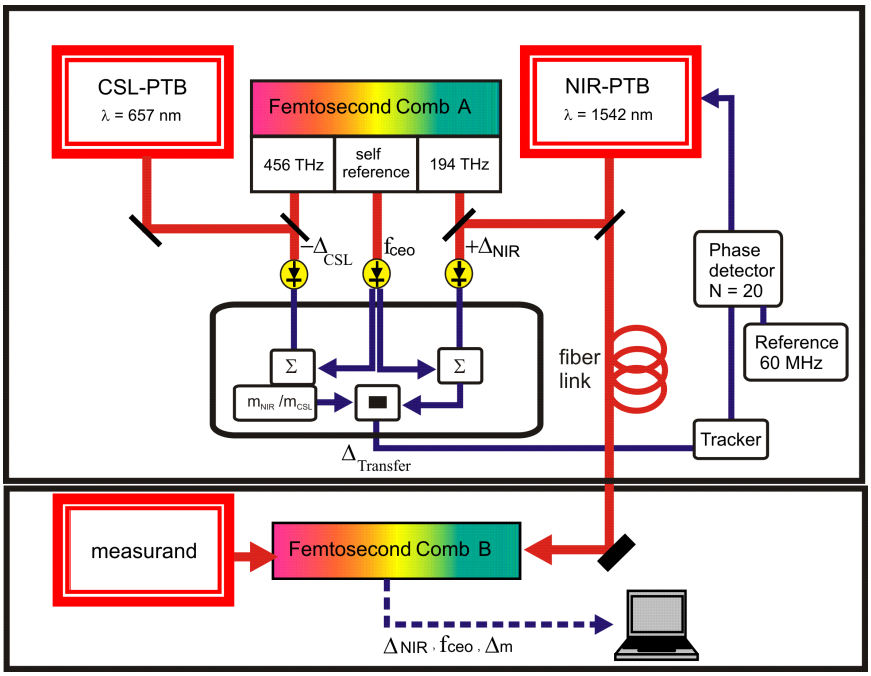

Figure 2.6: A fiber-based frequency comb A is used to transfer the stability of CSL-PTB to NIR-PTB laser using the transfer oscillator concept. Δ_{CSL}, Δ_{NIR}, Δ_m: the beats between the lasers and the corresponding frequency comb, f_{ceo}: the offset frequency of the comb, $\Sigma, -$: summation and difference operations, and m_{CSL}, m_{NIR}: the nearest comb mode to the lasers frequency. At a remote site, frequency comb B is used to measure the frequency of a remote laser (measurand).

In order to transfer the stability of the frequency reference CSL-PTB to the NIR-PTB laser, two beats between each of the two lasers and the corresponding comb mode (n_{CSL}, n_{NIR}) of comb A are derived. The two beats can be described by

$$[\Delta_{CSL}(t) = n_{CSL} f_{rep}(t) + 2f_{ceo}(t) - \nu_{CSL}(t)]_{PTB} \tag{2.3}$$

$$[-\Delta_{NIR}(t) = n_{NIR} f_{rep}(t) + f_{ceo}(t) - \nu_{NIR}(t)]_{PTB} \tag{2.4}$$

where $\nu_{CSL}(t)$ and $\nu_{NIR}(t)$ are the absolute frequencies of the two lasers (CSL-PTB, NIR-PTB). The mode n_{CSL} is the frequency doubled component at 657 nm (CSL-PTB wavelength) from the original mode $\frac{n_{CSL}}{2}$ at the normal emission wavelength of the Er-doped fiber comb at about 1550 nm.

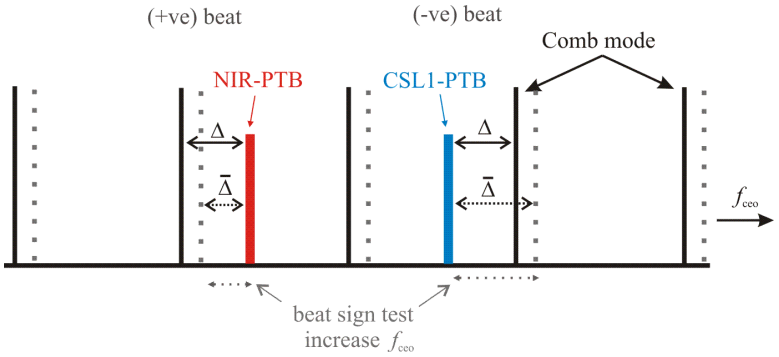

Figure 2.7: Beat sign test. By increasing f_{ceo} frequency, the positive beat frequency decreases while the negative beat frequency increases.

The sign in equations (2.3, 2.4) is due to the fact that, the NIR-PTB beat with the corresponding comb mode is positive while that of CSL-PTB is negative. In order to verify the sign of the beat a simple test is made by changing the f_{ceo} frequency. If the beat is negative, beat frequency increases when f_{ceo} frequency increases. If the beat is positive, beat frequency decreases when f_{ceo} frequency increase. Fig. (2.7) shows the beats between (CSL-PTB, NIR-PTB) and FFCS. The beat sign test is shown as dashed lines when f_{ceo} is increased.

The transfer beat between both lasers is generated without the phase noise contributions from the frequency comb (f_{rep}, f_{ceo}) using simple mathematical operation between the two beats in equations (2.3, 2.4). This is described as follows:

- The first step is to add (and subtract) f_{ceo} to (from) both beats in equations (2.3, 2.4) in order to drop f_{ceo} fluctuations. The f_{ceo} frequency is subtracted from the Δ_{CSL} beat after a division by two.

$$\left[\frac{\Delta_{CSL}(t)}{2} - f_{ceo}(t) = \frac{n_{CSL}}{2} f_{rep}(t) - \frac{\nu_{CSL}(t)}{2}\right]_{PTB} \tag{2.5}$$

  The f_{ceo} frequency is also added to Δ_{NIR} beat.

$$[\Delta_{NIR}(t) + f_{ceo}(t) = -n_{NIR} f_{rep}(t) + \nu_{NIR}(t)]_{PTB} \tag{2.6}$$

  Frequency mixers are used to generate the addition and the subtraction operations. Suitable filters are used to allow only the required operation (sum or difference).

- The second step is to drop the fluctuations in f_{rep} from the resulting frequencies. The electronic key element is a direct digital synthesizer (DDS) that is able to realize the rational number $(n_{CSL}/2n_{NIR})$ with high precision. The DDS is used to frequency divide equation (2.5) by $n_{CSL}/2n_{NIR}$.

$$\left[(\frac{\Delta_{CSL}(t)}{2} - f_{ceo}(t))\frac{2n_{NIR}}{n_{CSL}} = n_{NIR}f_{rep}(t) - \frac{2n_{NIR}}{n_{CSL}}\frac{\nu_{CSL}(t)}{2}\right]_{PTB} \tag{2.7}$$

- Finally, the sum is taken between the two frequencies in equations (2.7, 2.6) to obtain the transfer beat. Then, the transfer beat at PTB can be described by

$$\Delta_{transfer}(t) = \nu_{NIR}(t) - \frac{2n_{NIR}}{n_{CSL}}\frac{\nu_{CSL}(t)}{2} \tag{2.8}$$

Since in general, the reference laser (CSL-PTB) contributes negligible phase noise, the *transfer beat* between the PTB's frequency standard laser CSL-PTB and NIR-PTB reflects the stability of NIR-PTB laser. As shown in fig. (2.6), the *transfer beat* is tracked and compared with a reference oscillator at 60 MHz to generate an error signal. The error signal is directed to a built-in piezo-electric transducer (PZT) to stabilize the frequency of the NIR-PTB laser. The control bandwidth of the loop is limited to approximately 10 kHz by the first PZT resonance at about 30 kHz.

To measure the phase noise of the unstabilized NIR-PTB laser directly from the transfer beat, we slowly locked the NIR-PTB laser with an attack time of $\tau_{attack} <$ 0.1 s. to CSL-PTB to compensate only the frequency drift of the free-running NIR-PTB laser during the measurement. The spectrum of the transfer beat and hence the phase noise of the unstabilized NIR-PTB laser shown in fig. (2.8) as a black-dashed curve. It is dominated by flicker frequency noise $S_\phi \approx 1/f^3$ which is common for fiber lasers (further information about the noise types is found in chapter (3)). The flattening of S_ϕ at low frequencies is due to the low gain servo loop.

After locking the NIR-PTB laser to CSL-PTB using the transfer beat, the phase noise curve is dominated by white phase noise with an average value of $S\phi < 1 \times 10^{-6}$ rad^2/Hz up to a locking bandwidth of 8 kHz (red curve in fig. (2.8)). As demonstrated in [38], the stabilized NIR-PTB laser then exhibits approximately the same stability as CSL-PTB. Using eq.(2.8), its frequency can be calculated from the

frequency of CSL-PTB. Phase noise measurement are discussed in the next chapter (section 3.2).

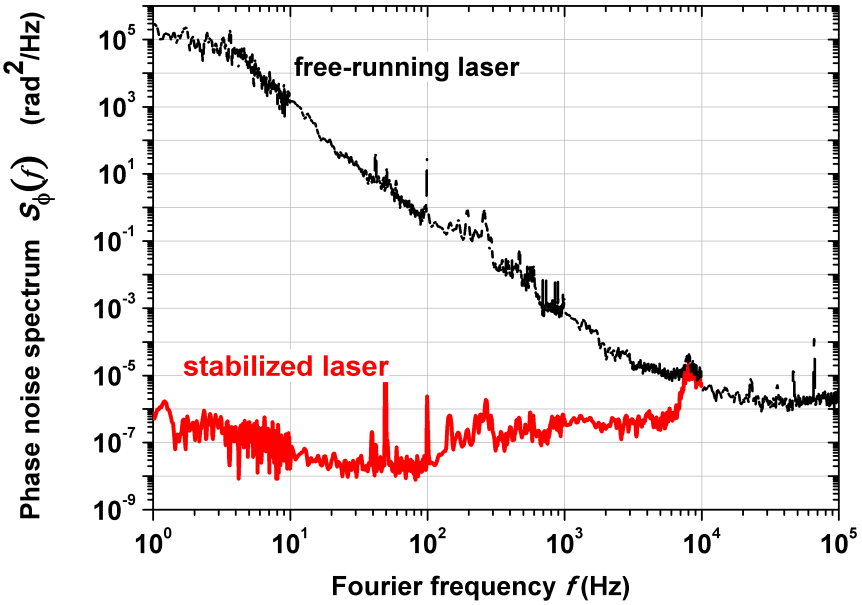

Figure 2.8: Phase noise of the *transfer beat* before (black-dashed line) and after (red-solid line) stabilizing NIR-PTB laser. The phase noise of the unstabilized transfer beat represents that of the free-running NIR-PTB laser.

When no frequency control is needed, it is not necessary to generate a hardware *transfer beat* (using mixers and DDS). As indicated in fig. (2.6) a *software transfer beat* allows one to measure the frequency stability of a measurand. A software *transfer beat* can be generated by the same steps discussed above, but using computer software to calculate the *transfer beat* mathematically.

However, in some cases, it is also useful to generate a *software transfer beat* combined with the hardware one, since it gives an out-of-loop indication for the achieved stability. It acts also as an indicator for some problems that may arise during the stabilization of the NIR-PTB laser frequency. Fig. (2.9) shows frequency fluctuations over about 5 hours for the hardware (blue), an optimized (red), and a cycle slipped (green) *transfer beat* between NIR-PTB and CSL-PTB. The latter indicates that the SNR of the NIR and CSL beats was not sufficient. As this cannot be detected with the hardware beat, an independent measurement using the software beat is required. Optimizing the SNR of the individual beat signals then removes the cycle slips. The corresponding stability measurements are shown in fig. (2.10).

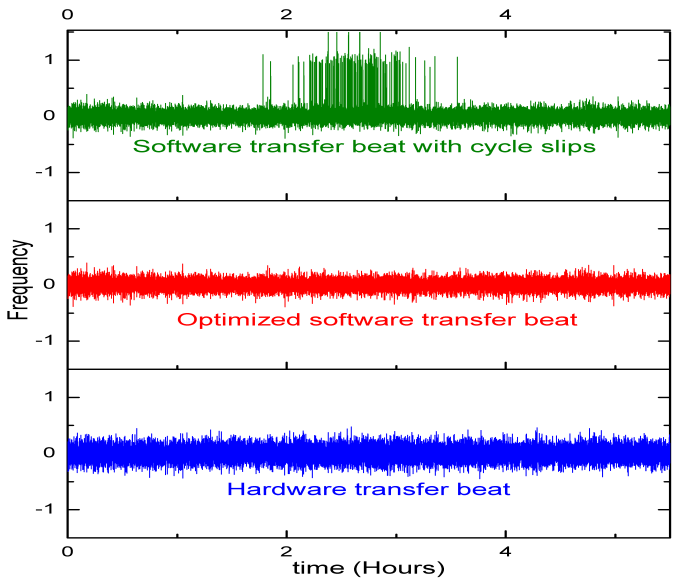

Figure 2.9: The time domain data for the frequency fluctuations of the hardware (blue), an optimized software (red), and cycle slipped (green) *transfer beats*, NIR-PTB is stabilized to CSL-PTB.

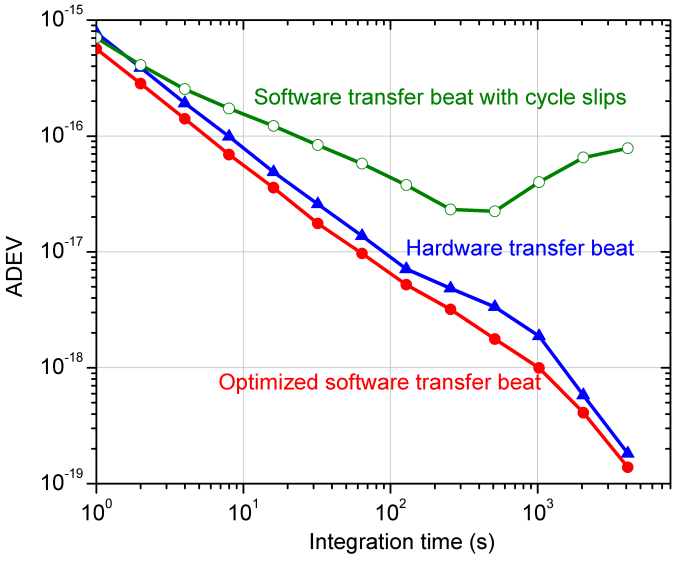

Figure 2.10: ADEV measurement for the hardware (blue triangle), an optimized software (red dots) *transfer beats*, and a *transfer beats* with cycle slipps (green open circle), NIR-PTB is stabilized to CSL-PTB.

2.2.4 Determination of the correct mode number (n)

In all of the above *transfer beat* calculations, the number of the nearest comb modes of NIR-PTB and CSL-PTB must be known. In the case of CSL-PTB, eq. (2.1) is used to obtain $n_{CSL-PTB}$, since CSL-PTB has a well known absolute frequency. This is not trivial for NIR-PTB. Due to the large tuning range of several 10 GHz, its absolute frequency is not yet known. The comb mode next to NIR-PTB frequency ($n_{CSL-PTB}$) could be easily determined if the absolute frequency of the NIR-PTB laser is known within 50 MHz (for $f_{rep} \approx 100$ MHz). A high accuracy wavemeter is used to obtain a value for $\nu_{NIR-PTB}$ (within 50 MHz) and hence $\nu_{NIR-PTB}$.

Another method is suggested by Ma et al. to determine the nearest comb mode to a measured laser (NIR) [43]. This method is based on varying f_{rep} of the frequency comb while counting the number of swept comb modes. Although this method is not applicable in this work, a short description of this method is given here, since it is the basis for the method used in this thesis. Two beat frequencies ($\Delta_{NIR1}(t),\ \Delta_{NIR2}(t)$) are obtained between the comb and the NIR laser, which correspond to mode numbers of ($n_{NIR},\ n_{NIR}+m$), where m is a small integer that can be obtained by counting the number of swept comb modes by smoothly changing f_{rep} and monitoring the beat between the NIR laser and the comb on a rf spectrum analyzer. Therefore, n_{NIR} can be expressed as:

$$n_{NIR} = \frac{m f_{rep2} \pm \Delta_{NIR2} \pm \Delta_{NIR1}}{f_{rep1} - f_{rep2}} \tag{2.9}$$

The accuracy of determining n_{NIR} is:

$$\delta = \frac{\Delta_{NIR2} - \Delta_{NIR1}}{f_{rep1} - f_{rep2}}$$

If the laser is not stable during the duration of measurement, this will increase the inaccuracy of determining $\Delta_{NIR2},\ \Delta_{NIR1}$. This will increase the inaccuracy of determining n_{NIR}, as inferred from the above equation. In our case of free-running laser with a frequency change of about Δ_{NIR} =1 MHz during the measurement time, the change in repetition rate should be 10 MHz to obtain $\delta \approx 0.1$. The laser wavelength of 1542 nm corresponds to a mode number in the order of 2×10^6. Therefore, the required mode number change is $m = \Delta f_{rep} \times n / f_{rep} = 2 \times 10^5$, which is impossible to count.

The method used here is based on the use of two femtosecond frequency combs with different repetition rate at the same time to measure the frequency of the NIR laser. By synchronizing the measurement for both combs, the problem of the free-running laser is solved. This method is applied to determine the nearest comb mode to the NIR-PTB laser. The two frequency comb systems at PTB and IQ (comb A, comb B) are used. From equation (2.9), by assuming values for the counted m, this equation can be modified for the two-combs-approach to be:

$$n_{NIRA} = \frac{m_{assumed} f_{repB} \pm \Delta_{NIRA} \pm \Delta_{NIRB}}{f_{repB} - f_{repA}} \tag{2.10}$$

where the number $m_{assumed} = n_{NIRB}(assumed) - n_{NIRA}(assumed)$ is the difference between the assumed mode numbers of the two combs, $\Delta_{NIRA}, \Delta_{NIRB}$ is the beats between the NIR laser and the two combs (the signs are calculated such that the NIR laser makes positive beat with the comb at PTB, while it makes a negative beat with the comb at IQ). The f_{ceo} frequencies assumed here to be the same for both combs for simplifications, while the real values are discussed later in this work.

Substituting different values for $m_{assumed}$ in eq. (2.10) until the calculated value for the mode in equation (2.10) for the beat with comb A equals the assumed value($n_{NIRA} - n_{NIRA}(assumed) \approx 0$). This gives the correct mode number.

2.3 Properties of optical fibers

Optical fibers are used instead of metal wires for frequency transfer because signals traveling along optical fibers suffer less loss and are also immune to electromagnetic interference. It allows also the transmission of stable optical frequencies carriers as well as the modulated RF or microwave frequencies. However, a signal transmitted through fibers still face some losses. The transmitted signal frequency can be distorted by the environmental perturbations (temperature variations and acoustic perturbations) and the dispersion caused by the random polarization changes and chromatic phase changes. In this section, these limitations are discussed, while in the next chapters methods are discussed to overcome these difficulties.

2.3.1 Attenuation

Fiber attenuation is one of the most important properties of an optical fiber in the context of frequency transmission. It mainly determines the maximum span for an optical link without optical amplifiers. It depends on the wavelength of the propagating light as shown in fig. (2.11) [44]. There are physical (absorption, scattering) and technical (bending and connectors) loss mechanisms in fused silica glass (SiO_2) fibers. At higher wavelengths (λ >1700 nm), the vibrational transition of the glass Si-O bond and the OH^- impurities in the glass cause light energy to be absorbed. The absorption by OH^- impurities is dominant in this wavelength region. For lower wavelengths (800 nm< λ <1700 nm), the intrinsic absorption of the fiber is very low and it is negligible compared to Rayleigh scattering losses. At wavelengths λ <500 nm, intrinsic UV absorption is the dominant factor.

Rayleigh scattering (RS) occurs from the interaction of light with the random density variations in the optical fiber due to the manufacturing process. The size of these variations (defects) must be less than one-tenth of the light wavelength for RS to occur [44]. The scattered intensity is proportional to $1/\lambda^4$, where λ is the transmitted light wavelength.

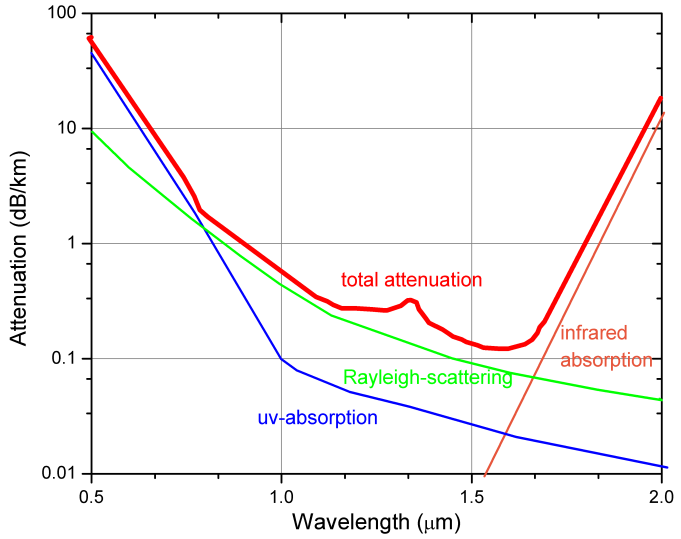

Figure 2.11: Wavelength dependence of silica-glass fiber attenuation coefficient [44].

As a result of these combined effects, the attenuation is minimum in the telecommunication wavelength window around 1550 nm. Therefore, a laser at 1542 nm is used in this work to transfer the stability of optical frequency standards through

the link to remote sites. This wavelength has an attenuation of about 0.2 dB in the fused silica single mode fiber (SMF-28) used here.

The technical loss mechanisms in the fibers are dominated by bending and connectors. Bending lowers the total internal reflection at core-cladding boundary and forces some light to leave the core. Care must be taken not to form a curvature with a radius less than the bend radius of 10 mm specified by ITU-T-G.657 standard. In our experiment, the bend radius was kept larger than 5 cm. Connectors introduce not only losses, but also back-reflections that effect the fiber noise stabilization scheme discussed in section (3.5). Angle polished connectors (APC) are used to minimize the back-reflections. An APC connector is polished with 8^o angle from the flat surface to reduce the reflections and direct the reflected light back out of the fiber. Another solution to avoid back-reflections and losses is to use index matching gel (IMM). IMM is a gel with refractive index close to that of the fiber core, and it is used to reduce Fresnel reflections at the surface of the fiber input in connectors. In this work, IMM is used only in the route between PTB and MPQ (900 km). All fiber connectors and devices used in this work are equipped with APC connectors.

The loss in the signal power resulting from the reflections at a discontinuity (connector) is called the *return loss*. *Return loss* is defined in decibel as $RL(dB) = 10log(P_i/P_r)$ where P_i is the input power and P_r is the reflected power. The loss of the signal power resulting from the insertion into the fiber is called *insertion loss*, and it is given by $IL(dB) = 10log(P_i/P_s)$ where P_s is the received power. Connectors should have an *insertion loss* of $IL < 0.5$ dB, while good splices have IL < 0.05 dB. The typical return loss of an APC connector is $RL > 50$ dB.

An optical time domain reflectometer (OTDR) is used to spatially measure the attenuation and the Fresnel reflections at connectors and fiber ends along a fiber. The OTDR launches short pulses into a fiber to measure the optical signal power returned to the instrument as a function of time. It measures the attenuation by detecting the Rayleigh back scattered light (RBS) from different parts in the fiber.

2.3.2 Stimulated Brillouin scattering (SBS)

Brillouin scattering can occur spontaneously at low optical powers. It results from the photon scattering on thermally generated phonons [45]. For higher input optical

powers, the optical field substantially contributes to the phonon population. The two counter-propagating waves generate a moving refractive index grating; the higher the reflected power, the stronger the grating and the higher the effective reflectivity. Above a certain threshold of incident light power, stimulated Brillouin phonons can scatter most of the incident light power back to the input of the fiber [46]. For silica fibers, the material nonlinearity is not very high, however, the small effective mode area and the long propagation length in the fiber strongly favor the nonlinear effects.

The frequency of the reflected beam is slightly lower than that of the incident beam, which corresponds to the frequency ν_B of the emitted phonons. This frequency shift is called the Brillouin frequency shift and is determined by the phase matching conditions. The Brillouin frequency shift can be calculated from the refractive index n, the speed of sound $v_a = 6 \times 10^3$ m/s, and the vacuum wavelength λ_o as:

$$\nu_B = \frac{2nv_a}{\lambda_o}$$

The Brillouin frequency shift depends on the material composition and to some extent on the temperature and pressure of the medium. For silica fibers, the Brillouin frequency shift is of the order of 11 GHz. The Brillouin gain has an intrinsic bandwidth of typically 10 to 100 MHz. The Brillouin linewidth $\Delta\nu_B$ is determined by the phonon life-time $\Delta\nu_B = 1/\text{lifetime}$. In principle, a strong acoustic absorption leads to a short phonon lifetime and hence to a narrow linewidth. However, the Brillouin gain spectrum is strongly broaden by various effects, such as transverse variations of the acoustic phase velocity or longitudinal temperature variations [47, 48].

The SBS threshold power is calculated from:

$$P_{th} = \frac{21A}{\gamma L_{eff}}(1 + \frac{\Delta\nu_{laser}}{\Delta\nu_B}) \tag{2.11}$$

where A: is the effective mode area of the fiber (1×10^{-10} m^2), L_{eff}: the effective gain length is $L_{eff} = (1 - e^{\alpha L})/\alpha = 21$ km ($\alpha = 0.2$ dB/km), and γ is the gain coefficient of the nonlinear process. The latter can be obtained from the following equation:

$$\gamma = \frac{2\pi n^7 p_{12}^2 k}{c_o \lambda^2 \rho_o v_A \Delta\nu_B}$$

where $c_o = 2.997 \times 10^8$ is the vacuum speed of light, λ is the wavelength, $\rho_o = 2.2 \times 10^3$ kg/m^3 is the density of the fused silica of the fiber core, $\Delta\nu_B$ is the SBS linewidth, $n = 1.451$ is the fiber phase refractive index at the used wavelength, $p_{12} = 0.29$ is the elasto-optic coefficient, and $k = 0.5$ (for SMF-28 fiber) is a polarization correction factor with a maximum value of 1 for the polarization maintaining fiber. The value of the gain coefficient is calculated to be $\gamma = 5 \times 10^{-11}$ m/W for a measured Brillouin linewidth of a $\Delta\nu_B = 10$ MHz.

SBS introduces the most stringent power limit for propagation of narrow-band optical signals in fibers. In our case, the linewidth of the laser is much less than the Brillouin linewidth. It follows from equation (2.11), for a laser linewidth of 1 kHz and a SBS linewidth is about 10 MHz, that the SBS threshold is at about 2 mW. Further increase in the power of the input light will increase the SBS scattered power until almost all the input light will be backscattered.

2.3.3 Fiber induced phase fluctuations

When light propagates through an optical fiber, acoustic perturbations or thermal fluctuations along the fiber lead to refractive index changes, and consequently to phase changes in the light propagating through the fiber. A phase change ($d\phi_{fiber}$) during a time t leads to the following frequency shift:

$$\Delta\nu_{fiber} = \frac{d\phi_{fiber}}{dt} = \frac{2\pi}{\lambda}\frac{d(nL)}{dt}$$

where L is the fiber physical length, n is the fiber refractive index, and λ is the propagating light wavelength. If these changes are caused by temperature variations dT, the above equation can be rewritten as:

$$\Delta\nu_{fiber} = \frac{2\pi}{\lambda}(n\frac{dL}{dT}\frac{dT}{dt} + L\frac{dn}{dT}\frac{dT}{dt})$$

where dn/dT is called the thermo-optic coefficient, and $(dL/dT)/L$ is called the expansion coefficient. The thermo-optic coefficient is two orders of magnitude larger than the thermal expansion coefficient [49]. Therefore, only the contribution from the refractive index changes are considered here.

$$\Delta\nu_{fiber} = \frac{2\pi L}{\lambda}\frac{dn}{dT}\frac{dT}{dt} \tag{2.12}$$

Eq. (2.12) describes the frequency shift according to temperature variations. A refractive index variation caused by acoustic (pressure) perturbations also leads to a frequency shift. This shift can be derived similarly by replacing $(\frac{dn}{dT}\frac{dT}{dt})$ by $(\frac{dn}{dP}\frac{dP}{dt})$.

In order to detect and correct the frequency shift of $\Delta\nu_{fiber}$, an interferometer is used. For example, if a single mode fiber (SMF-28) of a length L=100 km affected by a temperature change of dT=1 K in a period of one hour, the interferometer operating on a wavelength of 1550 nm will detect a frequency shift of about 1 kHz. This can be easily corrected using any optical frequency shifter, like an acousto-optic modulator. However, equation (2.12) considers only the instantenous frequency shifts. In a very long optical fiber, the time delay caused by the fiber to detect and compensate this frequency shift must be considered. Consequently, the noise compensation is possible only to a certain bandwidth. From appendix (A), the compensation bandwidth is limited to $1/4\tau$, where τ is time delay introduced by the fiber. Moreover, residual phase noise remains after appling the compensation scheme. It can be described from Appendix (A) by:

$$S_{remote}(\omega) = \frac{\tau^2\omega^2}{3} S_{fiber}(\omega) \tag{2.13}$$

2.3.4 Chromatic Dispersion (CD)

Chromatic dispersion (CD) describes the dependence of group velocity on the wavelength. In frequency transmission systems, each wavelength component of a transmitted signal travels at slightly different speed. The chromatic dispersion coefficient $D(\lambda)$, which is used to describe the effect is defined as [44]:

$$D(\lambda) = S_o(\lambda - \lambda_o) = \frac{\tau_{CD}}{L\ d\lambda} \tag{2.14}$$

where S_o is the slope at the zero dispersion wavelength λ_o, L is the fiber length and τ_{CD} is differential group delay due to CD and is equivalent to the velocity difference of the propagating wavelengths.

The phase shift between two propagating modes with different speeds can be expressed as

$$d\phi_{CD}(t) = 2\pi\nu\ d\tau_{CD}$$

Changing the fiber refractive index, changes the CD time delay by $d\tau_{CD}$ and at the same time the overall fiber delay time by $d\tau$ such that

$$\frac{d\tau}{\tau} = \frac{d\tau_{CD}}{\tau_{CD}}$$

Since the phase fluctuations in $d\tau$ is the one way fiber phase noise S_{fiber}, the spectral density of the CD induced phase noise can be described by:

$$S_{CD}(f) = (\tau_{CD}/\tau)^2 S_{fiber}(f) \tag{2.15}$$

From equations (2.15, 2.13), the CD contribution to the phase noise exceeds the one-way unsuppressed fiber phase noise at Fourier frequencies

$$f < \frac{\sqrt{3}\tau_{CD}}{2\pi\ \tau^2} \tag{2.16}$$

From the SMF-28 fiber datasheet one finds $S_o \leq 0.092$ ps/(nm^{2}km) and $\lambda_o \approx$ 1312 nm. The dispersion coefficient for a laser with a wavelength of $\lambda = 1542$ nm is $D(\lambda)$=21.1 ps/(nm.km). The linewidth of the free-running laser is about 5 kHz, therefore the time delay τ_{CD} between two wavelengths spaced by 5 kHz can be calculated for L=146 km from eq.(2.14) to be $\tau_{CD} = 1 \times 10^{-4}$ ps. Since $\tau = 0.7$ ms for the same fiber, then the CD contribution exceeds the unsuppressed fiber phase noise at frequencies $f < 5 \times 10^{-11}$ Hz (a period over thousand years). This effect will no longer be considered in this work.

2.3.5 Polarization Mode Dispersion(PMD)

Mechanical stress, bending and non-circularity cause a refractive index change between the two orthogonal axes of a single mode fiber (birefrengance). The fiber axis with lower refractive index is called the *fast axis* while the axis with higher refractive index is called the *slow axis*. When light enters this fiber, it decomposes into two orthogonally propagating modes with different speeds, leading to what is called polarization mode dispersion (PMD). The time difference between the two polarization modes is called the differential group delay τ_{DGD}. Since the slow and the fast axis are different for different sections of the fiber and vary randomly in time, the time delay caused by the PMD cannot be calculated analytically, but is only predicted by statistical methods [44]. The time delay changes (jitter) caused by PMD lead to phase noise of the transfered frequency, as reported by [25]. A

full treatment of the PMD effect is complicated due to the statistical nature of the PMD. However, an estimate for the magnitude of PMD induced phase noise has been derived in [24]. If polarized light propagates in a single mode optical fiber, the phase change caused by the PMD effect can be described in terms of the differential group delay τ_{DGD} by:

$$\Delta\phi_{PMD} = 2\pi\nu\ \tau_{DGD} \tag{2.17}$$

Changing the fiber length by contraction and expansion changes the differential group delay by $d\tau_{DGD}$ and at the same time the overall fiber delay by $d\tau$ such that

$$\frac{d\tau}{\tau} = \frac{d\tau_{DGD}}{\tau_{DGD}} \tag{2.18}$$

From (2.17, 2.18), the spectral density for the PMD induced phase noise is described by:

$$S_{PMD}(f) = (\tau_{DGD}/\tau)^2 S_{fiber}(f) \tag{2.19}$$

From equations (2.19, 2.13), the PMD contribution to the total phase noise exceeds the one-way unsuppressed fiber phase noise at Fourier frequencies:

$$f < \frac{\sqrt{3}\tau_{DGD}}{2\pi\ \tau^2} \tag{2.20}$$

According to the SMF-28 fiber datasheet the PMD coefficient is 0.1 ps/$\sqrt{\text{km}}$. For L=146 km, $\tau_{PMD} = 14.6$ ps and $\tau = 0.7$ ms, the PMD contribution exceeds the unsuppressed fiber phase noise at frequencies $f < 8 \times 10^{-6}$ Hz (a period over 100 hour), which is considered to be negligible.

In the compensation interferometer a Faraday mirror (FM) is used to reflect light from the remote end to the local end, see section (3.5). The FM rotates the reflected polarization by exactly 90^o. This causes an asymmetry between the local and remote end, since the time the light takes in the forward is not like that of the return direction. Environmental changes on the fiber can cause different effects on each direction. To calculate the frequency instability caused by the maximum effect, the forward light is considered to propagate in the fast axis and the return light propagates in the slow axis. The frequency instabilities caused by this effect can be described by:

$$d\nu_{DGD}/d\nu = \tau_{DGD}/\tau \tag{2.21}$$

Therefore, the instability due to PMD can be calculated using (2.21):

$$d\nu_{DGD}/\nu_o = (d\nu/\nu_o)(\tau_{DGD}/\tau)$$

For the case of 146 km fiber ($\tau_{DGD} = 14.6$ ps and $\tau = 0.7$ ms), the fiber induced instability is measured in chapter (5) to be 2×10^{-15}. Therefore, the PMD induced relative frequency instabilities is 4×10^{-23}, which is totally negligible and does not effect the frequency transfer.

In this chapter, the frequency standards used in this work are listed. The basics of a femtosecond frequency comb is illustrated. The ability to use a frequency comb as a transfer oscillator to compare frequency standards is discussed. Finally, the properties of optical fibers, which limit the transfer of stable optical frequencies are described.

Chapter 3

Phase noise measurement and compensation

The phase of an ideal oscillator $E_o cos(\omega_o t + \phi_o)$ can be predicted at any time from the initial conditions (E_o, ω_o, ϕ_o). However, for real oscillators the amplitude and the phase are effected by "noise" causing a fluctuation of the amplitude or the phase of the oscillator. Thus, the amplitude or the phase of a real oscillator can be predicted only with an uncertainty. In order to describe this uncertainty, the concept of amplitude or phase modulation is widely used. It considers small variations $(\Delta\phi, \Delta E)$ of the carrier wave. While amplitude noise decreases the signal to noise ratio of the carrier, phase noise decreases the frequency stability of the oscillator. In this chapter the phase noise is discussed. Discussion of amplitude noise is given in the next chapter.

In general, the measurement of phase noise requires an oscillator with superior performance. Phase noise can be measured and analyzed in the frequency or in the time domain. In the time domain, frequency counters are widely used to measure frequency fluctuations. In the frequency domain, phase demodulation techniques are used to obtain the phase noise spectral density of the phase fluctuation.

Disturbances occur at different Fourier frequencies. For example, acoustic perturbations occur around 1 kHz, while thermal fluctuations occur at the sub-Herz range. For Fourier frequencies above 1 Hz, spectrum analyzers or phase detectors are used, while for frequencies below 1 Hz, frequency counters are more convenient to use.

In this chapter, the techniques to measure phase noise in the time and frequency domains are described. An interferometer to measure and compensate the phase noise introduced by optical fibers is constructed. The performance of this interferometer is studied.

3.1 Phase noise sources

A polynomial model is used to represent the five most common types of noise effecting an oscillator [50]. The power spectral density of the phase fluctuations is given by:

$$S_\phi(f) = \sum_{a=-4}^{0} \nu_o^2 h_\alpha f^\alpha \tag{3.1}$$

where ν_o is the frequency of the oscillator, h_α is phase noise spectral density at 1 Hz.

The five noise types (phase (PM) or frequency (FM) noise) that effect the frequency stability of an oscillator are:

1. Random walk FM $(1/f^4)$ usually relates to the oscillator's physical environment, such as, mechanical shock, vibration, temperature, or other environmental effects may be causing "random" shifts in the carrier frequency. Random walk noise is difficult to measure since it is usually very close to the carrier.

2. Flicker FM $(1/f^3)$ is due to environmental perturbations that effect the resonance conditions. It is observed in quartz crystal oscillator, hydrogen masers, Cs clock as well as fiber lasers with Gaussian line profile.

3. White FM $(1/f^2)$ is common in actively controlled oscillators. It is observed in semiconductor laser with Lorentzian line profile, in lasers stabilized to cavities or in a quartz oscillator locked to high quality filter device.

4. Flicker PM $(1/f^1)$ is usually added by noisy control electronics, specially amplifiers. It can be reduced with good low-noise amplifier design.

5. White PM $(1/f^0)$ is broadband phase noise. It is produced from the amplification stages. It is also observed in phase compensated optical fiber links, as will be demonstrated later in this work.

In fig. (3.1), the phase noise spectral density (S_ϕ) is plotted against the Fourier frequency (f). It illustrates the different slops for the five different types of noise.

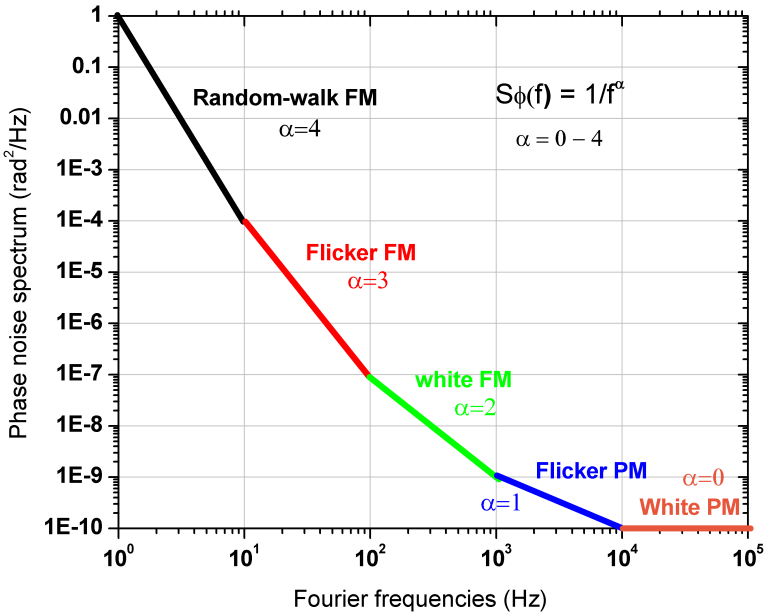

Figure 3.1: Phase noise slope for different noise types.

There are many other types of noise which cannot be described by this polynomial. For example the narrow band noise present at frequencies of 50 Hz and its harmonics, resulting from the AC line source. Many oscillations appear also if the oscillating device is sensitive to acoustic vibrations. This process is usually described by a single frequency modulation of the frequency of an ideal oscillator. Usually, the stability of an oscillator is not much effected by such narrow band small amplitude noise processes since the stability is calculated from the integral of the phase noise spectral density.

3.2 Frequency domain measurement

Phase noise describes random fluctuations of the phase of an ideal oscillator. The ideal oscillator is described in frequency domain by Dirac-delta function $\delta(\omega - \omega_o)$. The random phase noise can be treated as a phase modulation on the ideal oscillator. In this section, two methods are given to measure the amplitude of the phase noise. In the rf domain, phase noise can be obtained from the power of the sidebands relative to the power of the carrier, or in the baseband from the demodulation of

the phase noise using phase detector and reference oscillator. The phase noise is described by the phase noise spectral density ($S_\phi(f)$), which is a measure of the phase noise power at each Fourier frequency in the base band.

3.2.1 Power spectral density of phase fluctuations

Phase noise can be described, from equation (B.5) in appendix (B), as the ratio between the sideband and the carrier if phase deviations are so small that ($\Delta\phi_{rms}$ <<1 rad) is satisfied. Then

$$(\Delta\phi_{rms})^2 = \frac{2}{\sqrt{2}}\frac{E_{SB}^2}{E_c^2}$$

where E_c, E_{SB} are the amplitudes of carrier and sideband.

The power spectral density, in units of W^2/Hz, can be used to obtain the phase noise spectral density, in units of rad^2/Hz. This is done by applying the autocorrelation function to equation (B.5) and then using the Wiener-Khintchin theorem to get the phase noise spectral density (PNSD). This procedure is equivalent to squaring eq. (B.5).

$$S_\phi(f) = \frac{2P_{SB}(f)}{BW \times P_c}(\text{rad}^2/\text{Hz})$$

$$S_\phi(f) = 10log(P_{SB}(f)) - 10log(P_c) - 10log(BW) + 3\text{dB} \tag{3.2}$$

Where BW is the measurement bandwidth. A radio frequency spectrum analyzer (RFSA) is used to measure the power spectral density, in units of W^2/Hz. The RFSA's local oscillator is swept across the spectrum, so that a narrow band filter can acquire the power content of each individual frequency in the span. The phase noise spectral density is then obtained using the relation (3.2). Note that, the RFSA measures what is called the double-sideband spectral density ($L(f)$) at the positive and negative sides of the frequency spectrum. However, $S_\phi(f)$ is reported only for positive Fourier frequencies. Since both sides of the spectrum are equal, $L(f)$ has to be multiplied by two (+ 3 dB) to obtain S_ϕ.

The PNSD is normalized to a bandwidth of 1 Hz, by dividing the spectral density by the used filter BW. Figure (3.2) illustrates the spectrum of a carrier frequency in the presence of noise.

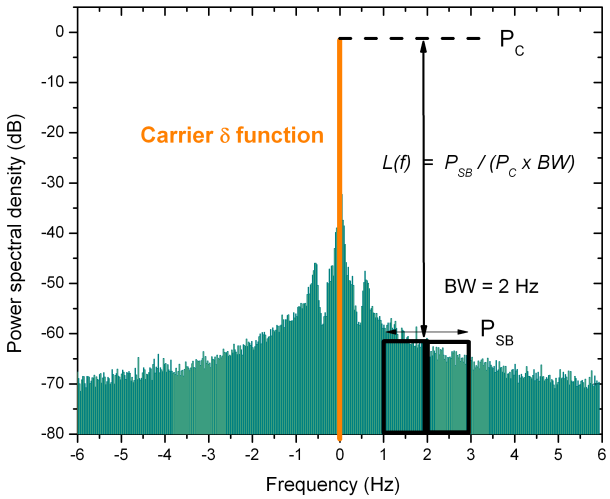

Figure 3.2: The spectrum of a carrier frequency in the presence of noise

Care should be taken that the carrier power does not saturate the detector. This check is made by changing the laser power and notice the change in the detected RF power. The RF power should increase linearly with laser power outside the saturation region.

The disadvantage of using this measuring technique is, that it is not possible to determine whether the spectrum at different Fourier frequencies results from amplitude fluctuations $\Delta E(t)$ or from phase fluctuations $\Delta\phi(t)$.

3.2.2 Phase demodulation

Phase demodulation is used to measure phase fluctuations without the effect of amplitude fluctuations. The phase noise of an oscillator can be measured by comparing the phase of the oscillator with a reference oscillator with superior performance. By holding the two oscillators at quadrature, it is possible to convert small phase variations into voltage variations using a double balanced mixer. By the detection at phase quadrature, the sensitivity to phase noise becomes maximum while the sensitivity to amplitude noise becomes minimum.

when phase fluctuations are larger than π, a mixer is not applicable. In the case of $(\Delta\phi > \pi)$, digital phase detectors are used instead. They are usually combined with a prescaler to divide the phase fluctuations by N. Note that, the original

phase fluctuations are reduced by (N^2). This allows the detection of large phase fluctuations $\Delta\phi > \pi$, and extendes the frequency capture range of the digital phase locked loop. They are also less sensitive to amplitude fluctuations than the analog phase detectors. However, they require high signal to noise ratio and are intrinsically noisier than standard rf mixers.

The power spectral density of phase fluctuations can be obtained from

$$S_\phi(f) = \frac{|\Delta\phi_{rms}(f)|^2}{BW} = \frac{N^2 \Delta V_{rms}^2(f)\ (\text{Volt})^2}{K^2\ (\text{Volt/rad})^2} \frac{1}{BW} \tag{3.3}$$

where N is the division ratio for digital phase detectors, K (Volt/rad) is the phase detector sensitivity coefficient. This conversion is only valid for phase fluctuations $\Delta\phi << \pi$.

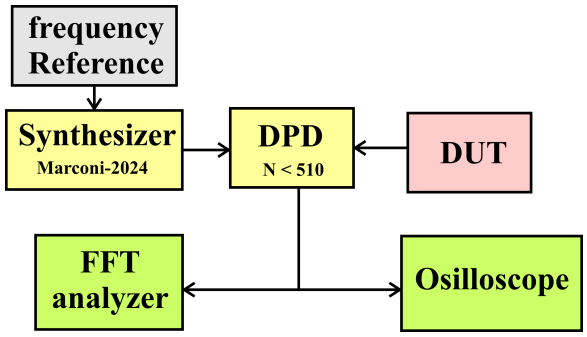

Figure 3.3: Phase noise measurement system; DUT: device under test, DPD: digital phase detector, FFT analyzer: fast Fourier transform analyzer.

In order to obtain the sensitivity coefficient (K) of the digital phase detector used in this work, the device under test in fig. (3.3) is replaced by another synthesizer (Synth2). Synth2 is phase modulated with known modulation amplitude. This modulation is demodulated with the above system and measured using an fast Fourier transform analyzer (FFT) or an oscilloscope. For example, if Synth2 is phase modulated with a modulation amplitude of 0.1 rad and modulation frequency of 1 kHz, a signal with a voltage of 2.4 mV is measured at 1 kHz with the FFT spectrum analyzer. From equation (3.3) the sensitivity coefficient of the phase detector is K= 24 mV/rad. To measure the linearity of the phase detector, the phase of one of the synthesizers is swept from $(\pi/2)$ to $(-\pi/2)$, while the corresponding voltage at the output of the digital phase detector is measured with an oscilloscope.

The phase detector is found to be linear over a range of about π rad, see fig. (3.4). The sensitivity coefficient can be obtained also from the slope of the curve in fig. (3.4). However, for the digital phase detector used here, K has to be divided by 2 due to the detection mechanism, since it counts at both the rising and the falling edges. The sensitivity coefficient is found consistent with the above measurement (K = 48/2 mV/rad= 24 mV/rad).

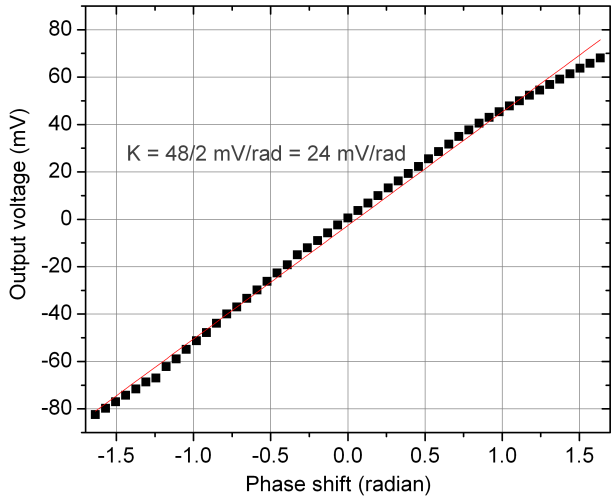

Figure 3.4: The linearity of the digital phase detector used in this work to analyze phase noise in the baseband.

3.3 Time domain measurement

Since the phase of the measured oscillator requires to be in quadrature (90^o) with the reference oscillator, slowly locking the reference oscillator to maintain quadrature is required. However, it is more convenient to analyze the oscillator's long term behavior by measuring its frequency in the time domain using a frequency counter. From equation (B.1) in appendix (B), the instantaneous frequency is then given by:

$$\nu(t) = \nu_o + \frac{1}{2\pi}\frac{d\phi(t)}{dt}$$

where $\phi(t)$ is the phase value at time t. For the comparison of frequency standards operating at different carrier frequencies ν_o, it is useful to define the normalized frequency deviations

$$y(t) = \frac{\nu(t) - \nu_o}{\nu_o} = \frac{1}{2\pi\nu_o}\frac{d\phi(t)}{dt}$$

The measurement of $y(t)$ is performed using frequency counters. As a result, the continuous function $y(t)$ is reduced to a discrete series of consecutive measurements averaged over the measurement time τ. In general, the averaging process depends on the used frequency counter. In the following section, two types of frequency counters (Π-type and Λ-type) are discussed. The Λ-type frequency counter offers higher resolution than the Π-type frequency counter, because the Λ-type frequency counter averages multiple highly overlapped measurements, which reduces the contribution of white phase noise.

3.3.1 Π-type frequency counters

The Π-type frequency counter estimates the frequency of a signal by counting all periods (N) occurring during a time interval τ, see fig. (3.5). Then, it takes the average over this time interval to estimate the measured frequency as:

$$\langle\nu\rangle = \overline{\nu} = N/\tau$$

where $\langle\nu\rangle$, $\overline{\nu}$ is the expectation and the average values of a frequency ν.

The expectation value of the measured frequency can be written using the weight function w_Π as:

$$\langle\nu\rangle \;=\; \int_{-\infty}^{+\infty} \nu(t)\; w_\Pi(t)\; dt \tag{3.4}$$

where

$$w_\Pi(t) = \begin{cases} 1/\tau, & 0 < t < \tau \qquad\qquad \Pi \text{ estimator} \\ 0, & \text{elsewhere} \end{cases}$$

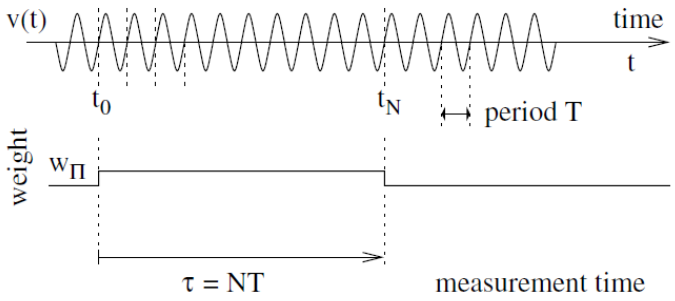

Figure 3.5: Rectangular averaging mechanism in FXM frequency counters

In this work, a multi-channel synchronous digital phase recorder, called "FXM", is used as a Π-type frequency counter. The FXM uses strobe pulses to periodically transfer the contents of the counters to the computer, without interrupting the counting process and without resetting the counters [51]. It counts frequencies from $5MHz$ to $50MHz$ with resolution of 0.001 period (0.1 ns at 10 MHz).

3.3.2 Λ-type frequency counters

In contrast to the "Π"-type frequency counter, a "Λ"-type frequency counter performs an additional averaging process over n series of frequency measurements. Each of this measurements is similar to the one obtained by the "Π"-type frequency counter, but shifted by a time $\tau_o = DT$ from the previous measurement, see fig. (3.6). The estimated value of the frequency can be written as [52]:

$$\langle \nu \rangle = \frac{1}{n} \sum_{i=0}^{n-1} \overline{\nu_i}$$

The expectation value of the measured frequency can be written using the triangle weight function w_Λ as:

$$\langle \nu \rangle = \int_{-\infty}^{+\infty} \nu(t) w_\Lambda(t) dt \tag{3.5}$$

where

$$w_\Lambda(t) = \begin{cases} t/\tau, & 0 < t < \tau \\ 2 - t/\tau, & \tau < t < 2\tau \\ 0, & \text{elsewhere} \end{cases} \qquad \Lambda \text{ estimator}$$

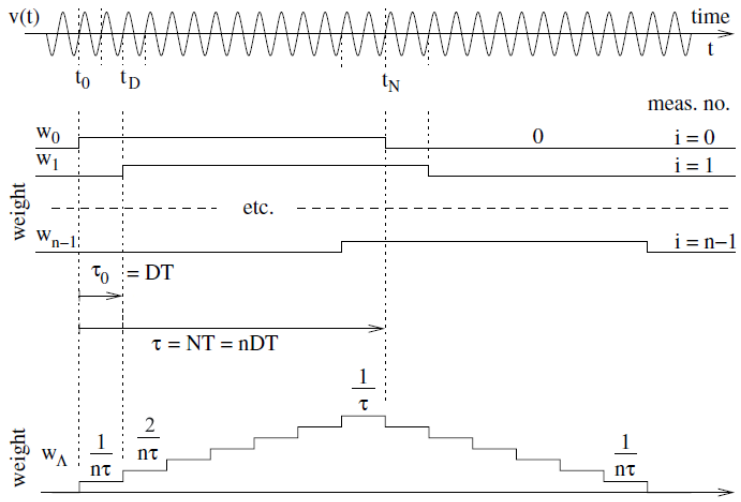

Figure 3.6: Triangular averaging mechanism, implemented in a FXE phase-averaging frequency counter.

This process of averaging acts as a low pass filter with a cut-off frequency that equals the reciprocal of the counter gate time. It is designed to further suppress the contribution of white phase noise.

In this work, a multi-channel synchronous digital phase recorder, called "FXE", is used as a Λ-type frequency counter. The FXE can be operated either as a Π counter or as a Λ counter.

3.3.3 Allan deviation (ADEV)

One of the most common statistical method to estimate the frequency stability is the two-sample Allan variance (AVAR). The AVAR is based on analyzing the fluctuations of two adjacent samples of the fractional frequency averaged over a period τ. For a sequence of measurements generated by Π counter, the AVAR algorithm gives a measure of the frequency instability. The AVAR is defined as:

$$\sigma_y^2(\tau) = \left\langle \frac{1}{2}(\overline{y}_{i+1} - \overline{y}_i)^2 \right\rangle \tag{3.6}$$

where

$$\overline{y}_i = \frac{1}{\tau}\int_{t_i}^{t_i+\tau} y(t)dt$$

The Allan variance can be described by a weighting function w_A as following, see also fig.(3.7):

$$\sigma_y^2(\tau) = \left\langle \left[\int_{-\infty}^{+\infty} y(t)w_A(t)dt\right]^2 \right\rangle \tag{3.7}$$

where

$$w_A(t) = \begin{cases} -\frac{1}{\sqrt{2}\tau}, & 0 < t < \tau \\ \frac{1}{\sqrt{2}\tau}, & \tau < t < 2\tau \\ 0, & \text{elsewhere} \end{cases}$$

Strictly, the Allan variance algorithm should only be applied to a sequence of measurements generated by Π-type frequency counters. However, when applied to a measurement generated by a Λ-type frequency counter, the calculated instability will be significantly lower and will not represent the AVAR [53].

In the following, the term Allan Deviation (ADEV), which is the square root of the AVAR, will be used as a measure of the frequency instability.

3.3.4 Modified Allan deviation (ModADEV)

Another type of variance commonly used is the the modified Allan variance (ModAVAR). The ModAVAR is less sensitive to white phase noise than the AVAR. thus, it offers a better estimate for the frequency stability of an oscillator. Moreover, it is also useful of distinguishing white from flicker phase noise, as will be discussed later in this section.

The ModAVAR is estimated from a set of n frequency measurements for each averaging time $\tau = n\tau_0$, where τ_0 is the basic measurement interval. The ModAVAR defined as:

$$\text{mod } \sigma_y^2(\tau) = \left\langle \frac{1}{2} \left[\frac{1}{n} \sum_{i=0}^{n-1} \frac{1}{\tau} \left(\int_{(i+n)\tau_0}^{(i+2n)\tau_0} y(t)dt - \int_{i\tau_0}^{(i+n)\tau_0} y(t)dt \right) \right]^2 \right\rangle \tag{3.8}$$

The ModAVAR can be described by a weighting function ω_M as following, see also fig.(3.7):

$$\text{mod } \sigma_y^2(\tau) = \left\langle \left[\int_{-\infty}^{+\infty} y(t) w_M(t) dt \right]^2 \right\rangle \tag{3.9}$$

where

$$w_M(t) = \begin{cases} -\frac{1}{\sqrt{2\tau^2}} t, & 0 < t < \tau \\ \frac{1}{\sqrt{2\tau^2}} (2t + 3), & \tau < t < 2\tau \\ -\frac{1}{\sqrt{2\tau^2}} (t - 3), & 2\tau < t < 3\tau \\ 0, & \text{elsewhere} \end{cases}$$

The weighting functions of the AVAR and the ModAVAR are shown in fig. (3.7). Note that, because of the averaging process of the ModAVAR the weighting function is to some extent similar to that of the Λ-type frequency counters but it is not identical.

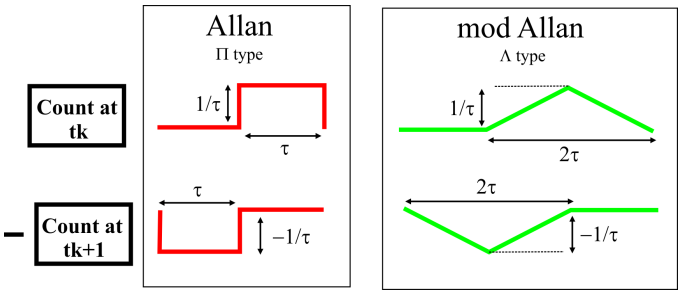

Figure 3.7: (left) AVAR Π type, (right) modAVAR Λ type weighting functions.

Note from equation (3.8) that, for $n = 1$, the ModAVAR and AVAR are identical. This means that the result will be the same for the first measured point, which corresponds to the gate time of the Π frequency counters. Therefore, by using a Π type frequency counter (FXM) to obtain the ModAVAR from eq. (3.8), the counter gate time τ_0 should be as low as possible. This allows to calculate the ModAVAR for averaging times (τ) larger than the gate time (τ_0).

The ModAVAR can be obtained from the Λ frequency counters (FXE-phase average mode), by making measurements with different gate times and then applying the normal Allan variance (AVAR) equation (3.6) for each gate time [52].

Fig. (3.8), shows a measurement of a stabilized beat signal using a Π-counter when processed according to ADEV (red squares) or ModADEV (blue circles). While it is not clear from the ADEV calculations whether the dominating noise is white phase noise or a flicker phase noise (both should follow $1/\tau$). The ModADEV classifies the noise type as a white phase noise, since the slope follows $1/\tau^{3/2}$. The instability calculated by the ModADEV is lower than that of the ADEV due to the filtering effect caused by the averaging process of the ModADEV. This is to some extent similar (but not identical) to the filtering of the Λ-type frequency counters discussed in subsection (3.3.2).

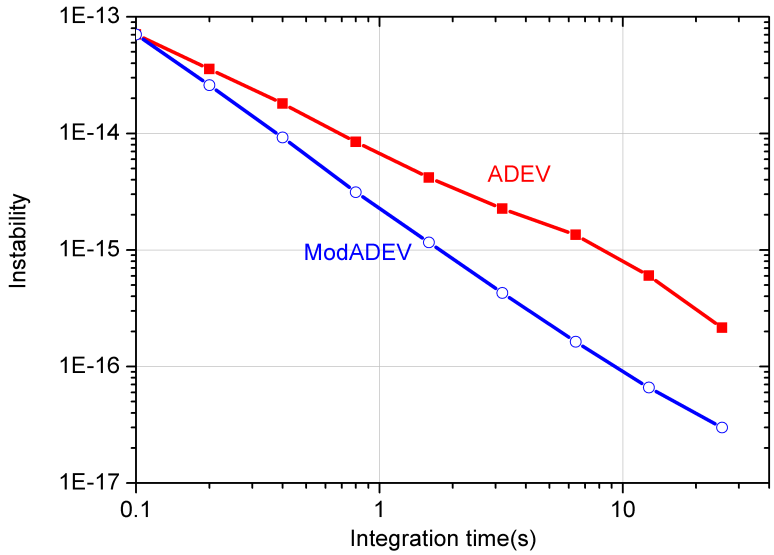

Figure 3.8: A stabilized beat signal; measured with a Π-counter when processed as ADEV (red squares) or ModADEV (blue circles).

3.4 Relation between S_ϕ and ADEV

In the previous sections, the description of the instability in the frequency and time domains are given. It is now important to relate both measurements in order to compare and validate the results. It helps also to identify the noise process from the time domain measurements only. For the five noise types, the Allan deviation can

Type of noise	$S_\phi(f)$	$(ADEV)^2$	$(ModADEV)^2$
Random walk	$\nu_o^2 h_{-4} f^{-4}$	$(\frac{2}{3}\pi^2 h_{-4})\tau$	same as $(ADEV)^2$
Flicker frequency	$\nu_o^2 h_{-3} f^{-3}$	$2ln(2)h_{-3}$	same as $(ADEV)^2$
White frequency	$\nu_o^2 h_{-2} f^{-2}$	$\frac{1}{2}h_{-2}\tau^{-1}$	same as $(ADEV)^2$
Flicker phase	$\nu_o^2 h_{-1} f^{-1}$	$h_1[1.038 + 3ln(2\pi f_h \tau)]\tau^{-2}/(4\pi^2)$	same as $(ADEV)^2$
White phase	$\nu_o^2 h_0 f^0$	$3h_0 f_h \tau^{-2}/(4\pi^2)$	$3h_0 f_h \tau^{-3}/(4\pi^2)$

Table 3.1: Illustration of the slope of the ADEV for different noise types (f^α).

be obtained from the phase noise spectral density by substituting equation (3.1) in the following equation (3.10) for each noise type:

$$\sigma_y^2(\tau) = 2\int_0^\infty S_\phi(f)\frac{sin^4(\pi\tau f)}{(\pi\tau f)^2} \tag{3.10}$$

The Allan deviation for each noise type is summarized in table (3.1) , see also fig. (3.9):

where h is the phase noise density at 1 Hz for each noise type, and f_h is the stop frequency.

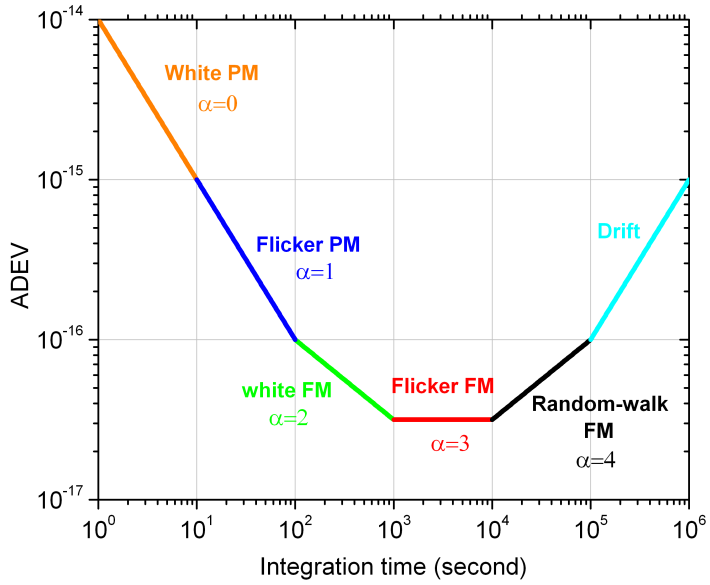

Figure 3.9: Illustration of the slope of the ADEV for different noise types (f^α)

Fig. (3.9), illustrate the slope of the ADEV for the five noise types. It also shows the ADEV slope for a drifting oscillator, which is proportional to τ.

3.5 Interferometer for phase noise compensation

The phase and hence the frequency of light propagating through a fiber is influenced by acoustic and thermal perturbations along the fiber, as discussed in section (2.3). In order to detect and compensate these phase changes, an interferometric approach is used. In this section, we explain the design of such interferometer in details. To study the compensation performance of the compensation interferometer, a second independent interferometer that measures the phase stability at the remote end is used.

3.5.1 Interferometer Design

In order to measure and compensate phase fluctuations of an optical fiber (M-fiber), an interferometer is constructed as shown in fig. (3.10). This setup is similar to a scheme described by Ma et al. [16], however, it is based on commercial fiber components. A beam splitter (BS1) couples light into a reference arm and a measurement arm. In the measurement arm, the light is transfered through the fiber (M-fiber) to a beam splitter (BS3) at the remote end. BS3 sends light to a Faraday mirror (FM) that reflects the light back towards the input of the fiber (local end). A circulator (OC) is used to redirect the backreflected light to interfere with the light from the reference arm on the photodetector PD1. At the input and the remote end of the fiber acousto-optic modulators are installed. The acousto-optic modulator (AOM1) at the local end is used for phase noise compensation, while AOM2 at the remote end is used to discriminate the desired reflection by the Faraday mirror from backscattered light within the fiber and reflections from the connectors or the splices. Moreover, it allows heterodyne detection of the phase noise at a convenient rf frequency. The FM at the remote end rotates any state of polarization (SOP) of the incoming light by 90 degrees, such that any polarization component traveling in the fast fiber axis in the forward direction returns in the slow axis. Consequently, SOP fluctuations that occur anywhere along the fiber are to a large extent compensated in the reflected light by this fully passive technique [54], and a beat signal with a stable amplitude is obtained.

The signal from PD1 is further processed using a tracking oscillator (TOS) and a phase/frequency comparator (DPFC). The phase of the TOS is compared with that of a fixed reference frequency using the DPFC. The DFPC generates an error

signal that shifts the frequency of AOM1 to compensate for any phase or frequency fluctuations in the measurement arm.

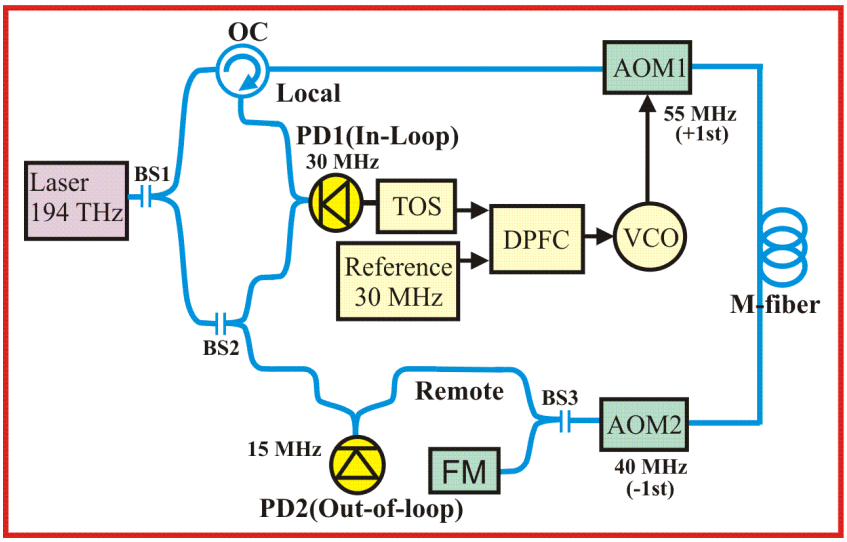

Figure 3.10: Setup for active fiber noise compensation. OC: optical circulator, AOM: acousto-optical modulator, VCO: voltage controlled oscillator, DPFC: digital phase-frequency comparator, TOS: tracking oscillator, PD1: in-loop photodetector, PD2: out-of-loop photodetector, FM: Faraday mirror, and M-fiber:measured fiber.

In our case, the in-loop beat is detected at 30 MHz since AOM1 shifts the light with 2×(+55) MHz and AOM2 shifts the light 2×(-40) MHz, for the forward and the return directions. A voltage controlled oscillator at 30 MHz is used here as a narrowband tracking filter and amplitude stabilizer. A digital phase-frequency comparator (DPFC) is used to compare the phase of the tracked in-loop beat with a reference frequency (derived from the hydrogen maser (H5)). A predivider with division up to $N = 512$ is installed in the first stage of the DPFC. The error signal produced from the DPFC is used to control the frequency shift of AOM1 using a voltage control oscillator (VCO).

The in-loop interferometer is similar to Michelson interferometer since the reference light interferes with the round-trip light from the measurement fiber. The in-loop beat holds twice the phase noise introduced by the measurement fiber due to the round-trip in the fiber.

In order to check the performance of the phase compensation system, a second interferometer at the remote end generates an out-of-loop signal by heterodyning

with a reference light on another photodetector (PD2) to obtain the out-of-loop beat. The out-of-loop beat is used to characterize the stability and the accuracy of the transmitted frequency at the user end. The out-of-loop interferometer is similar to a Mach-Zehnder interferometer since the the light passes the measurement fiber only once before it interferes with the reference light.

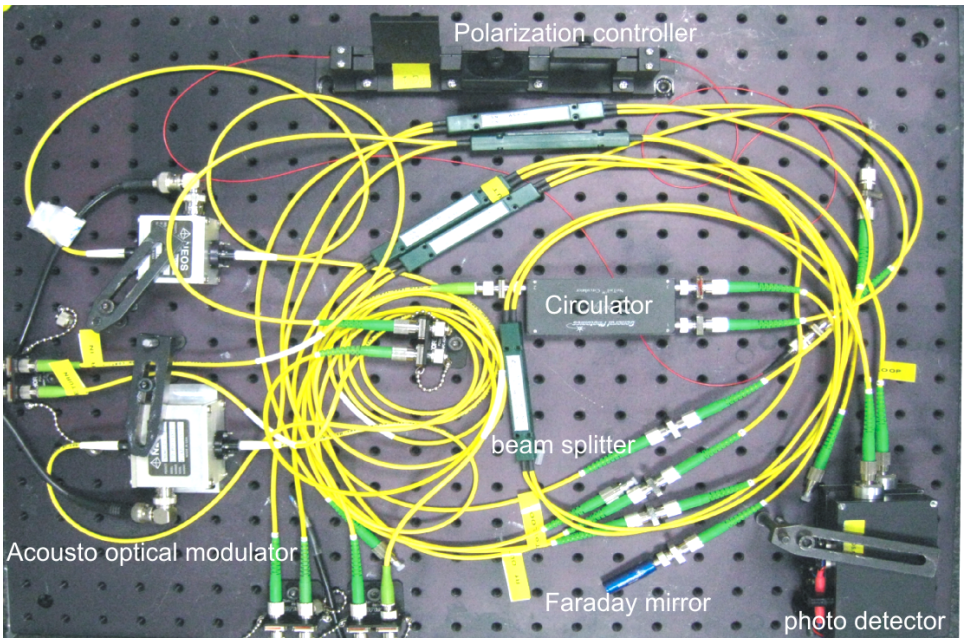

Figure 3.11: All-in-fiber interferometer used to detect and compensate phase noise

We used all-in-fiber components such as AOMs, beam splitters, circulator, polarization controller, Faraday mirror, and photodetectors to construct the interferometer. The all-in-fiber system is shown in fig. (3.11). Although fiber components are cheap and easy to use and connect, care must be taken while designing an interferometer since it is very sensitive to acoustic and thermal perturbations. The length of the reference arm should be designed as short as possible. The distance light travels to the local end should be exactly twice that of the remote end, otherwise additional noise appears because of the extra uncompensated parts. The interferometer is covered with a box to avoid air flow in the room and to minimize acoustic perturbations.

3.5.2 Interferometer transfer function

In this section, the transfer function of the DPFC is derived which helps to optimize the system performance. From appendix (A), the transfer function of the

compensation system can be represented by the following figure:

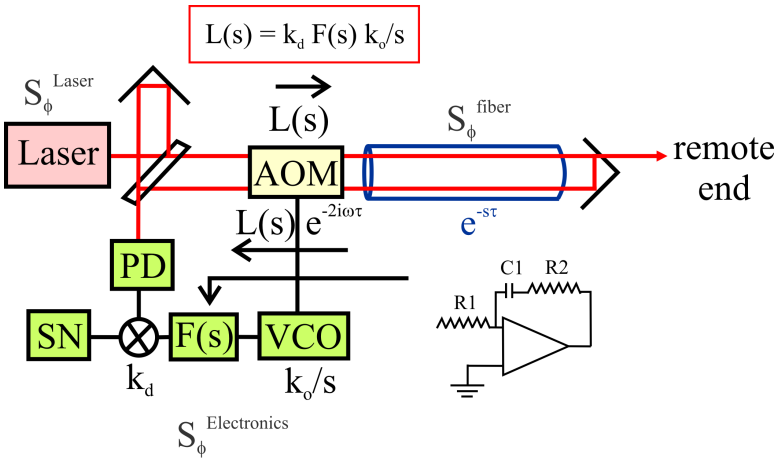

Figure 3.12: Phase noise compensation system transfer function and noise sources.

From fig. (3.12), the open loop transfer function ($G(s)$) for the round-trip light can be described by:

$$G(s) = \frac{k_o}{s}\frac{k_d F(s)(1+e^{-2s\tau})}{N}$$

Where k_d is the phase detector gain factor (in V/rad), k_o is the voltage controlled oscillator gain factor (in rad/V), N is the divider ratio, τ the time needed to propagate the one-way fiber, $F(s)$ is the transfer function of the proportional integrator, which can be described by [55], $F(s) = (1+s\tau_2)/s\tau_1$, where $\tau_1 = R_1C$, $\tau_2 = R_2C$ are the time constants of the regulator.

The magnitude and the phase of the gain are expressed as:

$$A(\omega) = 20log\,|G(s)| = 20log\sqrt{\Re(G^2(\omega)) + \Im(G^2(\omega))} \quad \text{Magnitude (dB)}$$

$$\phi(\omega) = tan^{-1}(\frac{\Im(G(\omega))}{\Re(G(\omega))}) \qquad \text{Phase (rad)}$$

As an example, we simulate the 146 km link used in frequency transmission between PTB and IQ (see chapter (5)). We used resistors $R_1, R_2 = 10$ kΩ and capacitor $C = 100$ nF for the regulator, while the one-way time delay in fiber is $\tau = nL/c = 0.7$ ms. The gain factors for VCO and phase detector are adjusted to be k_d=1 V/rad and k_o=150 kHz/V. A bode-plot for magnitude and phase of the 146 km phase noise compensation system is shown in figs. (3.13, 3.14). Both figures show a Mathcad simulation for the open-loop (red-solid line), closed-loop (blue-dashed line), and error (green-dashed line) transfer functions.

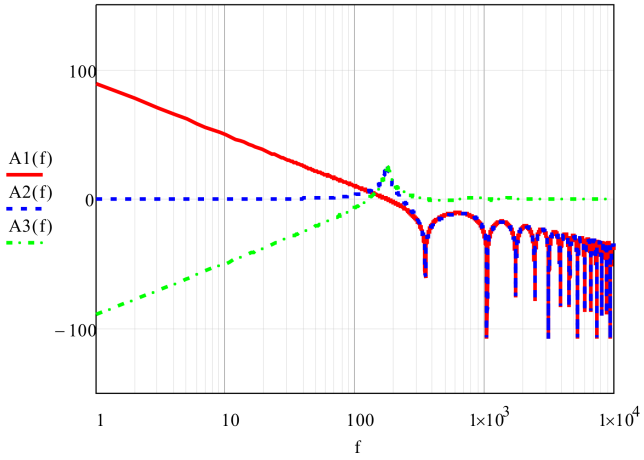

Figure 3.13: Magnitude of the open-loop (red-solid), closed loop (dashed-blue), error (dashed-green) transfer functions for the frequency transmission system over 146 km.

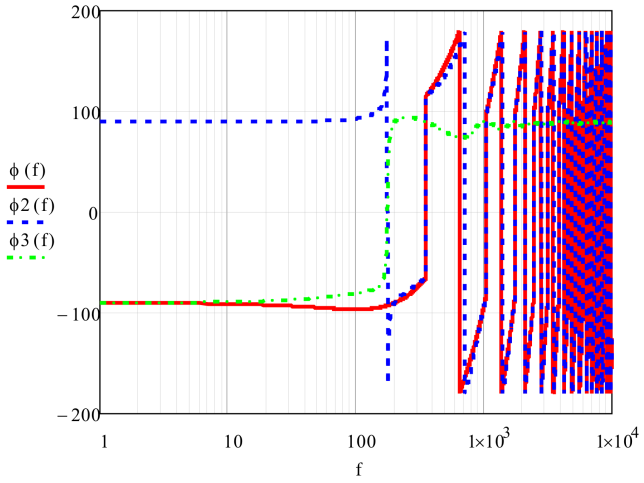

Figure 3.14: Phase of the open-loop (red-solid), closed loop (dashed-blue), error (dashed-green) transfer functions for the frequency transmission system over 146 km.

The gain factors and integrator time constants are chosen to maintain stable operation. With higher gain factors, a better compensation for lower frequencies will be obtained. However, the noise at the unity gain frequency will increase. This leads to a decrease of the stability, since it is obtained from integration of the overall noise spectrum. By further increasing the gain, oscillations may occur. These oscillations prevent the compensation scheme from working properly, because they change the sign of the compensation signal. The integrator time constant is chosen to be larger than the time delay in the fiber τ to prevent oscillations.

3.5.3 Interferometer phase noise

There are three phase noise contributers that should be considered during phase noise compensation. Phase noise from the laser, phase noise from the transmission fiber, and phase noise from the compensation interferometer including the electronics.

The first phase noise contributer is the phase noise from the laser through self-heterodyning. The in-loop beat results from the interference of the round-trip light with reference light. Both round-trip and reference light become uncorrelated if the round-trip time ($2\tau_{delay}$) is much longer than the coherence time of the laser. The round-trip and the reference light can be regarded as independent oscillators, which have the same phase noise. Laser light of a phase noise $S_{\phi}^{laser}(f)$ and a vacuum velocity c takes a time $\tau_{delay} = nL/c$ to propagate through a fiber of length (L) and refractive index (n), the laser phase noise contributes the in-loop beat by:

$$S_{\phi}^{SH}(f) = 4[sin(2\pi f\, nL/c)]^2 S_{\phi}^{laser}(f) \qquad [24] \qquad (3.11)$$

Assuming that the laser has a Lorentzian spectrum for simplicity, the coherence time can be approximated by $0.8/\Delta\nu$ [44], where $\Delta\nu$ is the laser linewidth. The fiber laser (NIR-PTB) used for frequency transmission has a free-running linewidth of about 5 kHz which corresponds to a coherence length of about 32 km. Therefore, using a free-running laser in frequency transmission over the long distances discussed in this work is not possible. The in-loop beat contains not only fiber induced phase noise but also a contribution from laser phase noise. As a result, the compensation scheme works improperly. After stabilizing the laser to the optical reference as described in section (2.2), it reaches a linewidth in the order of 10 Hz which corresponds to a coherence length of about 16000 km. This is totally sufficient for the distances discussed in this work. An example to the contribution of laser phase noise by self-heterodyning is given in section (5.3).

The second contributer to the phase noise is the transmission fiber induced phase noise. It is compensated with the fiber interferometer with a compensation limit determined by delay time in the fiber as discussed in appendix (A).

The third contributer to the phase noise is the compensation interferometer itself. The achieveable stability in the frequency transfer is limited by the residual noise in

the phase noise compensation interferometer at long measurement times. We have analyzed different designs of the interferometer and optimized the interferometer for compactness and minimized uncompensated fiber leads in the setup. We then measured the interferometer's noise floor when both AOMs were directly connected with a short patch cord. The frequency stability of the out-of-loop beat signal was measured for the unstabilized and stabilized interferometer. The stabilized interferometer allows us to assess the attainable noise cancellation limit without suffering from bandwidth limitation or any excess noise due to the fiber delay. Fig. (3.15) and fig. (3.16) show PNSD and ADEV for the out-of-loop and in-loop beat signals of the unstabilized and the stabilized interferometer, respectively. A calculation of the ADEV from the phase noise data [54] shows that time and frequency domain measurements agree quantitatively.

The phase noise of the free-running interferometer (black-dashed curve in fig.(3.15)) is represented by the unstabilized out-of-loop beat. It is dominated by white frequency noise of $S\phi(f) = 6 \times 10^{-5}$ $/(f^2/\mathrm{Hz}^2)$ $(\mathrm{rad}^2/\mathrm{Hz})$ up to a Fourier frequency $f = 1$ kHz, while above 10 kHz a white phase noise level of $S\phi(f) = 3 \times 10^{-11}$ $(\mathrm{rad}^2/\mathrm{Hz})$ is reached. This is found to be in good agreement with the measured ADEV of $\sigma_y(1s) \approx 2 \times 10^{-17}$ (black dots in fig. (3.16)). After 10 s, environmental perturbations start to dominate the stability of the unstabilized interferometer. It should be noted that even for the unstabilized interferometer the flicker noise floor is well below 1×10^{-17} up to an averaging time of $\tau = 10000$ s.

For the in-loop beat, the PNSD and the ADEV are shown also in the figures (3.15, 3.16), as a gray-dashed line for the unstabilized in-loop beat, and as a gray-solid line for the stabilized in-loop beat. For the free-running interferometer, the PNSD of the in-loop is about 2 dB higher than that of the out-of-loop, while the ADEV of the in-loop is about 3 dB higher than that of the out-of-loop. From Appendix (A), the difference between the round-trip and the one-way PNSD for low frequencies should be 6 dB and not only 2 dB. This discrepancy can be attributed to the very short lengths of fiber interferometer.

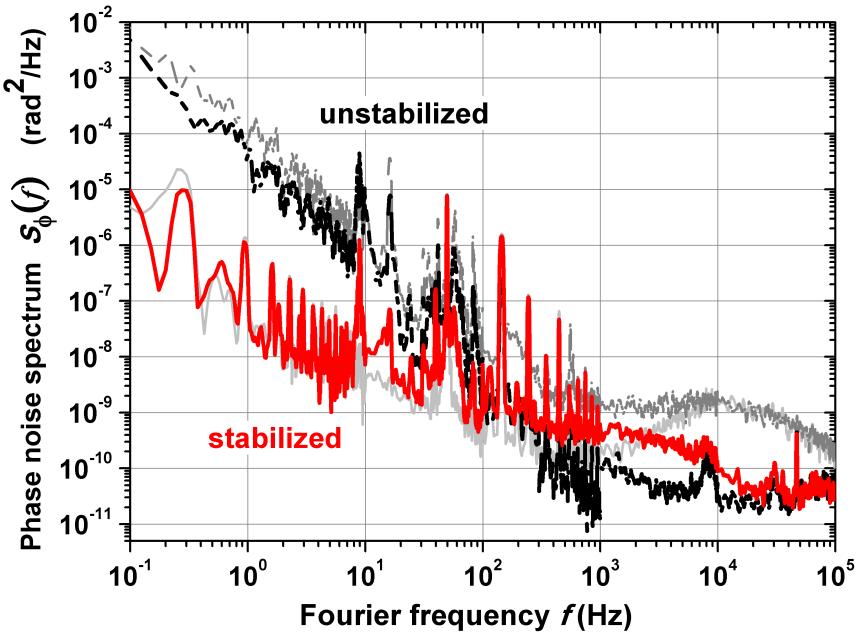

Figure 3.15: Residual noise of, Out-of-loop: black-dashed (unstabilized), red (stabilized); In-loop: gray-solid (stabilized), gray-dashed (unstabilized).

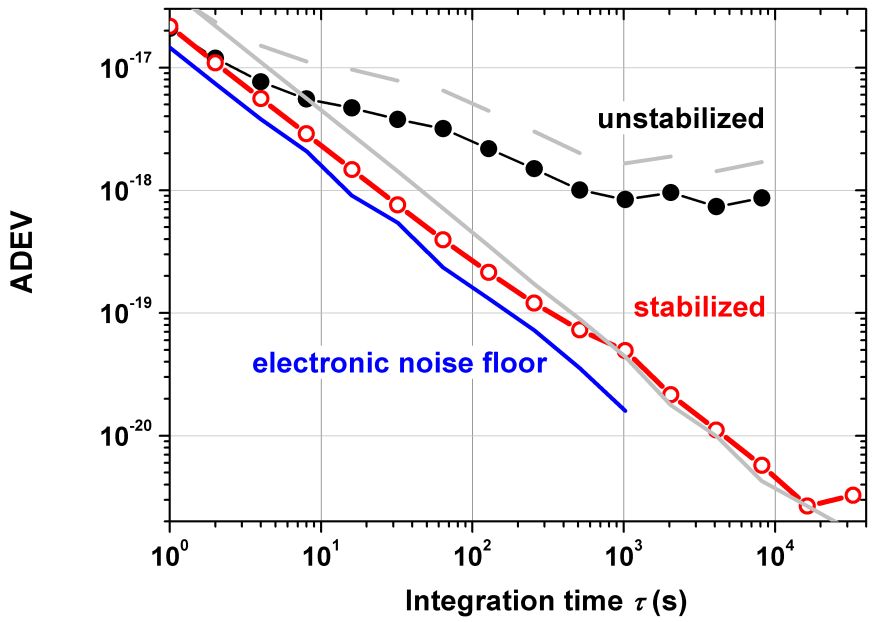

Figure 3.16: Relative frequency instability of out-of-loop signal: black-dots (unstabilized), red open-circle (stabilized); in-loop: gray-solid (stabilized), gray-dashed (unstabilized). The electronic noise is represented by the blue line.

For the stabilized interferometer, the ADEV and PNSD of the in-loop beat and the out-of-loop beats should be similar, because the interferometer is very short. However, the ADEV of the stabilized in-loop is higher than that of the out-of-loop. This is attributed to the 10 kHz bump in the in-loop beat, since the ADEV is equivalent to the integration of the PSND spectrum. The ADEV of the out-of-loop doesn't follow $1/\tau$ as that of the in-loop. This is attributed to the stability degradation of the out-of-loop beat caused by the imperfection in the interferometer symmetry.

Once the interferometer is stabilized using the DPFC with prescaler set to N = 8, fluctuations of the path length and those arising from AOMs are corrected. The phase noise is then suppressed by approx. 28 dB at 1 Hz with only a slight increase of the white phase noise level between 300 Hz and 10 kHz (red curve in fig.(3.15)). The stabilized interferometer is dominated by flicker phase noise for $f < 1$ kHz and white phase noise for $f > 10$ kHz; for this type of noise the ADEV depends on the effective bandwidth of the frequency counting system. Assuming a high frequency cut-off of 100 kHz, we calculate an instability of $\sigma_y(s) \approx 2 \times 10^{-17}/(\tau/\mathrm{s})$.

At an averaging time of $\tau = 1$ s the measured instability of the stabilized interferometers (red open circles in fig. (3.16)) $\sigma_y(1s) \approx 2 \times 10^{-17}$ coincides with that of the unstabilized interferometer; after 1 hour averaging the instability drops below 10^{-20}.

To determine the electronic noise limit of our measurement, the TOS is locked to a rf synthesizer (blue line in fig. (3.16)) and its frequency is counted. A fractional frequency instability of $\sigma_y(s) \approx 1.6 \times 10^{-17}/(\tau/\mathrm{s})$ was achieved which includes electronic noise due to the TOS, rf-synthesizer and the frequency counting system. From these measurements we conclude that the measurement noise floor of the complete systems is $\sigma_y(1s) \leq 5 \times 10^{-17}$ and averages approximately as $1/\tau$ with no indication of a flicker floor up to 10000 s.

The phase noise of the unstabilized interferometer indicates an upper limit to the frequency transfer stability, since it is not possible to measure the noise of the reference arm only. Thermal fluctuations lead to flicker frequency noise or random walk of the unstabilized interferometer at long measuring times, see fig.(3.16). The stabilized interferometer should follow $1/\tau$, when the compensation works properly.

Introducing an asymmetry in the interferometer (in-loop trip $\neq$ 2 $\times$ out-of-loop trip), the stability curve will deviate from the $1/\tau$ slope. In fig(3.17), an additional 0.5 m long fiber is introduced in the one-way trip such that round-trip fiber length equals twice that of the one-way fiber plus 0.5 m (asymmetrical interferometer). The ADEV of the asymmetrical interferometer is shown as orange circles in the figure. In the symmetrical case (red dots), the ADEV follows the expected $1/\tau$ slope.

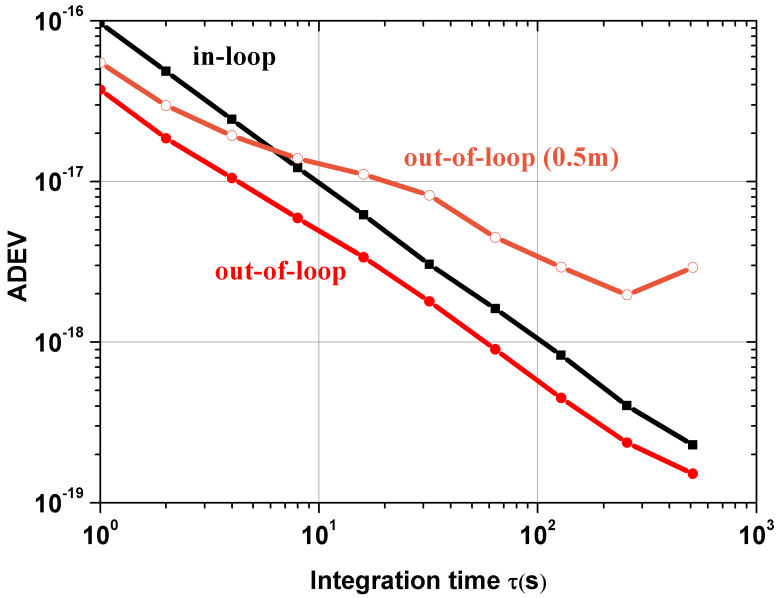

Figure 3.17: Relative frequency instability of stabilized in-loop (black squares) and out-of-loop beats for a symmetrical (red dots) and an unsymmetrical (orange circles) interferometer.

In this chapter, time and frequency domain measurements of the phase noise have been described. An interferometer to compensate the phase noise introduced by optical fibers is constructed. The stability in the time domain and the phase noise in the frequency domain for this interferometer are characterized. The instability of the free-running interferometer exhibit a flicker floor of about 10^{-18}. After compensating the interferometer phase noise, the instability of the interferometer reaches $\sigma_y(s) \approx 1.6 \times 10^{-17}/(\tau/\mathrm{s})$. The compensation system is optimized by using the system transfer function.

Chapter 4

Optical signal detection and amplification

In frequency transmission systems, it is essential to study the amplitude noise for each component in the system. Amplitude noise can either result from the detection process, from the laser source itself, or from the optical amplification. Amplitude noise decreases the signal-to noise ratio (SNR), therefore, care must be taken during optical amplification not to add plenty of noise to the optical signal.

In long distance frequency transmission, optical amplifiers are used. They are selected such that maximum amplification is obtained with the least added amplitude noise. Furthermore, the separation between amplifiers is kept below a certain limit to avoid degradation of the SNR of the transmitted signal. This limit is investigated before installing the amplifiers.

In the first part of this chapter, sources of amplitude noise and their measurement are discussed. In the second part, two methods for amplification of optical signals either using erbium-doped fiber amplifiers (EDFA) or Fiber Brillouin amplifiers (FBA) are described. Both methods are compared at the end of this chapter.

4.1 Amplitude noise

Amplitude noise decreases the oscillator signal to noise ratio (SNR), hence, it effects the detection efficiency. Optical frequencies can't be measured directly due to their high frequencies $\approx 10^{14}$ Hz. The measurement of optical signals requires establishing

a heterodyne beat signal with a reference optical frequency using a photodiode. This beat signal holds the phase and the amplitude fluctuation of the measured signal when the reference beam contributes negligible phase change amount. This beat signal produces a current $I(t)$ from the photodetector.

$$I(t) \propto 2(I_S I_R)^{1/2} cos[(\omega_R - \omega_S) + \phi] \tag{4.1}$$

where I_R, I_S is the current from the reference and the signal beams and ω_R, ω_S are frequencies of the reference and the signal beams.

therefore, the mean-squared current produced by the photodetector is:

$$< i_{beat}^2 >= 2 I_S I_R \tag{4.2}$$

Equation (4.2) describes the signal mean square current produced by the photodetector, which in the ideal case should be measured. However, noise is added to the detected signal from four fundamental contributions. These are laser intensity noise, optical amplifier intensity noise, thermal noise from electronics, and photonic shot noise. The total system noise, $\delta P_{TN}(f)$, is the linear summation of these four noise contributions [56].

$$\delta P_{TN}(f) = \delta P_{LN}(f) + \delta P_{ThN}(f) + \delta P_{qN} + \delta P_{AN}(f) \qquad \text{W/Hz}$$

where $\delta P_{LN}(f)$ is the laser intensity noise, $\delta P_{AN}(f)$ is the optical amplifiers intensity noise, δP_{qN} is the photonic shot noise power and δP_{ThN} is the contribution of thermal noise power. All noise power contributions are measured in W/Hz.

The SNR is a quantitative description of the amplitude noise. It can be expressed as the mean-square ratio between the signal to noise currents, since the power is $P =< i^2 > R_L$ where R_L is the transimpedence of the photodetector.

$$SNR = \frac{P_{Beat}}{\delta P_{TN}} = \frac{i_{Beat}^2}{i_{TN}^2} \tag{4.3}$$

where i_{TN}^2 is the mean-square current due to the total noise.

4.1.1 Thermal Noise

In photodetectors, the electronics that follow the photodiode (especially amplifiers) produce thermal noise δP_{ThN}. Thermal noise limits the sensitivity of the receiver

and can also lead to restriction in the distance between transmitter and receiver in both analog and digital systems. Thermal noise can be expressed in several ways. It is often described as a noise factor in dB relative to the room temperature lower limit of -174 dBm/Hz. The mean-squared thermal noise current from the photodetector is:

$$< i_{th}^2 >= 4kTBW/R_F \tag{4.4}$$

where k is Boltzmann's constant, T is the absolute temperature, BW corresponds to the measurement filter bandwidth and R_F is the amplifier feedback resistance.

Thermal noise can be measured by connecting the dark detector to a RF spectrum analyzer. The thermal current of the photodetector $< i_{th}^2 >$ can be determined from the analyzer RF power level.

4.1.2 Shot noise

Shot noise directly results from the quantum nature of the photons arriving at the detector, and it is related to the detection statistics. Shot noise is directly related to the amount of light incident on the photodetector. The mean-squared shot noise current from the photodetector is:

$$< i_q^2 >= 2qI_{dc}BW \tag{4.5}$$

where: q is the electron charge (1.6×10^{-19} C), I_{dc} is the output current from the photodiode due to the incident light, and BW is the bandwidth of the measurement system.

The shot noise can be calculated by measuring the DC current I_{dc}, when the measured light falls on the photodetector. The system in fig. (4.1) is used to measure the shot noise reported in fig. (4.3).

4.1.3 Intensity Noise (Laser and amplifier)

Laser intensity noise, δP_{LN}, refers to the noise due to laser intensity fluctuations, which are primarily due to spontaneous emission. Intensity noise of a laser can be measured by making a beat between light from the laser and a frequency shifted copy of itself. The frequency shift of several MHz is introduced to avoid detector

noise at low frequencies. Intensity noise is commonly specified by a quantity called relative intensity noise (RIN). RIN is the noise power (δP_{LN}) normalized to the average power ($\bar{P}_L$) of the oscillator in units of $\mathrm{dB}_c/\mathrm{Hz}$.

$$RIN = \frac{\delta P_{LN}}{\bar{P}_L BW} \mathrm{dB}_c/\mathrm{Hz},$$

where BW is the measurement bandwidth and dB_c is the decibel level with reference to the carrier. Figure (4.1) shows the system used to measure RIN of the fiber laser used for frequency transmission, see section (2.2.3).

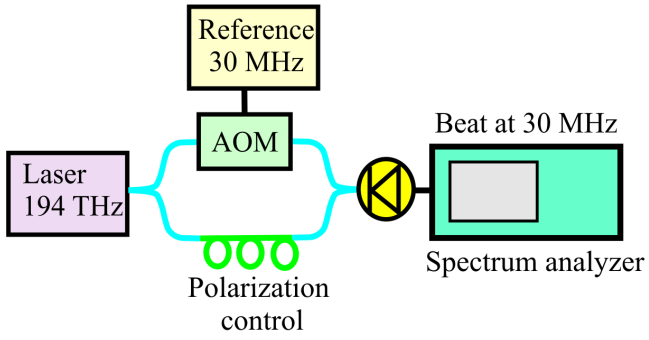

Figure 4.1: System used to measure laser relative intensity noise (RIN).

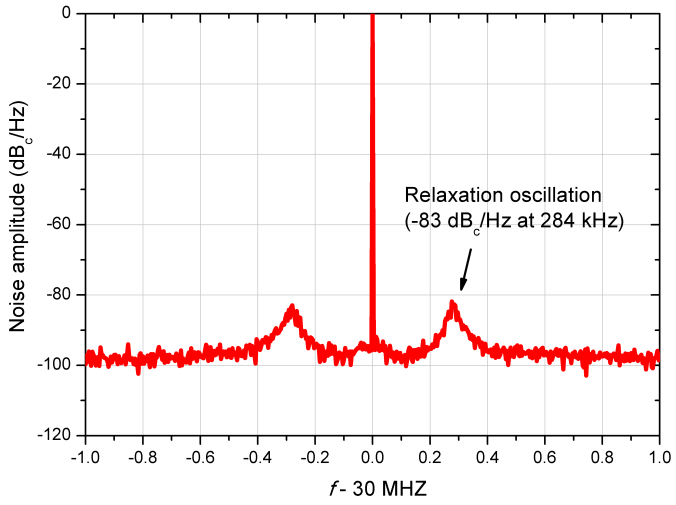

Figure 4.2: Fiber laser Relative intensity noise (RIN), a relaxation oscillation is observed at 284 kHz.

Figure (4.2) shows the measured relative intensity noise of the fiber laser. The peaks at 284 kHz arise from the relaxation oscillation of the laser. Relaxation

oscillations occur because the upper state life time of the laser is longer than the cavity damping time [57].

Unlike in lasers, in transsmision systems signal passes the amplifier only once which increases the probability for more spontaneous emissions especially at small signal powers. Optical amplifier intensity noise can be measured using optical spectrum analyzer (OSA). However, this method is widely used in the case of optical amplifiers with high intensity noise and broad spectrum. This method is not applicable in the case of lasers or narrowband spectrum amplifiers, as in the case of Brillouin amplifiers. In both cases, the bandwidth of the OSA or RF analyzer measurement filter have to be taken into account.

Figure (4.3) shows the thermal noise measured with the system shown in fig. (4.1) for one of the detectors used for phase noise compensation. It shows also laser noise and other types of noise for comparison with thermal noise. Due to the careful design of the amplifiers during the construction of this detector, Thermal noise is lower than shot noise.

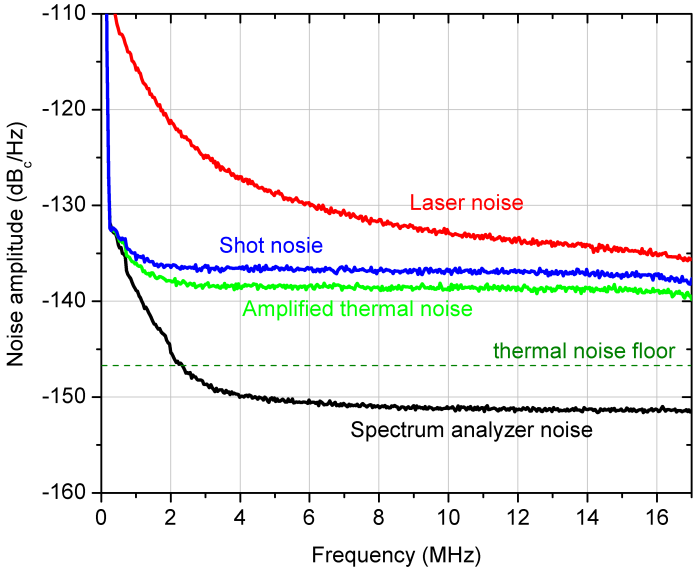

Figure 4.3: Measurement of laser noise, detector thermal noise, shot noise and spectrum analyzer noise.

4.2 Optical amplification

Optical fibers are used to transfer ultra-stable optical frequencies to distant users, provided that the attenuation of the signal and frequency fluctuations introduced by acoustic and thermal fluctuations on the fiber are compensated. Such a compensation scheme requires to reflect part of the light back to the transmitting station to form a phase detection interferometer. Thus part of the light has to travel twice the distance to the destination, see section (3.5). In fiber networks, Erbium doped fiber amplifiers (EDFA) are currently used to amplify the signal coherently. Typically, one uni-directional EDFA is used to amplify light for each direction [58]. The problem of using two separate EDFA is not only that the system will become more complex but also that the assumption that the forward and the return directions have the same noise will break down. Thus the uncompensated residual noise will increase. To avoid this, our colleagues at Max-Plank Institute for Quantum optics (MPQ), recently built a bi-directional EDFA using the same gain medium for amplification of light in both directions [59]. Another promising method is the fiber Brillouin amplification (FBA). FBA amplifies bi-directionally with high gain especially for low input signals. We explain in the following section the basics of an EDFA, its bi-directional version (BEDFA), and the operation of a FBA. Finally, a comparison is made between both amplifiers.

4.2.1 Erbium doped fiber amplifier (EDFA)

Erbium-doped fiber amplifiers (EDFAs) are widely used in optical communication systems because they operate in the wavelength region of 1.55 μm, can be pumped efficiently (3 dB/mW) with commercially available semiconductor lasers, and provide a broad-gain (35 nm), and are nearly polarization independent [60, 44, 61].

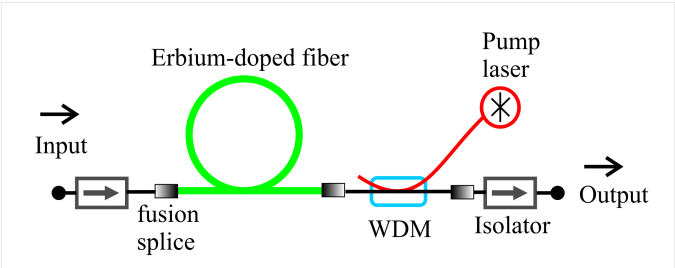

Figure 4.4: EDFA components, WDM: wavelength division multiplexer.

The essential components of an EDFA are shown in fig. (4.4). The EDFA comprises a pump laser, a wavelength division multiplexer (WDM), an optical isolator, and an Erbium doped fiber. A pump laser provides optical power in the range of 10-400 mW at a wavelength of 980 nm or 1480 nm. The WDM serves to efficiently couple signal and pump light into, or from, the Erbium-doped fiber. The optical isolator suppresses any light reflected back to the amplifier which might degrade the amplifier gain performance and cause parasitic lasing effects. Pumping can be either counter propagating, or co-propagating or both together with respect to the input light. The length of the Erbium-doped fiber is selected according to the required gain. A gain up to 40 dB can be achieved with 30 m of Erbium-doped fiber.

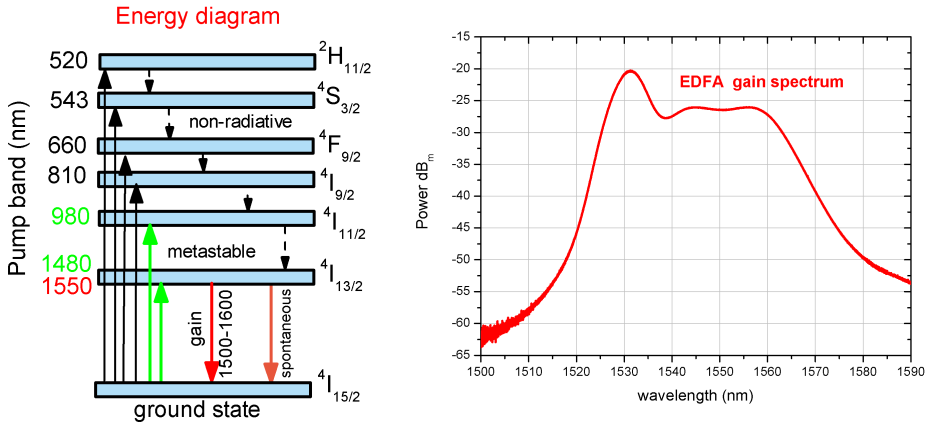

Figure 4.5: (left) Er^{+3} Energy levels in fused silica fiber, (right) EDFA spectrum.

The optical gain is provided by Er^{3+} ions. The erbium-doped fiber core diameter is about 5 μm with Er^{3+} ion centrally concentrated. The high concentration of Er^{3+} ions (1×10^{19} ions/cm^3) minimize the required fiber length to achieve similar gain. The relevant optical transitions are shown in fig. (4.5) (left). Pumping at 980 nm constitutes a three-level system, where the ion energy quickly decays (τ=2 μs) non radiatively from the $^4I_{11/2}$ to the long-lived $^4I_{13/2}$ metastable state. The excited ions relax spontaneously with a spontaneous life time of about 10 ms. This long lifetime should in principle lead to narrow emission spectrum. However, the spectrum is considerably broadened in the presence of randomly located silica molecules. Structural disorders of silica molecules lead to an inhomogeneous electric field and in turn to inhomogeneous broadening of the gain spectrum due to the Stark splitting of energy levels. Fig. (4.5) shows a measured spontaneous emission for one of our EDFA.

Stimulated emission to the ground state occurs when the incident light arrives at the excited Er^{3+} ions. The stimulated emission creates additional photons with the same optical phase and direction as the incident signal, thus amplification is achieved. Excited ions which don't interact with the incident light, spontaneously decay. The spontaneously decayed photons will be amplified and contribute to noise which degrades the SNR of the amplified signal and therefore is called the amplified spontaneous emission (ASE).

In order to be used in a phase noise compensation scheme, an EDFA must be operated bi-directionally. A "home-made" bi-directional EDFA has been built by our colleagues at Max-Planck Institute for Quantum Optics (MPQ). The bi-directional EDFA (BEDFA) components are shown in fig. (4.6). The pump laser is a fiber Bragg grating stabilized diode laser, operating at a wavelength of 980 nm with a maximum output power of 450 mW. The pump laser linewidth is about 0.2 nm. The length of the Erbium-doped fiber is about 6 m. The Erbium-doped fiber is pumped in both directions.

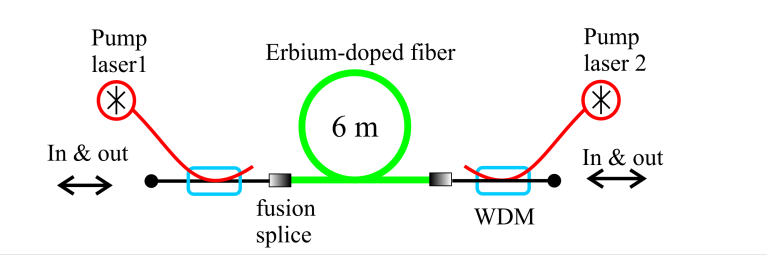

Figure 4.6: Bi-directional EDFA parts

If the isolator is moved, the gain must be lowered to avoid back-reflection. When the BEDFA is installed on a 146 km fiber link, see chapter (5), saturation of the gain medium and parasitic lasing effects are observed. This is mainly caused by Rayleigh scattering [60], but also due to some reflections at the BEDFA ends. This becomes more severe when the BEDFA is implemented in an amplifier chain for long distance transmission, like the 900 km link discussed in chapter (8). In consequence, the gain has to be reduced to overcome these effects, which limits the achievable distance of the bi-directional EDFA to not more than 120 km.

4.2.2 Fiber Brillouin amplifier (FBA)

Another approach to overcome limitations discussed in the previous section is to make use of the stimulated Brillouin scattering (SBS). As discussed before in section (2.3), the SBS process causes the propagating light to be back-scattered. This light is frequency shifted by about 11 GHz with respect to the input light and has a linewidth of about 10 MHz. The threshold for this process is about 2 mW, for a laser with a linewidth of 5 kHz which is injected into a fiber with an effective length of more than L_{eff}=21 km.

The peak gain (g) of the Brillouin process is described by [62]:

$$g = \frac{\gamma L_{eff} P_{pump}}{A} \tag{4.6}$$

where P_{pump} is the pump laser power, A is the effective mode area of the fiber (1×10^{-10} m^2) and γ is the gain coefficient of the nonlinear process. From equation (2.11), we calculate $\gamma = 5 \times 10^{-11}$ m/W. Using equation (4.6), the gain is calculated to be 9 dB/mW.

If pump laser light with a frequency ν_{pump} is injected in opposite direction to a signal laser with frequency ν_{signal}, it will be amplified by a process called fiber Brillouin amplification (FBA) [63, 64], if the pump frequency is shifted up by ν_B, such that, $\nu_{pump} = \nu_{signal} + \nu_B$. This shift frequency is about 11 GHz. Since SBS can start at pump laser power of 2 mW, we can also obtain amplification with such low pump laser power. Moreover, this amplification is high because of the high gain (9 dB/mW) of SBS. The achieved amplification can reach 50 dB for very low signal powers (around tens of nW's). This is equivalent to 250 km distances that can be spanned without amplifier, if the FBA is used.

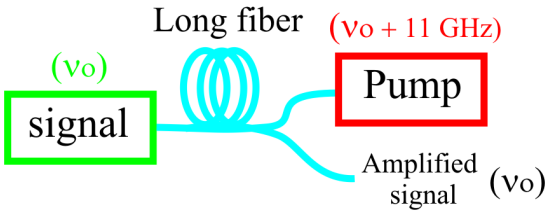

Figure 4.7: FBA amplification setup

4.2.3 Comparison between FBA and EDFA

Amplification and signal-to-noise ratio

For measuring the amplification of FBA we performed a simple test. A 25 km spool of single mode fiber (SMF28) was used as FBA gain medium. Narrow linewidth fiber lasers were used as pump and signal lasers. These lasers have a wavelength of λ=1542 nm, a linewidth of about 5 kHz, up to 100 mW output power, and a tuning range of about 2 nm.

With our 10 GHz resolution optical spectrum analyzer it is not possible to resolve the amplification caused by FBA, because the SBS linewidth itself is only about 10 MHz. Therefore, we constructed a Mach-Zehnder interferometer with the 25 km fiber spool in the measurement arm and an AOM in the reference arm, as shown in fig. (4.8). The AOM introduces a frequency shift (55 MHz) in the reference arm to produce a heterodyne beat signal at the photodetector. A variable attenuator is installed in the front of the 25 km arm to adjust the input power for the 25 km fiber without changing the power in the reference arm. The pump laser is injected from the opposite end of the fiber, with a power of around 20 mW and with frequency up-shifted by $\nu_{pump} - \nu_{sig} = \nu_B$=10.972 GHz. We tuned the variable attenuator at the input of the 25 km fiber to inject different signal powers into the FBA, to simulate different fiber lengths. The pump power is optimized to obtain the maximum amplification for every signal power. This allows the gain and the SNR of the device to be measured electrically with a RF spectrum analyzer. The measurement was recorded with 100 kHz filter bandwidth.

For comparison, we performed the same measurement for a BEDFA and a commercial single-pass EDFA and include the result in fig. (4.9). Note, the latter is not usable in the optical frequency transfer scheme, since bi-directional operation is required to compensate the fiber phase noise. Fig. (4.9) shows the gain (a) and the SNR (b) for different signal powers for the devices under test. Although both, the BEDFA and FBA, achieve almost the same SNR, the gain of the FBA is significantly higher than that of the BEDFA. This is especially true for low signal powers. As an example, the gain of the FBA is about 1000 times higher than that of the BEDFA for signal powers less than 50 nW.

For a transparent network, the amplifier gain has to compensate the loss in each

section of the network. A BEDFA with gain of 25 dB allows a span of about 120 km. In contrast, a FBA with 50 dB gain can compensate the loss of a 250 km long fiber with a typical attenuation coefficient of 0.2 dB/km.

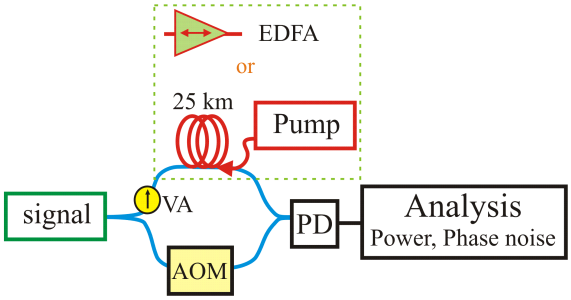

Figure 4.8: Set-up to measure the amplification of the FBA, a one-way or a bi-directional EDFA, VA: variable attenuator, PD: photodetector, signal: signal laser with isolator, pump: pump laser, AOM: acousto-optic modulator.

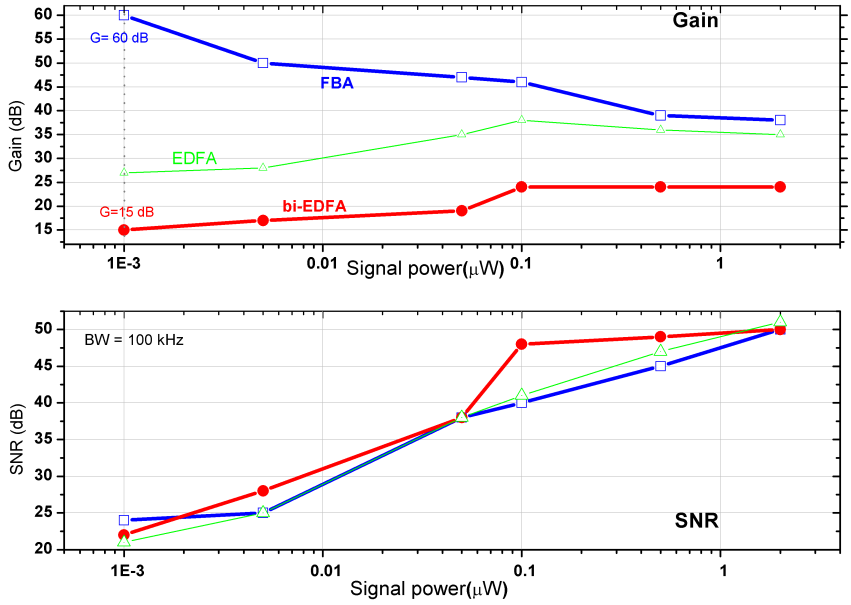

Figure 4.9: FBA in comparison to EDFAs (uni-directional and bi-directional) for different signal powers received at the output of a 25 km fiber: (a) gain (b) SNR. The spectrum analyzer bandwidth is 100 kHz.

This opens two possibilities when implementing the FBA for light amplification: using an additional fiber spool as discrete FBA-module is a suitable solution when operational or safety requirements forbid injecting more than a few mW optical

power into the transmission fiber. However, when higher power levels are allowed in the installed transmission fiber, this fiber itself can be used as gain medium.

In order to test this option of a distributed amplifier further, we performed measurements using the FBA and the BEDFA on 148 km and 332 km of installed, commercial fibers. The installed underground dark fiber is part of a wide-area network connecting PTB with other research institutes in Germany, (see chapters 5, 7, 8). Replacing the 25 km fiber spool by either the 148 km link or the 332 km link, the setup in fig. (4.8) is used to measure the gain and the SNR of the amplified light out of these fibers. The FBA and the EDFA amplifiers are used to amplify the light coming out from each of the fibers, similar to the 25 km fiber in fig. (4.8). The measurements are shown in fig. (4.10) for the 148 km fiber and in fig. (4.11) for the 330 km fiber. The measurements show that for the 148 km link, the intrinsic FBA achieves 18 dB more gain than our bi-directional EDFA.

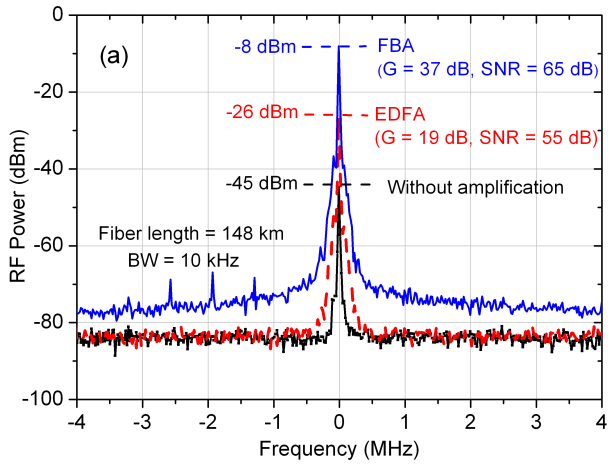

Figure 4.10: Detected heterodyne beat power (RF) obtained with FBA and with bi-directional EDFA, when 5 mW signal power are injected into 148 km fiber (P_{pump} = 20 mW, ν_B = 10.974 GHz).

For the 332 km link, the difference is even larger: The FBA gives 45 dB more gain than the EDFA. This result shows that the FBA is more suitable for use in long fiber links. The Brillouin shift frequency was measured to be 10.974 GHz and 10.970 GHz for the 148 km and the 332 km fiber link, respectively, with only 4 MHz difference.

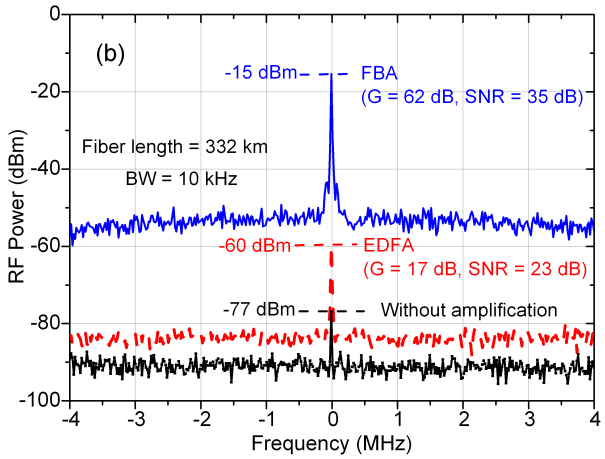

Figure 4.11: Detected heterodyne beat power (RF) obtained with the FBA and with a bi-directional EDFA, when 5 mW signal power are injected into 332 km fiber (P_{pump} = 40 mW, B = 10.970 GHz).

Phase noise

One of the most important aspects in frequency transfer applications is how much additional phase noise is added by the amplifier to the signal propagating through the fiber. We used the Mach-Zehnder interferometer shown in fig. (4.8) to measure the phase noise of the bi-directional EDFA and FBA. Fig. (4.12) shows the measured phase noise for the free-running interferometer without (black line) and with installed EDFA (red-open circles). At low Fourier frequencies ($f < 30$ Hz) the EDFA possibly adds a small amount of phase noise - this is still less than 0.1 rad^2/Hz at $f = 1$ Hz. We attribute this phase noise to the approximately 6 m fiber used as gain medium inside the amplifier.

To measure the phase noise introduced by the FBA, a 25 km fiber spool is used as FBA gain medium. Such a spool is quite sensitive to environmental perturbations, which results in additional phase noise. To reduce this effect, we put the spool inside an acoustic isolation box.

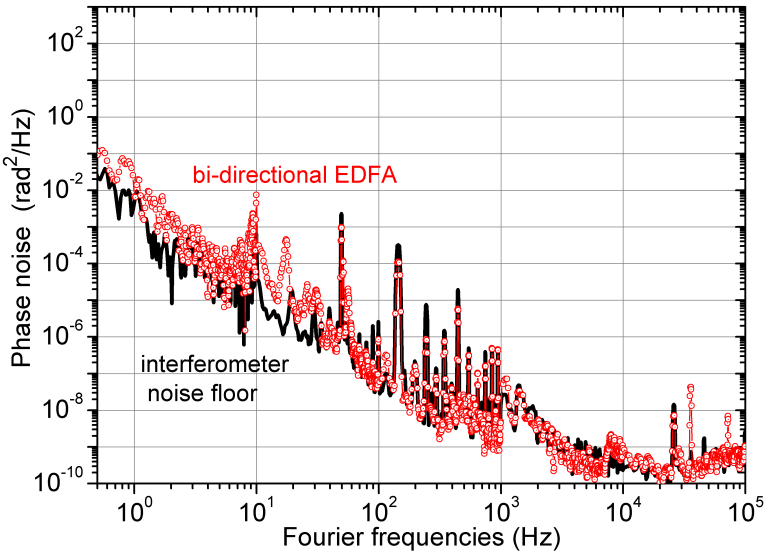

Figure 4.12: Phase noise of the free-running interferometer without (black line) and with a bi-directional EDFA (red-open circle).

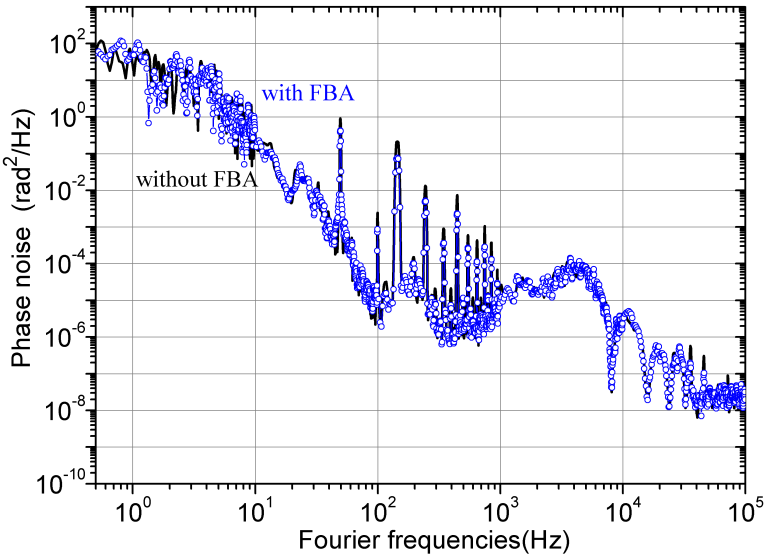

Figure 4.13: Phase noise of 25 km spooled SMF28 fiber without (black line) and with using FBA (blue-open circle).

Still, the measured phase noise for the unstabilized 25 km fiber (black line in Fig. 4.13) exceeds one rad^2/Hz at frequencies below 10 Hz. With the pump laser turned on, we then measured the phase noise of FBA (blue-open circles). The phase noise due to the FBA process is less than that of the 25 km fiber alone, since both curves coincide. The total phase noise is significantly less than that encountered on long fiber links. It can therefore be compensated with the standard technique.

4.2.4 FBA pump laser stabilization

The maximum amplification is achieved when the pump frequency matches the condition $\nu_{pump} = \nu_{sig} + \nu_B$. Therefore, the pump laser frequency has to be controlled. If pump and signal lasers are at the same site, a beat between the signal and the pump laser can be detected with a fast photodetector (bandwidth > 11 GHz). The beat signal is then locked to a microwave reference. But this technique needs complex and expensive equipment, which handles GHz frequencies. Furthermore, this technique will not be practical if the pump laser is located at an intermediate station.

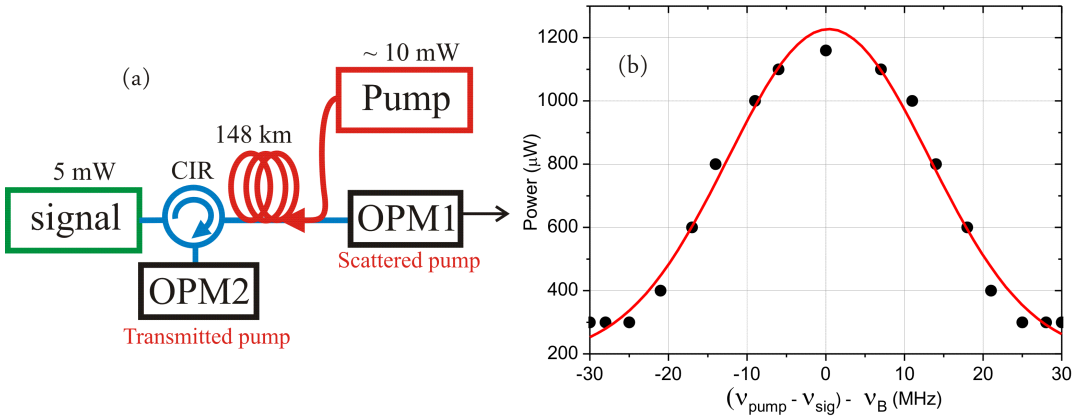

Figure 4.14: (a) Measurement setup for the scattered and transmitted pump power changes. The pump is injected in the opposite direction to the signal laser. CIR: circulator and OPM: optical power meter. (signal power is about 1 μW after 148 km fiber) (b).The change of the scattered pump power when the pump frequency is swept around ($\nu_{sig} + \nu_B$) and a Gaussian fit.

We have developed a simpler method based on the observation that the back-scattered pump power increases when the pump frequency is equal to ($\nu_{sig} + \nu_B$). Fig. (4.14.a) shows the system used to measure the scattered and transmitted pump

powers when the pump is injected in the opposite direction of the signal in the 148 km fiber. Although the signal power is less than 1 μW at the output of the 148 km fiber, the back-scattered pump power increases when the pump frequency is swept around ($\nu_{sig} + \nu_B$), see fig. (4.14.b). The transmitted pump power is decreased also by the same amount. A small modulation of the pump laser frequency and lock-in detection was used to monitor this change in the scattered pump power and stabilize the pump laser frequency at ($\nu_{sig} + \nu_B$).

When the fiber link is acting as the FBA gain medium, the change in the fiber temperature causes the Brillouin frequency (ν_B) to be changed. If the signal frequency does not match the Brillouin frequency (within $\pm$5 MHz), the amplification scheme will not work any more. To determine the Brillouin frequency change with temperature [65], we measured the temperature dependence of the 25 km fiber in the range from 16 ^{o}C to 25 ^{o}C. The Brillouin frequency temperature dependence is found to be 0.4 MHz/K. Typical peak to peak diurnal temperature variations for a buried fiber (depth $<$ 1.5 m) are well below 1 K. Even if we assume an upper limit for temperature variations of about 10 K, the stabilization circuit can easily handle a pump laser frequency shift of about 4 MHz.

To conclude, amplitude noise limits the detection of the frequency of an optical frequency standard. It is represented by "SNR". It originates from the detection process (shot and thermal noise), the optical signal itself (laser noise), or from the optical amplification. Thermal noise is minimized by optimizing the design of electronics, and shot noise is minimized by optimizing the light power on the photodetectors. Optical amplification is required to maintain the signal before it drops below the noise. Two types of optical amplifiers (BEDFA and FBA) are presented and compared to each other. FBA provides amplification up to 60 dB for small optical signals (in order of 50 nW), while Bi-EDFA is only suitable for amplification of signals in order of few micro watts. Therefore, a span up to 250 km can be bridged using an FBA, while only 120 km can be bridged using an BEDFA.

Chapter 5

Optical frequency transfer over 146 km urban fiber

In the previous chapters, the basics concepts for optical frequency transfer have been considered. We now use the results for the design of a 146 km fiber link, that allows to test the full concept. The 146 km fiber consists of a pair of 73 km long commercial fibers which connect the frequency standards at the Leibniz University of Hannover (LUH) to the frequency standards in PTB, Braunschweig. This link enables a remote comparison between frequency standards in both institutes. In order to perform such a comparison, the phase noise induced by the fiber link should be less than the phase noise induced by the frequency standards. Therefore, the phase noise induced by the fiber link is characterized and compensated.

In order to characterize the fiber link, a fiber ring topology that begins and ends at the same laboratory is necessary. Therefore, the two fibers, which are linking PTB, Braunschweig to the LUH, are connected at LUH while the measurement is made at PTB. This is the first worldwide characterization of installed commercial fiber over such a long distance (146 km).

5.1 Description of the fiber link

A dedicated pair of commercially used single mode dark fibers (SMF28) is connecting PTB in Braunschweig to the Institute of Quantum Optics (IQ) at the Leibniz University of Hanover (LUH) with a total fiber length of about 74 km. The pair of dark fibers is part of a larger fiber network currently being established. This network

will eventually connect the optical clocks at (PTB) with those at the Institute of Quantum Optics (IQ), Max Planck Institutes in Erlangen (Institute of Optics, Information and Photonics, (IOIP)) and Garching (Max-Planck-Institute for Quantum Optics, (MPQ)). The fiber route was established in collaboration with the German Science Network (DFN), GasLINE GmbH, and a local telecommunication provider in Braunschweig (EnBs).

A sketch of the fiber link is depicted in fig. (5.1) In a first step, our laboratory is connected to (PTB's) computing center that is linked to a local network provider (EnBs). The EnBs-network allows us to connect to the wide-area network of GasLINE. The networks of gas transmission and of regional distribution companies offer significant potential for developing a wide-area, fiber-optic infrastructure. The use of this infrastructure allows us to directly connect to the computing center at LUH that is located about 600 m away from IQ. An in-house fiber link provides access to the Mg frequency standard [29] at IQ.

Figure 5.1: Fiber route from PTB in Braunschweig to IQ in Hanover. A dedicated pair of dark fibers in a strand of commercially used fibers has been made available.

A commercial SMF-28 fiber according to the ITU-T G.652 standard is used to establish the full link. From the fiber data sheet, the refractive index of the fiber is $n = 1.4681$ at 1542 nm, the attenuation is 0.2 dB/km, the polarization mode dispersion is 0.1 pm/$\sqrt{\text{km}}$, and the chromatic mode dispersion is 16.52 ps/nm^2.km at 1542 nm. An Optical Time Domain Reflectometer (OTDR) was used to obtain detailed information about the attenuation along one of the 74 km fiber link. The OTDR measurement curve is shown in Fig. (5.2).

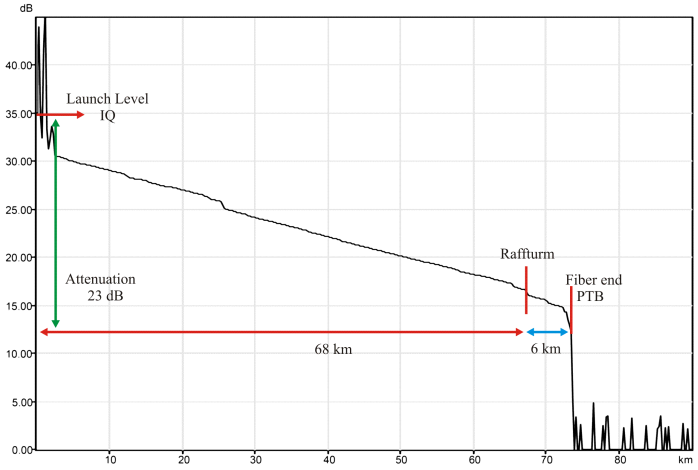

Figure 5.2: The 74 km fiber-link attenuation measured from IQ, Hanover, using an OTDR. At Raffturm the local-area network of EnBs is connected to the wide-area network of GasLINE.

Both fibers were connected at university LUH computer center which is located about 600 m away from IQ. Therefore, the fiber length from PTB to LUH computing center is about 73 km and the loop back to PTB is 146 km. The connection was established at LUH computing center and not at IQ due to a technical problem at that time. The measured overall attenuation of the 146 km fiber link after about 16 splices and 10 connectors is approximately -43 dB.

5.2 The frequency transmission setup

After transferring the frequency stability of a cavity stabilized laser at PTB (CSL-PTB) at 657 nm to the NIR laser at 1542 nm as mentioned in section (2.2), the NIR laser is used to transfer the frequency stability through the 146 km fiber to the user end. The setup is shown in fig. (5.3). The reason for locating the local and the user ends at PTB is to measure the compensation performance. Therefore, the in-loop and the out-of-loop beat signals can be obtained at the same laboratory. The in-loop beat holds the round-trip phase excursions accumulated along the 146 km fiber. This phase noise can be compensated by applying the error signal generated by the interferometer to control the shift frequency of AOM1. The out-of-loop beat characterizes the performance, since it represents the frequency stability at the user end.

The propagation time of the light in the fiber determines the compensation bandwidth. For the single path it amounts to $\tau = 0.7$ ms. However, as described in Appendix (A), the compensation bandwidth is only $1/4\tau$. Therefore, we expect a unity gain peak at about 350 Hz. The DPFC integrator corner frequency should be lower than 350 Hz to avoid oscillations. The accumulated in-loop phase fluctuations are so large that the DPFC prescaler is set to N = 256. This enables stable locking of the in-loop signal.

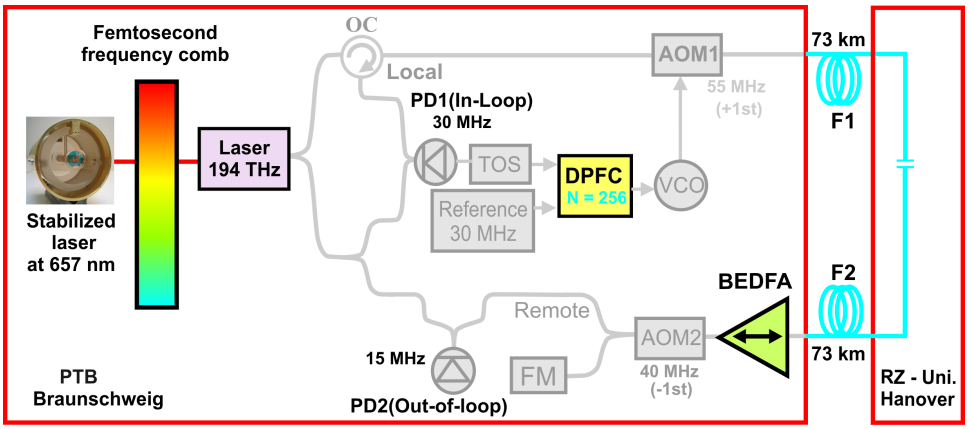

Figure 5.3: Setup for frequency transfer through 146 km fiber. N = 256: divider value, EDFA: Erbium-doped fiber amplifier. The compensation set up is discussed in more details in section (3.5).

The in-loop beat is obtained after a round-trip fiber length of 292 km. The attenuation is about 86 dB. Launching 4 mW into the fiber, only 10 pW contribute to the in-loop beat. Therefore, a BEDFA optical amplifier, discussed in section (4.2), is installed at the remote end. The BEDFA as a bi-directional amplifier is used to avoid interferometer asymmetry, discussed in section (3.5). As the one-way attenuation is about -43 dB, a power of 0.2 μW is available at the input of BEDFA. According to fig. (4.9), this input power is enough to obtain an amplification of 25 dB. At the output of the BEDFA, the power is about 60 μW. About 10 % of this power is sent to the out-of-loop interferometer to generate a beat with a SNR = 90 dB at a bandwidth of 1 Hz. In the return direction the gain medium of the BEDFA is saturated by the forward direction which limits the backward to less than 10 dB. Thus, 0.5 mW are injected back into the fiber, less than 30 nW reach the in-loop detector. However, this is enough for an in-loop beat with a SNR = 70 dB at BW = 1 Hz.

5.3 Laser noise and self-heterodyning

Using a laser with a coherence length less than the fiber length can lead to the self-heterodyning effect (described in section (3.5.2)) when compensating the fiber noise. This effect occurs because the return signal becomes uncorrelated with that of the reference arm. The in-loop beat then contains not only the fiber noise but also a contribution from the laser noise $S_\phi^{laser}(f)$. From section (3.5.2), the self-heterodyne beat can be expressed as:

$$S_\phi^{SH}(f) = 4[sin(2\pi f\, nL/c)]^2\ S_\phi^{laser}(f)$$

In our case, the light travels about 292 km in the fiber to form the local beat signal. The NIR laser has a free-running line-width of about 5 kHz, thus a coherence length of about 20 km, which is obviously smaller than the round-trip length in the fiber. For Fourier frequencies $f < (c/nL)$, $n = 1.468$, and a one-way fiber length of $L = 146$ km, the above equation can be approximated by $S_\phi^{SH}(f) = 8 \times 10^{-5} f^2\ S_\phi^{laser}(f)$.

We have measured the noise of the interferometer signal at the remote end (out-of-loop signal) for the unstabilized and stabilized link and the results for the PNSD and ADEV are shown in fig. (5.4) and fig. (5.5), respectively. The contribution of the laser noise to the interferometer signal, fig. (5.4) (green open squares) at the remote end is calculated from the measured laser noise (blue-open squares) using eq. (3.11) and replacing L by L/2 for the one-way light. The flicker frequency noise ($1/f^3$) of the NIR laser is converted into flicker phase noise ($1/f$) by the interferometer transfer function.

The measured phase noise of the unstabilized fiber link (black dots) is dominated by this laser noise for $f > 1$ Hz (except the peak at about 17 Hz); only for very low frequencies $f < 1$ Hz the noise of the optical link S_ϕ^{fiber} exceeds S_ϕ^{SH} of the free running laser. The corresponding ADEV shows a constant floor of 4×10^{-14} for $\tau < 100$ s, fig.(5.5) black dots, and some averaging for longer integration times.

When the fiber control loop is closed it correlates laser noise and fiber noise in order to minimize the total noise $S_\phi^{tot}(f)$, corresponding to a linear combination of $S_\phi^{fiber}(f)$ and $S_\phi^{sh}(f)$.

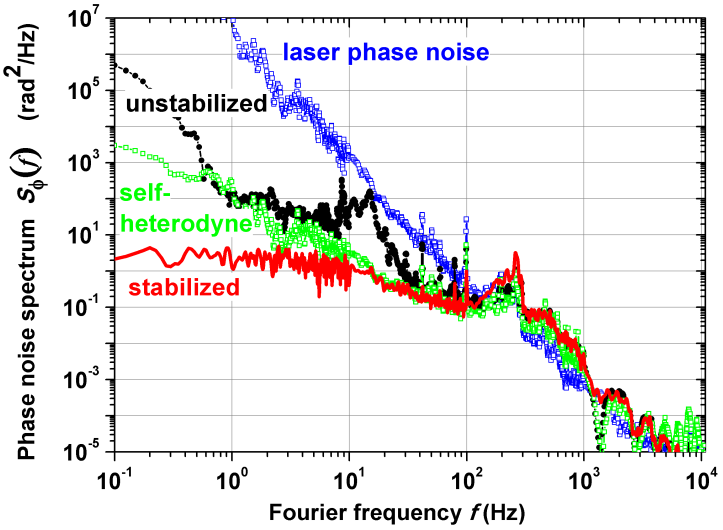

Figure 5.4: Phase noise of the remote beat without stabilizing the NIR laser before (black dots) and after (red line) link stabilization. The phase noise of the free running laser is shown as blue-open squares, and the calculated laser self-heterodyne signal as green open squares.

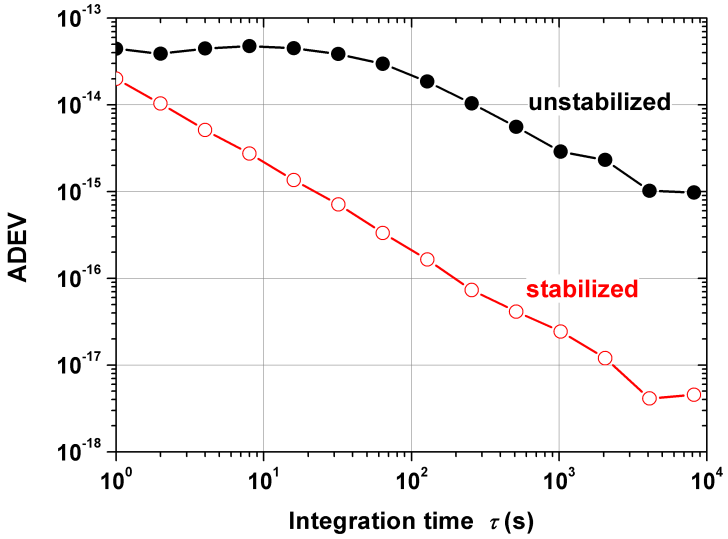

Figure 5.5: Relative frequency instability of the remote beat with the unstabilized NIR laser before (black dots) and after (red open circles) stabilizing the link.

For the stabilized interferometer the total phase noise $S_\phi^{tot}(f)$ at the remote end is shown as red curve in fig.(5.4), and the measured ADEV of $\sigma_y(s) < 2 \times 10^{-14}/(\tau$ /s) is shown as red curve in fig. (5.5). However, the stability of the beat signal measured at the remote end should not be confused with the stability of the optical carrier frequency at the remote end that remains limited by the noise of the free-running laser as long as $S_\phi^{laser} > S_\phi^{fiber}$. Therefore, frequency stabilization of the transfer laser before compensating the phase noise resulting from the fiber link is essential.

5.4 Frequency transfer stability and accuracy

5.4.1 Frequency transfer stability

The phase noise of the fiber link S_ϕ^{fiber} can be measured after stabilizing the NIR laser to avoid the self-heterodyning effect, discussed in the previous section. The out-of-loop beat represents the one-way phase noise of the 146 km fiber link. The uncompensated noise of the fiber link is shown as black-dashed curve in Fig. (5.6). It can be approximated by (blue line):

$$S_\phi^{fiber}(f) = [\frac{100Hz}{f} \times (\frac{1+f}{10Hz})^{-2} + const] \text{ rad}^2/\text{Hz}$$

Above 100 Hz the noise decreases as $1/f^3$, while for $f < 10$ Hz the frequency dependence turns to flicker phase noise. The constant phase noise level of $\approx 10^{-5}$ rad^2/Hz at high frequencies is given by the noise floor of the phase detection system.

Beside the noise contributions associated with the interferometer and the transfer laser itself, a fundamental limiting factor of any fiber link is related to the time delay $\tau_{delay} = nL/c$ introduced by the fiber [24]. First, it directly affects the control bandwidth of the compensation loop. Second and more severe, the delay through the link results in an imperfect cancellation of the noise at the remote end. This incomplete suppression of the one-way fiber noise due to the delay dominates other limitations at low Fourier frequencies. For the round-trip signal used for the stabilization of the 146 km link, theoretically attainable noise suppression at a Fourier frequency $f = 1$ Hz is about 52 dB and the bandwidth of the loop is limited by $1/4\tau_{delay}$ to approx. 350 Hz. As a result, the stability at short averaging times

(high frequencies), is limited (due to the limited bandwidth) by unsuppressed fiber noise on the link, and at longer averaging times by the residual phase noise of the interferometer. When the fiber stabilization loop is closed the phase noise of the link is suppressed to a white phase noise level of approximately 6×10^{-3} rad^2/Hz, as shown as a red-solid curve in the same figure. Due to the locking bandwidth of about 350 Hz, the technical noise at 15 Hz is suppressed only by about 25 dB.

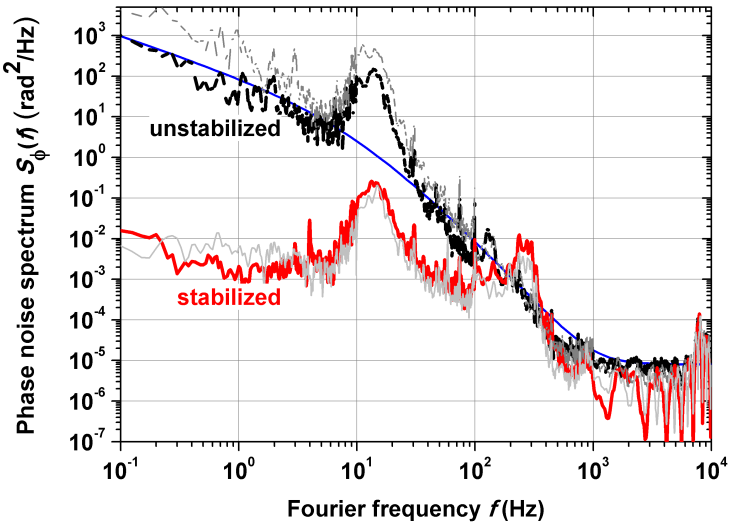

Figure 5.6: Phase noise of the 146 km link: out-of-loop beat before (black-dashed), and after (red-solid) stabilizing the link; in-loop beat: before (gray-dashed), and after (gray-solid) stabilizing the link. Blue line: approximation of $S_\phi(f)$.

The in-loop signal represents the round-trip phase noise in the 146 km fiber and is shown also in the same figure as a gray-dashed line before compensating the fiber phase noise and gray-solid line after compensating the noise. It is clear that, for low frequencies, $f <$ compensation bandwidth, the round-trip uncompensated phase noise is higher than the one-way phase noise. The experimental difference between both is as predicted in Appendix (A), where the noise of the round-trip should be 4 times higher than the one-way noise for Fourier frequencies significantly smaller that the compensation bandwidth and 2 times otherwise.

The corresponding ADEV measurement (Fig. (5.7)) shows a good agreement with the measured phase noise data. Note, that the instability of the unstabilized 146 km fiber link (black dots) is already at the low 10^{-14} level. Closing the interfer-

ometer loop, an instability of the transmitted frequency of $\sigma_y(\tau) \approx 3.3 \times 10^{-15}\ /(\tau/\mathrm{s})$ has been obtained (red open circles), reaching a level of $\sigma_y < 4 \times 10^{-19}$ after 10000 s. Note that the link instability follows a $1/\tau$-slope (red dashed line) over more than 6 orders of magnitude.

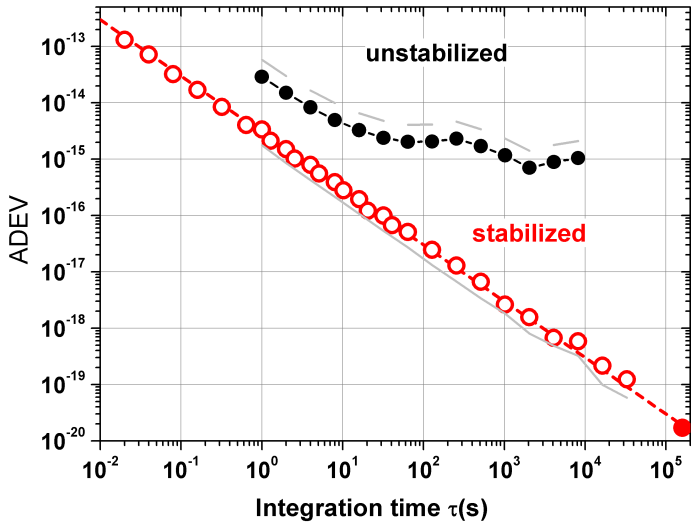

Figure 5.7: Allan deviation for the 146 km for out-of-loop beat, before (black dots) and after (red-open circles) stabilizing the link; for in-loop beat, before (gray-dashed line) and after (gray-solid line) stabilizing the link. The uncertainty of the relative frequency deviation $\Delta\nu/\nu_{NIR}$ of the transmitted signal is shown as a red dot; the red dotted line is equivalent to $\sigma_y(\tau) = 3 \times 10^{-15}\ /(\tau/\mathrm{s})$.

5.4.2 Accuracy of the transmitted frequency

Beside the attainable stability, any small residual frequency offset between the frequency at the local site and that at the remote end is of fundamental importance. The accuracy of the transmitted frequency was checked by comparing the measured mean value of the out-of-loop signal with the expected value. Passing both AOMs (55 MHz (+1st order) and 40 MHz (-1st order)), the frequency at the remote end should be shifted by exactly 15 MHz with respect to the local end.

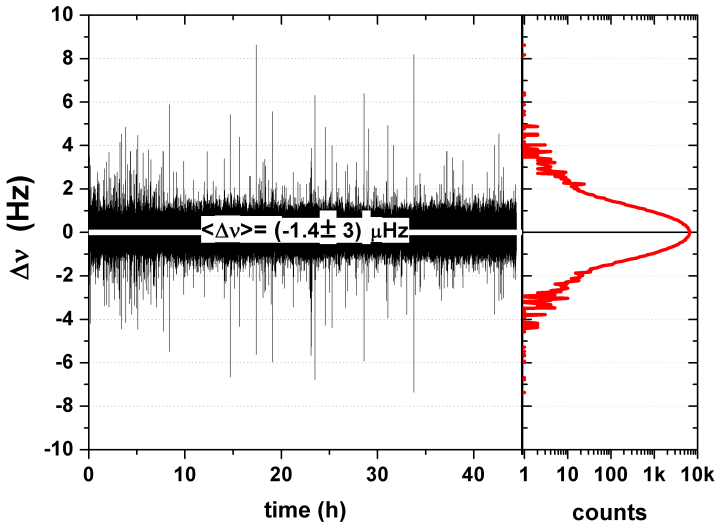

Figure 5.8: Time record of the frequency deviation of the transmitted signal from its nominal value of 15 MHz over a measurement period of 44 hours (left); histogram of the frequency values (right).

Fig. (5.8) shows a time record of the frequency deviation $\Delta\nu$ of the transmitted signal from its nominal value of 15 MHz. The observed mean deviation of the transmitted optical carrier frequency given by the sample average of the full data set was $\Delta\nu = (1.4 \pm 3.3)\ \mu$Hz. The statistical uncertainty of the mean was calculated from the standard deviation divided by the total number of data points, assuming that the $1/\tau$ dependence (white phase noise) continues over the full period of 44 hours. The division by the total number of data points instead of the square number of data points for white phase noise is reported in [66]. We have included the relative frequency uncertainty of the averaged frequency deviation of 1.7×10^{-20} as red dot in Fig. (5.7). This value coincides with the estimated ADEV for an averaging time of 44 hours. A more conservative estimate for the accuracy of the transmitted optical frequency is given by the last data point of the Allan standard deviation. After 9 hours, a relative frequency instability of 1.3×10^{-19} is reached.

To conclude, ultra-stable frequencies can be transfered over 146 km fiber with relative stability of $\sigma_y(\tau) \approx 3.3 \times 10^{-15}\ /(\tau/\mathrm{s})$ and relative uncertainty of 1.3×10^{-19}. In the next chapter, part of this fiber will be used to compare frequency standards located in two institutes separated by a geographical distance of about 60 km.

Chapter 6

Remote Measurement of frequency standards using the fiber link

In the previous chapter, a pair of optical fiber, connecting LUH and PTB, is characterized for ultrastable frequency transfer. It has been shown that, by compensating the fiber induced phase noise, it is possible to transfer frequencies over 146 km with a stability of $3.3\times10^{-15}/(\tau/\mathrm{s})$ and a relative uncertainty below 1×10^{-19}. This performance enables a relative comparison of the best available optical frequency standards within minutes.

In order to investigate the instability of an optical frequency standard at the Institute of Quantum Optics (IQ) at LUH, an optical frequency standard with superior stability is required. Such a standard is available at PTB. The optical fiber, connecting IQ to PTB, is used to perform this comparison. In this chapter, the setup used to measure the stability of two cavity stabilized lasers that are alternatively used to interogate the clock transition of a ^{24}Mg optical frequency standard at IQ is presented.

6.1 Frequency measurement setup

The comparison between the frequency standards at IQ and PTB is performed using a phase noise compensated 74 km fiber link. The 74 km fiber consists of the 73 km fiber and about 1 km long fiber that connects the computing center of LUH with IQ. The system used to perform this comparison is depicted in fig. (6.1).

The frequency stabilization system of the NIR laser at PTB is discussed in section

(2.2). The frequency comb (comb A) is stabilized to an active Hydrogen maser (H5). The frequency of H5 is corrected with CSF1.

At Hanover, a software transfer beat is generated between the transmitted signal and the Mg-laser using a local frequency comb (comb B), which is stabilized to a transportable passive H-maser (H7). Using this setup, the short term stability of the Mg-laser is measured against the CSL-PTB laser, while the long term stability of the ^{24}Mg frequency standard is measured against the microwave frequency standards (H5-CSF1).

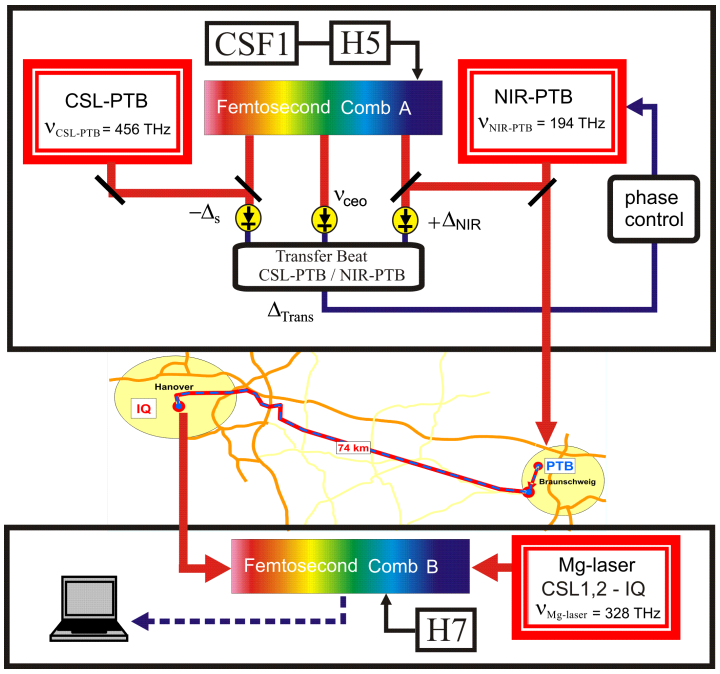

Figure 6.1: Setup for the remote measurement of a Mg-laser at 328 THz against CSL-PTB at 456 THz using a transfer laser (NIR-PTB) at (194 THz) and two frequency combs A and B. The PTB femtosecond frequency comb A is locked to a H-maser (H5) referenced to the Cesium fountain CSF1. At the remote end the transfer beat is calculated from the measured individual beat signals. The IQ femtosecond frequency comb B is locked to an H-maser (H7).

In order to detect and compensate the phase fluctuations introduced by the fiber link, an interferometer similar to the one discussed in section (3.5) is used, see fig. (6.2). In contrast to the system discussed in section (3.5), now the remote end is at IQ.

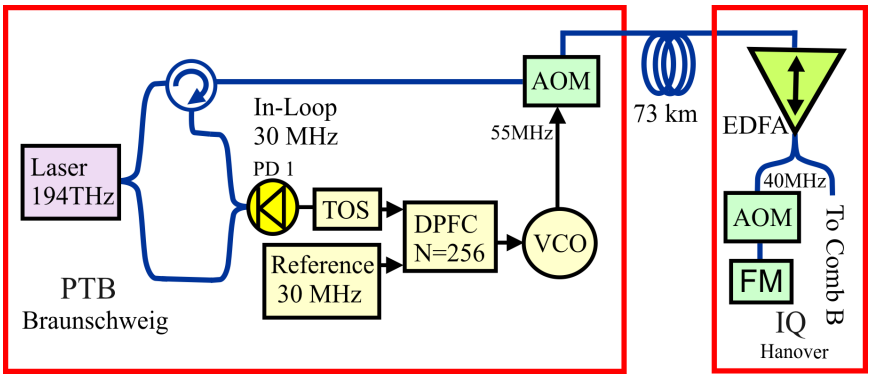

Figure 6.2: Setup for active fiber noise compensation during the frequency comparison. EDFA: Erbium-doped fiber amplifier, OC, DPFC, TOS, PD1, AOM, and FM: see fig. (3.10).

The instability of the 74 km fiber link cannot be measured without the out-of-loop beat. However, since the 146 km fiber (chapter 5) contains most of the 74 km fiber (73 km), an upper limit for the instability of the 74 km fiber can be given from the out-of-loop measurement of the 146 km fiber. The instability of the transmitted frequency through the 146 km link is $\sigma_y(\tau) \approx 3.3 \times 10^{-15}\ /(\tau/\mathrm{s})$, while the contribution of the link to the uncertainty of the optical standards frequency is 1.3×10^{-19}.

6.2 Short-term stability of the cavity stabilized lasers at IQ

In Hanover, currently two ultrastable laser systems are in operation, CSL1-IQ and CSL2-IQ. Both are diode lasers systems, which are stabilized to two independent ultrastable optical resonators. Since beat note measurements between the two systems display the combined instability, they only provide an upper limit for the individual performance. Thus, for characterization of the individual instability, a third laser is required. This one is provided by transferring the frequency of an ultrastable laser located at PTB via a 74 km long telecommunication fiber to IQ.

For all the measurements shown in fig. (6.3) a Π-type frequency counter was used. As discussed in section (3.3), the ADEV depends on the type of frequency counters used to record the beat signal. Frequency drifts of all the cavity stabilized

lasers (several 10^{-15}/s) are measured and corrected with respect to the Hydrogen maser H5. The beat between CSL1-IQ and CSL2-IQ shows the combined instability of both lasers (green squares). It has a flicker noise floor of about 6×10^{-15}. The beat between CSL-PTB and CSLYb-PTB at PTB gives the combined stability of both lasers (grey open squares). This combined instability shows an upper limit for the instability of CSL-PTB laser. It has a thermal noise floor of about 2×10^{-15}. Therefore, the CSL-PTB laser in PTB can be used to evaluate the performance of CSL1-IQ and CSL2-IQ lasers individually at IQ. The lasers at Hanover (CSL1-IQ and CSL2-IQ) are heterodyned with the laser at PTB (CSL-PTB) via the optical link to investigate their instability. The instability of CSL1-IQ is shown as blue dots and that of CSL2-IQ as red triangle [67].

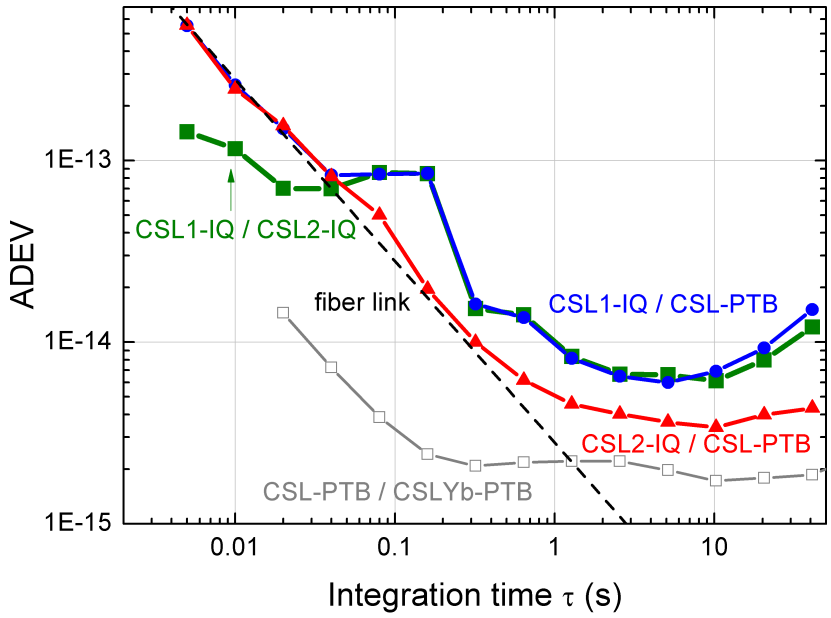

Figure 6.3: Allan Deviation of the beats between CSL1-IQ, CSL2-IQ against each other (CSL1-IQ / CSL2-IQ) (green squares), of CSL1-IQ laser against the NIR laser (CSL1-IQ / NIR-PTB) (blue dots), of CSL2-IQ laser against the NIR laser (CSL2-IQ/ NIR-PTB) (red triangles), and of two clock lasers (CSL-PTB against CSLYb-PTB) at PTB, shown as a grey open squares.

An upper limit for the instability of the 74 km fiber link can be obtained from the above measurements as follows: the remote instability measurement of both lasers at IQ deviate from their local measurement below an integration time of $\tau < 0.04s$. On the other hand, the instability of the 74 km fiber link should be less than that of the 146 km fiber link, since the 74 km fiber is part of the 146 km fiber. Indeed,

the instability of the 74 km link shows an instability of 2.8×10^{-15} (black dashed line), which is less than that of the 146 km, which is $\sigma_y(\tau) = 3.3 \times 10^{-15}/\tau$.

In order to obtain the ModADEV and further suppress the white phase noise a Λ-type frequency counter is used to measure the frequency instability of the CSL-PTB/CSL2-IQ beat. A number of ten measurements were made at different gate times (τ=5 ms, 10 ms, 20 ms, 50 ms, 100 ms, 200 ms, 500 ms, 1 s, 2 s, and 5 s). The ADEV equation (3.6) is then applied to each of the ten measurement gate times to obtain the ModADEV at each gate time, see section (3.3.2). The result is shown in fig. (6.4), as red triangles.

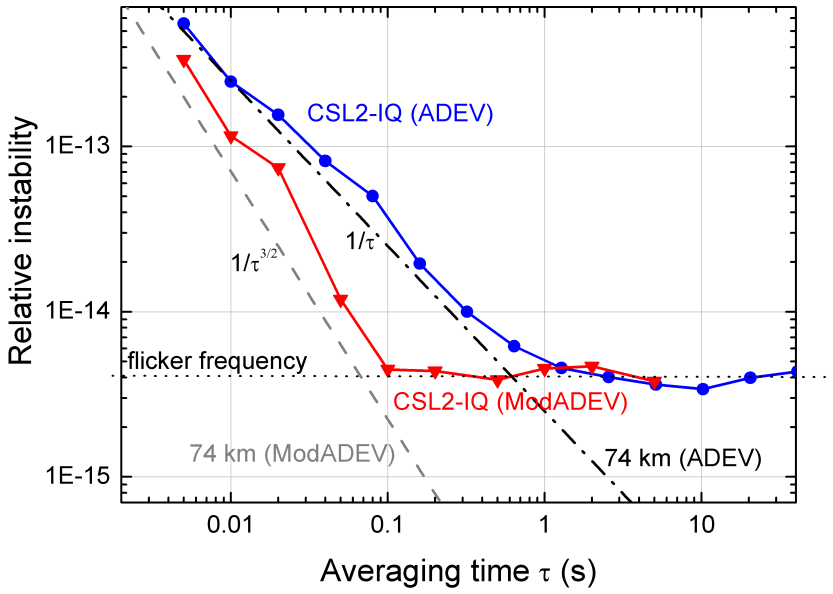

Figure 6.4: Relative instability of the CSL2-IQ laser measured with a Π-type frequency counter (blue dots) and with a Λ-type frequency counter (red triangle). The instability of the fiber transfer is shown as a black dashed-doted line for the ADEV and as gray dashed line for the ModADEV.

The ModADEV algorithm is used to distinguish flicker phase noise from white phase noise, while leaving the other types of noise (such as the flicker frequency noise) unaffected. In other words, it can be used to reduce the contribution of the white phase noise from $\sigma_y = 1/\tau$ to $\sigma_y = 1/\tau^{3/2}$. This white phase noise is mainly attributed to the fiber link. Therefore, using the ModADEV enables a faster measurement of the flicker frequency noise attributed to the frequency standard. Fig. (6.4), shows the ADEV of the white phase noise introduced by the 74 km fiber link which follows $1/\tau$ (black dashed-doted line). The instability curve is improved to

$1/\tau^{3/2}$ when applying the ModADEV (gray dashed line). By using the ModADEV, the instability of the CSL2-IQ reaches a flicker frequency floor of 4×10^{-15} from integration times of 0.1 s up to 30 s. In contrast, the ADEV reveals the flicker floor only after 1 s. Therefore, the frequency standard can be faster characterized by using the ModADEV.

6.3 Stability of the Mg-frequency standard

In the previous section, the lasers used to interrogate the "clock" transition ($^1S_0 - {}^3P_1$) in ^{24}Mg are characterized. The aim of this section is to characterize remotely those lasers after they are locked to this "clock" transition. An earlier measurement of the instability of the ^{24}Mg standard was limited by the instability of a portable Cs frequency standard (black squares in fig. 6.5) [29]. The short-term stability of the measurement could be improved using a transportable passive maser (H7). However, as indicated by the blue open circles, the measurement of the ^{24}Mg frequency standard is still limited by the instability of H7 and an even better frequency standard is required. The fiber link allows to benefit from frequency standards with superior stability at PTB; in the microwave domain (H5/CSF1) and in the optical domain (CSL-PTB laser).

Since the repetition frequency of the optical frequency comb at PTB is pre-stabilized to that of the H5, which is in turn corrected by CSF1 (the PTB primary frequency standard), the frequency of the NIR-PTB laser can be measured with respect to CSF1. Assuming that the fiber link adds negligible noise, then, the frequency of the NIR-PTB is the same as at IQ (NIR-IQ). At PTB, the frequency ratio ($\nu_{NIR-PTB}/\nu_{H5}$) results from the measurement of the frequency of the NIR-PTB against that of the H5. At IQ, the frequency ratio (ν_{NIR-IQ}/ν_{Mg}) results from the measurement of the frequency of the NIR-IQ against that of the Mg-standard. Synchronizing both measurements, allows one to eliminate the noise contribution of H7 and to relate the Mg-laser frequency to the primary standard at PTB (H5/CSF1). The result is shown as black open squares in fig. (6.5). Since the frequency instability of H5/CSF1 (dashed gray line) is lower than that of the remote Mg standard for τ >20 s, H5/CSF1 can be used to evaluate the long-term performance of the Mg frequency standard after only few minutes.

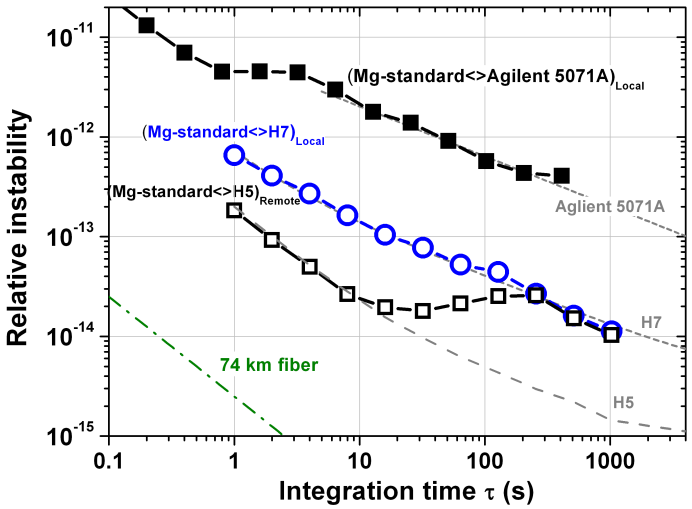

Figure 6.5: The relative instability of the Mg-standard against (H5/CSF1) at PTB (open squares), against H7 at IQ (blue open circles), and an earlier measurement against a portable Cesium clock (black squares) [29]. The instabilities of the H7, Agilent Cesium clock, and CSF1/H5 (grey dashed line), the fiber link (green-dashed line).

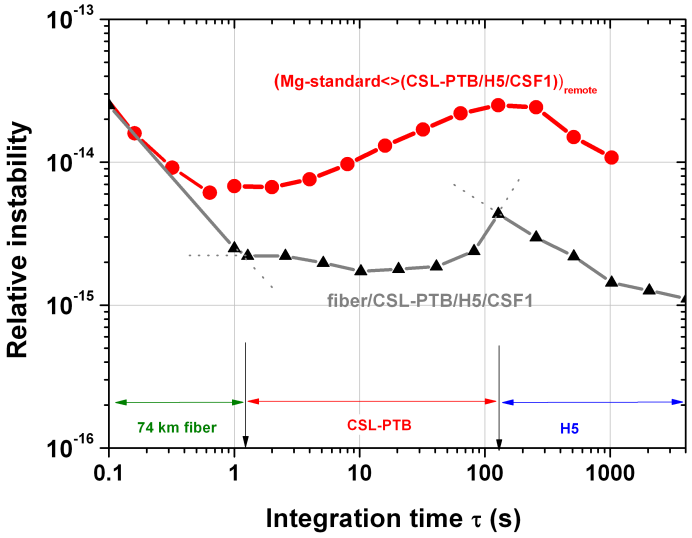

Figure 6.6: The relative instability of the Mg-standard measured against CSL-PTB laser (red dots) (a small linear cavity drift was removed). The instability contribution from different sources (black triangles).

However, to investigate the full performance of the Mg-standard at short and long time scales, an additional direct comparison with CSL-PTB is required. In order to measure the long term stability, a small drift of CSL-PTB is measured with respect to H5/CSF1. The red dots in fig. (6.6) show results of the Mg-standard for an integration time of 0.02 s$< \tau <$1000 s, derived from the measurement of the frequency ratio ($\nu_{Mg-laser}/\nu_{CSL-PTB}$). The black traingles show the contribution from different instability sources that may effect the measurement. Note that, using CSL-PTB together with the microwave frequency standards at PTB, the frequency of Mg-standard can be fully remotely characterized after only several seconds.

As discussed before, an upper limit of the accuracy of the frequency transfer over the 74 km fiber link is 1.3×10^{-19}. With such unprecedented transfer accuracy, the fiber link is used to remotely measure the absolute frequency of the Mg-laser with reference to the Cesium fountain at PTB. It also allows to investigate systematic frequency shift of the remote standard within several minutes. It was specially useful for determining the uncertainty contribution due to the pulsed Ramsey scheme used to interrogate the cold Mg atoms. The Mg-laser absolute frequency is found to be 655 659 923 839 796 (8) Hz. This value is not corrected for the systematic effects, for details about the systematic effects and the measurement of the Mg-laser absolute frequency please refer to the PhD thesis of Jan Friebe [68].

To conclude, the 74 km fiber link is used to remotely evaluate the short-term stability of the cavity stabilized lasers CSL-IQ at IQ against that of the PTB (CSL-PTB) within 0.1 s. It is used also to remotely evaluate the long-term stability of the Mg-laser with reference to the PTB primary frequency standard (CSF1). Due to the unprecedent accuracy in the frequency transfer, the fiber link is used also for the remote measurement of the absolute frequency of the Mg-laser with reference to CSF1. Moreover, it allows to evaluate systematic frequency shift of the Mg-laser within several minutes.

Chapter 7

Frequency transfer over 480 km fiber link using FBA

In the previous chapters, a frequency transfer over a distance of more than 140 km is demonstrated. Only one BEDFA was required to amplify the transfered optical signal over such a distance. For longer distances, a chain of BEDFA is required to amplify the optical signal. However, saturation of the gain medium and lasing effects are observed; as a consequence, the gain of the bi-directional EDFA has to be kept below 25 dB. For a typical attenuation of 0.2 dB/km for a typical optical communication fiber, the distance between two bi-directional EDFAs is therefore limited to about 125 km. In consequence, on long links the number of intermediate amplifier stations will increase, as well as the effort of controlling and maintaining these stations.

In order to keep the number of intermediate stations as low as possible, the FBA developed in chapter (4) is used. This technique enables the amplification of a very small input signal (a few nW) by more than 50 dB in a single gain step, with relatively low pump powers (about 30 mW). Moreover, it enables bi-directional amplification because it uses the fiber itself as the gain medium and different sections of the same fiber for each direction.

In this chapter, the capability to transfer an optical frequency over a 480 km fiber link using only one intermediate amplification station is investigated. The 480 km fiber link is constructed from two pairs of fibers connecting IQ, Hanover, PTB, Braunschweig, and a gasLINE station near Cörmigk. The four fibers are connected

to form a ring such that, it begins, passes through, and then ends at PTB. FBA's are used at the intermediate station, the input, and the output of the 480 km fiber.

7.1 Description of the fiber link

As discussed before in section (5.1), a dedicated pair of commercially single mode dark fibers (SMF28) is connecting (PTB) in Braunschweig to the Institute of Quantum Optics (IQ) at the university of Hanover (LUH) with a total fiber length of about 74 km. Another similar pair of fiber is connecting the PTB to a station in Cörmigk with a total fiber length of 166 km. This pair of fiber is a part of the link that connects PTB with the Max-Planck-Institute for Quantum Optics (MPQ) in Garching. A sketch of the fiber link is depicted in (7.1).

Both fibers in the pair (PTB - IQ) are connected at IQ to form a total fiber length of 148 km. The total attenuation at λ=1542 nm is about 45 dB. The other pairs (PTB - Cörmigk) are connected at Cörmigk forming a total length of 332 km. The total attenuation at λ=1542 nm for this 332 km long section is about 70 dB. Both pairs (PTB - IQ) and (PTB - Cörmigk) are connected at PTB to form a loop that starts, passes through and then ends at PTB. Thus, the total one-way length is 480 km with a total attenuation of 116 dB.

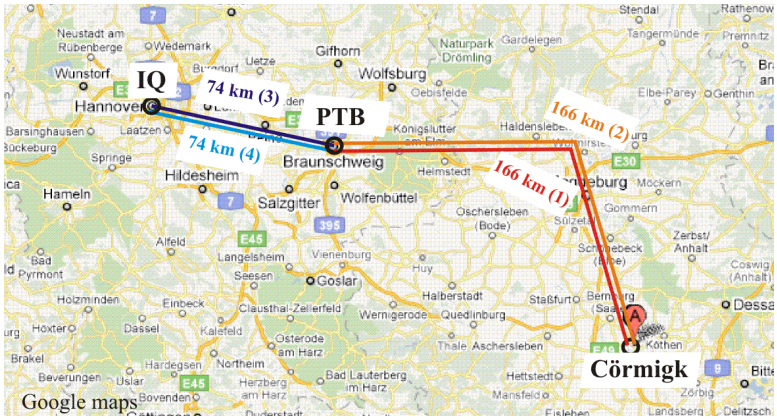

Figure 7.1: Fiber route between Cörmigk and IQ in Hanover passing through PTB in Braunschweig using a dedicated pair of dark fibers in a strand of commercially used fibers.

7.2 The frequency transmission setup

To transfer a stable optical frequency from one location to a remote user over an optical fiber link, phase noise accumulated along the fiber as well as attenuation have to be compensated. In this section we describe the transfer of an optical carrier over 480 km using the fiber stabilization scheme described in section (3.5), and an amplification scheme that utilizes FBAs, described in section (4.2.2), at each end of a 480 km fiber link and in one intermediate station only.

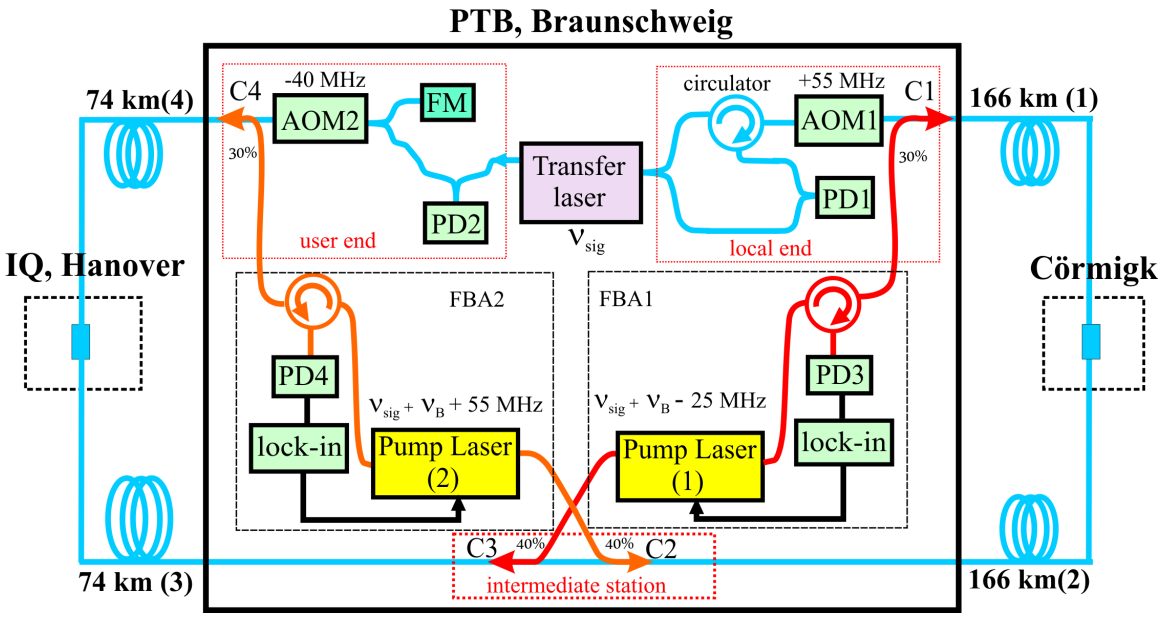

Figure 7.2: : Brillouin amplification in a frequency transfer system, AOM: Acousto-optic modulator, PD: photodetector, FM: Faraday mirror, C1: 30/70, C2: 40/60, C3:40/60, C4:30/70 simple fiber couplers.

In this setup local and user end as well as the intermediate station are located at PTB, which allows for easy testing. The light is sent in the first fiber (166 km) to Cörmigk, where it is returned to the intermediate station at PTB by the second fiber. The light is amplified and sent in the third fiber (74 km) to IQ, where it is connected to a fourth fiber to return the light back to PTB (the user end).

Fig. (7.2), demonstrate the frequency transfer system over 480 km fiber link. The phase noise compensation interferometer (PNCS) consists of AOM1, AOM2, PD1, PD2, circulator, FM, and some simple fiber couplers, for more details see chapter (3). A transfer laser is locked to an optical frequency standard with the help of a femtosecond frequency comb, see chapter (2).

For a full round-trip in the fiber the signal accumulates 232 dB loss before it reaches the phase compensation detector PD1. In order to compensate this loss, we used two FBA's for pumping four fiber sections. One FBA is used at the intermediate station to amplify the light in the return direction with a pump power of 45 mW and in the forward direction with a pump power of 30 mW. A second FBA with pump power of 9 mW amplifies the returned light, while the forward direction at the "virtual" user end is pumped with 18 mW. The pump light is injected into the fiber using simple fiber couplers with a coupling ratio depending on the available pump powers. The chosen coupling ratio compromises between signal loss at the expense of pump power loss. Because of the 80 MHz frequency difference between the forward and the return light introduced by the AOM, one amplifier is used for each direction. For the forward direction FBA2 is used with a frequency $\nu_{Fpump} = \nu_{sig} + \nu_B$+55 MHz and for the return direction FBA1 is used with a frequency $\nu_{Rpump} = \nu_{sig} + \nu_B$−25 MHz, where ν_B is the Brillouin frequency and ν_{sig} is the frequency of the transfer laser (signal).

As the gain of the FBA is $>$ 50 dB for an optical input power less than -50 dBm, it enables to bridge a distance of about 332 km without additional intermediate amplification stations. Thus, the overall distance of 480 km can be bridged with only one intermediate amplification station. The FBA is operated bi-directionally within the phase noise compensation interferometer. As we discussed in section (4.2), the ideal distance when using FBA is about 250 km. However, we still have a well detectable signal after a span of 332 km. The out-of-loop SNR is about 30 dB at BW=100 kHz, while the inloop is about 20 dB at 100 kHz. This SNR is enough for a stable operation of the phase noise compensation interferometer.

It is necessary to stabilize the frequency of the pump laser since it is drifting with time. However, stabilization within only ±5 MHz is required. In order to stabilize the pump laser, a part of the Brillouin-scattered light is directed by circulators to the DC photodetectors PD (3 and 4), where it is used to stabilize the frequency of the pump laser as discussed in section (4.2.4).

7.3 Frequency transfer stability and accuracy

A beat signal at the user end between the forward direction and the light from a reference arm (out-of-loop beat) measures the stability of the 480 km fiber link. The signal is analyzed in the frequency domain with a FFT spectrum analyzer; in the time domain we use a Π-type frequency counter with zero dead time. The phase noise of the out-of-loop beat is measured before and after applying the frequency/phase compensation by detecting the phase changes with respect to a reference oscillator using a digital phase detector [69]. Fig. (7.3) shows the phase noise in (rad^2/Hz) for the out-of-loop signal with and without compensation. The phase noise reduction is 39 dB at a Fourier frequency of 1 Hz. This is near to the theoretical limit of 41 dB at f=1 Hz predicted by Williams et al. [24]:

$$S_D = \frac{1}{3}(2 \times \pi)^2 \tau_{delay}^2 f^2 S_\phi(f) = 7.5 \times 10^{-5} f^2 S_\phi(f)$$

where $S_\phi(f)$ is the phase noise of the free-running fiber and f is the Fourier frequency. It is close to the optimum value (green-open circles in fig. (7.3)) up to the compensation bandwidth of about 100 Hz. The compensation bandwidth is $1/4\tau_{delay}$, where τ_{delay} is the one way time in the fiber.

Care must be taken not to include the phase noise of the laser during the compensation of the fiber noise through self-heterodyning. Since the linewidth of the transmitted laser is in order of 10 Hz, see section (2.2), we are not limited by the stability of the coherence length of the laser which is more than 3000 km. Therefore, the fiber stabilization beat still holds negligible laser noise due to self-heterodyning in the frequency range of interest.

We used a Π-type frequency counter with 1 second gate time to measure the frequency in the time domain and used the Allan deviation (ADEV) as a statistical measure of the frequency stability. Fig. (7.4) shows the ADEV of the out-of-loop signal before (black squares) and after (red-open circles) applying the phase compensation. After applying the compensation, the stability of the transferred frequency reaches $\sigma_y(\tau) = 2 \times 10^{-14}$ $/(\tau/\mathrm{s})$. This value is in good agreement with the value calculated from the phase noise (see Fig. (7.3)). The ADEV curve follows a $1/\tau$ slope and reaches a value of 2×10^{-18} after about 2 hours.

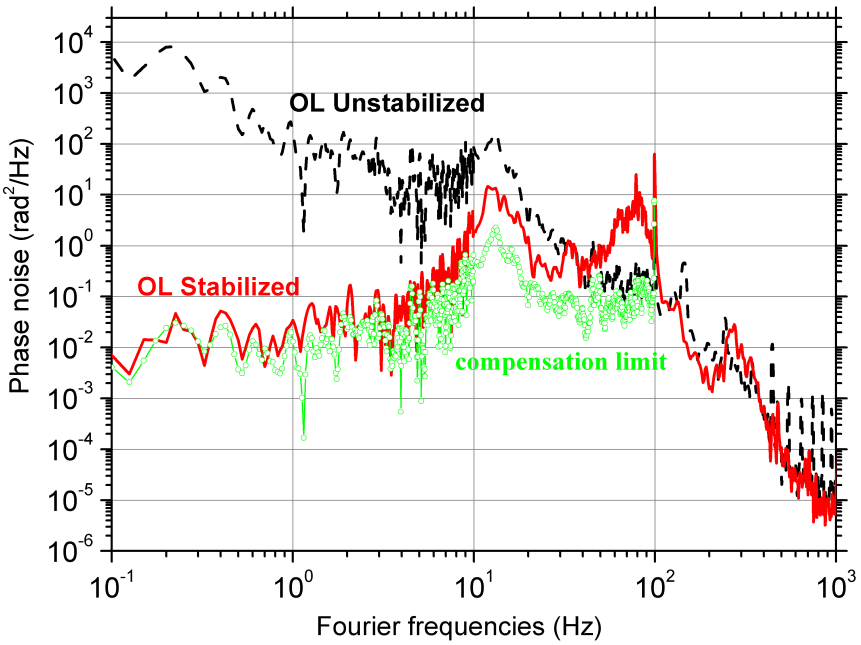

Figure 7.3: Phase noise of the out-of-loop signal (OL) before (black dashed), and after (red solid) phase compensation. The green-open circles give the theoretical compensation limit according to [24].

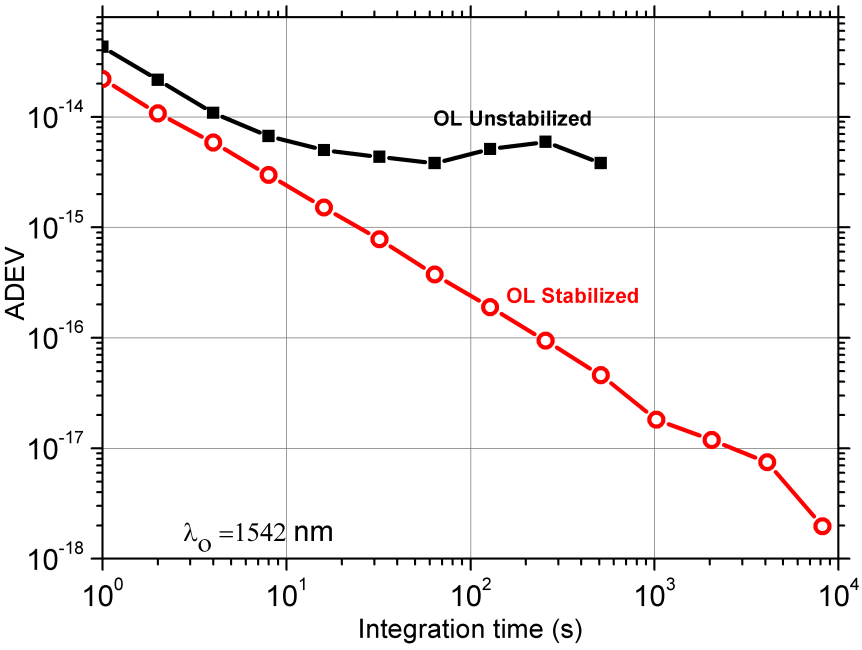

Figure 7.4: Out-of-loop signal (OL) with compensated (red-open circles) and uncompensated phase noise (black-squares).

Fig. (7.5) shows a time record of the frequency deviation $\Delta\nu$ of the transmitted signal from its nominal value of 15 MHz. The observed mean deviation of the transmitted optical carrier frequency given by the sample average of the full data set was 64 μHz with a statistical uncertainty of 54 μHz. The statistical uncertainty is obtained by dividing the standard deviation of the measurement by N since it is white phase noise and not by $\sqrt{N}$, as discussed in [66], where N = 65000 is the total number of data points. The relative frequency uncertainty of the averaged frequency deviation is 3.3×10^{-19}.

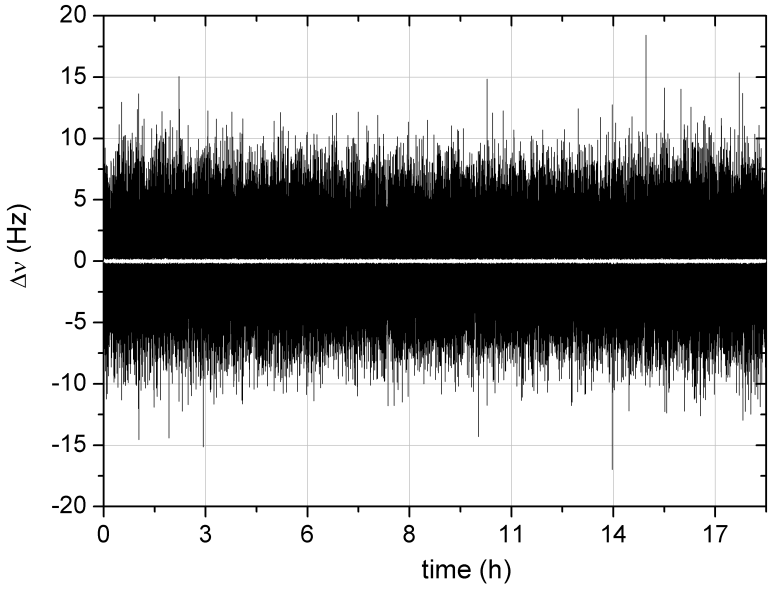

Figure 7.5: Time record of the frequency deviation of the transmitted signal from its nominal value of 15 MHz over a measurement time of 17 hours

In this chapter, the FBA is implemented for an ultrastable frequency transfer over 480 km fiber link using only one intermediate amplification station, together with FBA's at the remote and the local ends. The FBA is found to be able to bridge a distance of about 332 km without additional intermediate amplification stations. The FBA enables low phase noise bi-directional optical amplification, and it allows a frequency transfer over the 480 km fiber link with a relative instability of $\sigma_y(\tau)$=$2\times10^{-14}/(\tau/\mathrm{s})$ and a relative statistical uncertainty of 3×10^{-19}. This performance together with the bidirectional operation and the high gain ($> 50dB$) makes the FBA suitable for the implementation in a Eurpean fiber network for frequency transfer.

Chapter 8

Towards a European fiber network for frequency dissemination

In the previous chapters, a stable frequency has been transmitted over a distance of up to 480 km. Optical amplifiers were used to enable optical frequency transfer over such along distances. A simple BEDFA was used to bridge distance of 146 km. For longer distances, a chain of BEDFA is required to transfer the optical signal. However, saturation of the gain medium and lasing effects were observed. In consequence the gain of the bi-directional EDFA had to be kept below 25 dB. As an alternative to the BEDFA, The fiber Brillouin amplifier (FBA) was implemented for long distances. The FBA enables the amplification of a very small input signal (a few nano Watt) by more than 50 dB in a single gain step, see chapter (4). It is also possible to combine both FBA and BEDFA as will be shown for the 900 km fiber link discussed in this chapter.

The optical frequency transfer between PTB at Braunschweig and Max-Plank Institute for Quantum Optics (MPQ) in Garching over a distance of about 900 km of fiber is currently investigated. This link will enable a remote frequency comparison between a hydrogen optical frequency standard at MPQ and those at PTB.

All necessary steps to establish a fiber network connecting European laboratories which host optical frequency standards can be tested with this 900 km link. A plan to connect PTB to the LNE-SYRTE in Paris with fiber link of more than 1000 km is in preparation.

In this chapter, the 900 km link between PTB and MPQ is shortly described

and the expected stability of this link is discussed. The current optical amplification scheme is described. Finlay, the optical frequency standard laboratories in Europe are mentioned and the possible fiber network between them is sketched.

8.1 Towards a frequency comparison over 900 km (PTB-MPQ)

For a comparison of frequency standards at PTB-Braunschweig with those at MPQ-Garching, a dedicated pair of commercially single mode dark fibers (SMF28) connects both institutes with a total fiber length of about 900 km. The 900 km fiber route is shown in fig. (8.1). Eight containers are rented from GasLINE company in order to install the optical amplifiers (bi-directional EDFA).

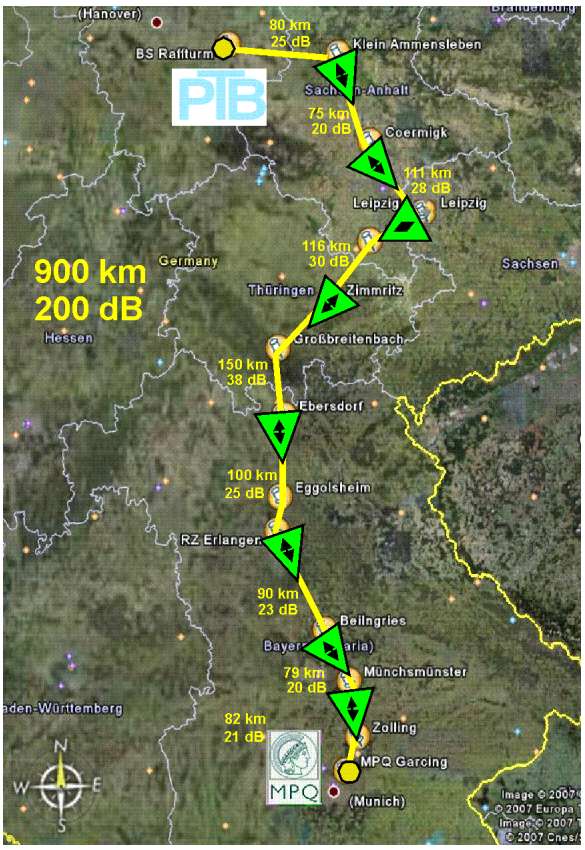

Figure 8.1: Route of the 900 km fiber link connecting PTB, Braunschweig to MPQ, Garching. Eight intermediate bi-directional EDFA amplification stations are used to amplify the optical signal. [source: google maps]

Since the fibers are part of a commercial network, safety precautions have to

be considered. One of these safety precautions is that the station can be remotely shut-down in the case of maintenance or at the occurrence of an error, like a fiber damage. Additionally, to obtain stable operation of the full link the BEDFA pump laser power should be optimized remotely on each amplification station. As external control of the stations is not provided by the fiber provider, optical communication between amplification stations using the same dark fiber needs to be established. A laser diode emitting at 1.3 μm with an optical power of about 1 mW is used to transmit control signals together with the 1.5 μm light from the local or remote fiber ends to each station. Wavelength division multiplexers (WDM) are used to separate and combine both wavelengths. In SMF-28 fibers, light at 1.3 μm is attenuated by about 0.3 dB/km, which means that the distance between stations should not exceed 100 km.

Distances between the stations and the corresponding attenuation of the fiber sections are given in fig. (8.1) and in table (8.1) for clarification.

Stations	Distance	Attenuation@1.5μm
PTB-Ammensleben	80 km	25 dB
Ammensleben-Cörmigk	75 km	20 dB
Cörmigk-Leibzig	111 km	28 dB
Leibzig-Zimmritz	116 km	30 dB
Zimmritz-Ebersdorf	150 km	38 dB
Ebersdorf-Erlangen	100 km	25 dB
Erlangen-Beilngries	90 km	23 dB
Beilngries-Müchsmünster	79 km	20 dB
Müchsmünster-MPQ	82 km	21 dB
Total	883 km	230 dB

Table 8.1: Distance and attenuation between the stations.

The fiber section between Zimmritz and Ebersdorf has a distance of about 150 km and an attenuation of about 38 dB at 1.5μm. According to section (4.2), this should degrade the SNR of the transmitted signal by about 10 dB. Indeed, we observed degradation of SNR after this connection, therefore, a BEDFA will be installed in Grossbreitenbach to enhance SNR of the transmitted signal.

There are two fibers installed between MPQ and PTB. Both fibers are stabilized independently to verify the performance of the link. In order to implement the phase noise compensation scheme the signal has to make a round-trip in the 900 km fiber. Since the gain of the BEDFA was only enough to transmit the light in one direction, a fiber Brillouin amplifier (FBA) is used to amplify the light by about 50 dB before sending it back in the fiber. For the first fiber, the light follows the route MPQ-PTB-MPQ and the stabilization is applied at MPQ while the FBA amplification is applied at PTB. For the second fiber, the light follows the route PTB-MPQ-PTB and the stabilization is applied at PTB while the amplification is applied at MPQ.

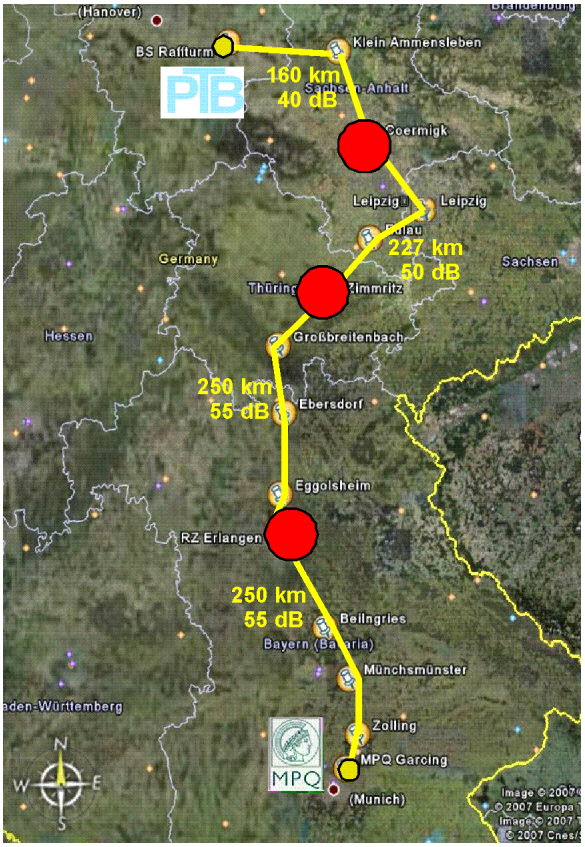

Figure 8.2: Future scheme of the 900 km fiber link connecting PTB to MPQ. Only three intermediate FBA amplification station are required. [source: google maps]

In future, one can think of using FBA optical amplifier stations instead of the recently installed bi-directional EDFA stations. By applying this amplification technique, only three intermediate FBA stations are sufficient, see fig. (8.2).

Using FBA, only three stations should be installed at a maximum distance of

about 250 km without intermediate amplification stations. Another two FBA amplifiers should be used at MPQ and at PTB in order to detect the round trip light at PTB. This method is not yet implemented since the BEDFA is already installed in the PTB-MPQ route.

8.1.1 Expected frequency stability of the 900 km link

As reported by Williams et al. [24], the instability of the phase noise compensated fiber link scales approximately as $L^{3/2}$. Therefore, the instability of the 900 km fiber link (PTB-MPQ) can be predicted from the instability of the 146 km and the 480 km fiber links discussed in chapters (5, 7), assuming that the phase noise is uniformly distributed along the fiber. Since the instability of the 146 km stabilized fiber link is 3.3 $\times 10^{-15}/(\tau/\mathrm{s})$, the expected instability of the 480 km fiber can be obtained by applying the scaling law $\sigma_y \propto L^{3/2}$ [24] as follows:

$$[\sigma_y(1s)]_{480\ km-expected} = 3.3 \times 10^{-15}(\frac{480\ km}{146\ km})^{3/2} \approx 2 \times 10^{-14}$$

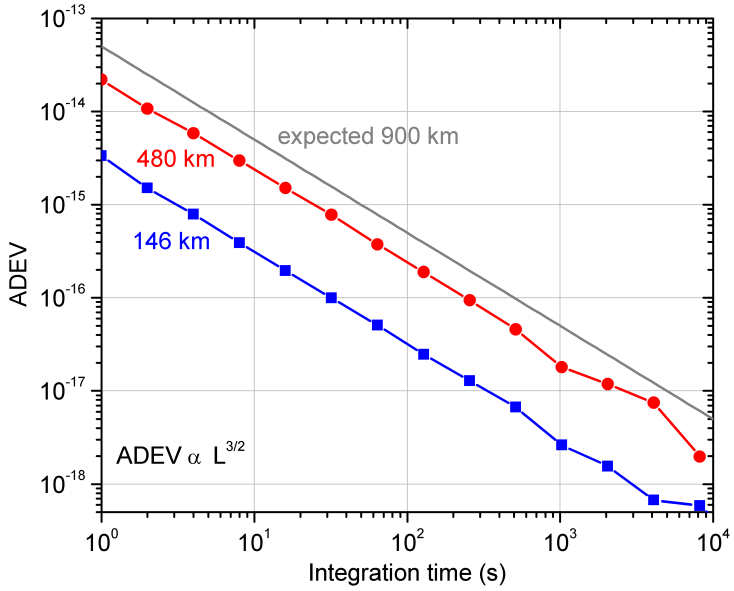

Figure 8.3: The measured instability for the stabilized 146 km (blue squares), 480 km (red dots) fiber links. The expected instability of the 900 km fiber link can be derived from the measured instability of the previous link applying the scaling law $\sigma_y \propto L^{3/2}$ [24].

From chapter (7), the measured instability of the 480 km is $\sigma_y(\tau)$=$2\times10^{-14}/(\tau/\mathrm{s})$

which is in good agreement with this prediction. The expected instability of the 900 km can be derived in similar manner as follows:

$$[\sigma_y(\tau)]_{900\ km-expected} = 3.3 \times 10^{-15}/(\tau/s)(\frac{900\ km}{146\ km})^{3/2} \approx 5 \times 10^{-14}/(\tau/s)$$

This link will be used to measure the instability of the optical hydrogen frequency standard in MPQ, which has an uncertainty of 1.4×10^{-14} [70]. The remote measurement of the frequency with such uncertainty is possible after only few seconds.

For future measurements of better frequency standards in MPQ, the stability of the fiber link can be improved by installing intermediate compensation modules. By this way the link will be divided into sections. Therefore, the instability scaling model with $L^{3/2}$ is then applied to each section of the fiber link to get its expected instability separately. The total link instability is obtained by applying the root-sum-of-squares (RSS) to these instabilities. For example, consider that a fiber with length L is divided into two sections L_1, L_2. The total link stability will be then

$$[\sigma_y]_{L-devided} = [\sigma_y]_L \sqrt{\frac{L_1^3 + L_2^3}{L^3}}$$

The stability of the divided link should then be better than the undivided link since $\sqrt{\frac{L_1^3+L_2^3}{L^3}} \leq 1$. For the case of 900 km link, the link can be divided as follows L_1=400 km and L_2=500 km. The reduced instability is then 2.5×10^{-14}.

8.1.2 Towards a European fiber network

A number of European laboratories have optical frequency standards based on cold atoms and ions. For example, PTB at Braunschweig has Yb^+, Ca, and Sr based optical frequency standards, the Center for Quantum Engineering and Space-Time research (QUEST) at Braunschweig currently develops an Al^+ based optical frequency standard, IQ at Hanover has a Mg based optical frequency standard, MPQ at Garching has a H based optical frequency standard, SYRTE at Paris has Sr and Hg based optical frequency standard, NPL at London has Yb^+ and Sr^+ based optical frequency standards, and INRIM at Turin has Yb based optical frequency standard. Those laboratories are shown in fig. (8.4).

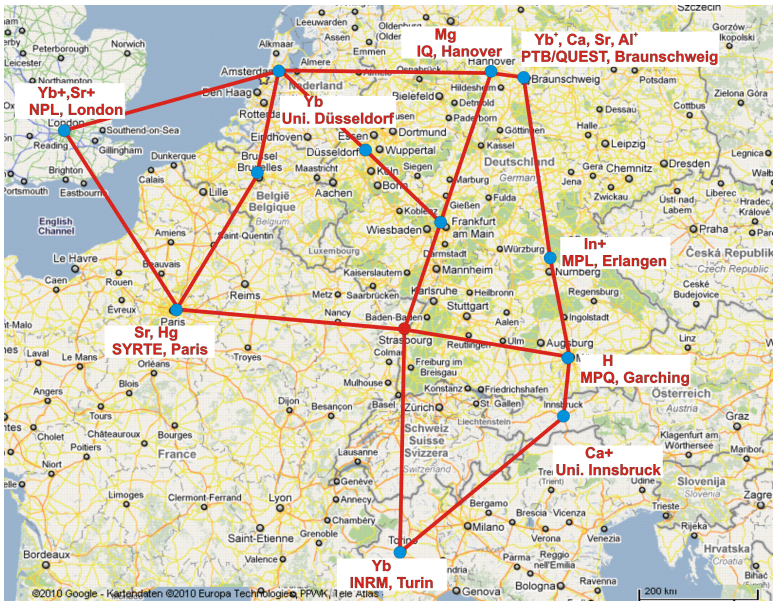

Figure 8.4: European laboratories which has optical frequency standards. Possible fiber link route between those laboratories is sketched.

In order to investigate the stability of those optical frequency standards, they must be compared with other optical frequency standards with similar performance. As shown in fig. (8.4), the distance between optical frequency standards can reach up to 1500 km. As none of these optical frequency standards is portable and the stability of the frequency comparison over GPS satallites is not sufficient, the only possible way is to compare those frequency standards over optical fiber links. Based on existing fiber networks, a network could be established as sketched in fig. (8.4) that connects European metrology institutes and other laboratories operating high performance frequency standards.

Currently, a first fiber link between PTB and Observatoir de Paris (SYRTE) in Paris over about 1300 km is discussed, that could serve as a backbone for the future European network.

Conclusion

In this thesis, the ability of optical fiber links to transfer ultrastable optical frequencies has been studied. For the first time worldwide, it has been shown that telecommunication fibers with lengths up to about 500 km are suitable to remotely compare the best available optical clocks within only few seconds [19, 21]. At this level of accuracy, a remote comparison is only possible after compensating the phase noise induced by the optical fiber due to thermal and acoustic fluctuations.

In order to detect and compensate the phase noise introduced by the fiber link, an all-in-fiber system has been developed. In order to test the best achievable phase noise compensation, the interferometer is stabilized after being connected to a short fiber. It reaches a relative instability of $\sigma_y(\tau) = 2\times10^{-17}/(\tau/\mathrm{s})$ that drops below 10^{-20} after about one hour [19]. Even for the free-running interferometer the relative instability reaches a flicker floor of 1×10^{-18} after a few seconds. This extremely low noise floor was achieved by the careful design of the interferometer.

The phase noise compensation interferometer has been implemented to test the ultrastable frequency transfer over a telecommunication fiber link of 146 km. The 146 km fiber consists of two 73 km fibers connecting the Physikalisch-Technische Bundesanstalt (PTB) in Braunschweig to the Leibniz University of Hanover (LUH). At PTB a cavity stabilized laser operating at a wavelength of 657 nm was used as optical frequency reference. In order to transmit the stability of this standard through such a long fiber without suffering huge attenuation, a telecommunication laser at a wavelength of 1542 nm is used as a transfer laser. This laser is phase locked to PTB's frequency standard by means of femtosecond frequency comb. Thus, it exhibits the same stability as the optical reference. To balance the attenuation of the fiber, one bi-directional erbium doped fiber amplifier (BEDFA) is used at the remote end. Over the 146 km fiber, the frequency transfer has been performed with a relative uncertainty below 1×10^{-19} and a relative instability of $\sigma_y(\tau) =$

$3.3\times10^{-15}/(\tau/\mathrm{s})$, limited by the time delay introduced by the link [19, 71, 72].

This technique has been applied to remotely characterize ultrastable lasers at IQ and to measure the frequency of an optical frequency standard at the Institute of Quantum Optics (IQ) in LUH against that of PTB using one of the tested fibers. The frequency standard at IQ is a cavity stabilized laser which is locked to the $^1\mathrm{S}_0-^3\mathrm{P}_1$ transition in the ^{24}Mg atom. The cavity stabilized laser at 914 nm is frequency doubled to match the transition frequency. In addition to the femtosecond comb at PTB, another comb is used at IQ to compare the frequency of the Mg standard frequency with that of the transmitted light from PTB. The ratio between the frequencies of the transfered light from PTB and the Mg interrogation laser showed a relative short term instability of about $\sigma_y = 4 \times 10^{-15}$ at 0.1 s limited by the instability of the Mg laser [67, 20].

For longer distances, a chain of BEDFA is required to transfer the optical signal with minimized loss. By using a chain of BEDFA, a saturation of the gain medium and lasing effects is observed. Therefore, the gain of the bi-directional EDFA has to be kept below 25 dB, which allows to bridge distances of about 120 km. The fiber Brillouin amplifier (FBA) is introduced as an alternative to the BEDFA for longer distances. The FBA enables the amplification of a very small input signal (a few nano Watt) by more than 50 dB in a single gain step. This enables to bridge distances of about 250 km in one step. This technique has been implemented to demonstrate an ultrastable frequency transfer over a 480 km fiber link with only one intermediate amplifier station, and additional amplifiers at the remote, and the local ends. The relative instability of the frequency transfer was $\sigma_y(\tau)=2\times10^{-14}/(\tau/\mathrm{s})$ and reached 2×10^{-18} after about two hours. The mean value of the transmitted frequency was shifted from that of the reference laser by 64 μHz with a statistical uncertainty of 54 μHz. This shift corresponds to fractional frequency deviation of 3×10^{-19} [21].

In collaboration with the Max-Planck Institute of Quantum Optics (MPQ) in Garching, a fiber link of about 900 km has been established. This allows to compare frequency standards at MPQ with those at PTB. Eight BEDFA stations are installed along the fiber route to maintain the required power level and the signal to noise ratio (SNR) of the transmitted signal. All stations are controlled remotely using another wavelength at 1.3 μm and built-in microcontroller with specially designed software. The BEDFA stations have been installed before testing the FBA. However,

one FBA is installed in addition to the BEDFA stations at the remote end. This allows to fully recover the power level before the light is sent back to the local end to implement the phase noise compensation. Further development in this link is still in process. The result obtained from this link will help to establish an European fiber network for frequency comparison of remote clocks. It will help particularly to know how many amplification stations are required for such links, to examine the remote control over a large number of amplification stations, to examine the scaling of the achievable stability with increasing the length, or to discover any other effects that could degrade the frequency transfer stability.

Appendix A

Model for phase noise compensation

In this appendix, a derivation for the relation between the round-trip and one-way phase noise for light propagating through a fiber is given, with some more details to what is given in [73]. After applying the phase noise compensation scheme described in section (3.5), the remaining phase noise at the remote user end is derived, with some more details to the derivation given in [24].

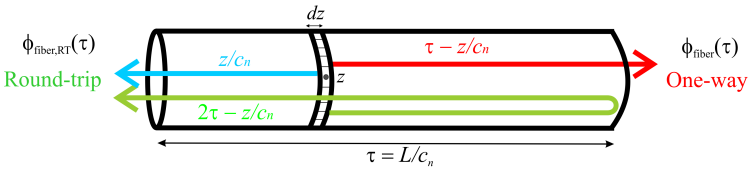

Figure A.1: Round-trip and one-way detection of an event take place at position z along a fiber with length (L).

Any acoustic or thermal perturbation over the fiber will induce a phase shift $\delta\varphi(z,t)$ of the frequency of the light passing the fiber at time t and position z, see fig. (A.1). This phase noise will accumulate as the light travels in the fiber. The accumulated phase noise in the forward direction from the position $z = 0$ to $z = L$ at time t is

$$\varphi_{fiber}(t) = \int_0^L \delta\varphi(z, t - (\tau - z/c_n))dz \tag{A.1}$$

where $\tau = L/c_n$ is the propagation delay in the fiber, c_n is the speed of light in the fiber.

Part of this light is then returned back in the fiber for phase noise detection and compensation. The Phase noise accumulated by the round-trip light at a time t is

$$\varphi_{fiber,RT}(t) = \int_0^L [\delta\varphi(z, t - z/c_n) + \delta\varphi(z, t - (2\tau - z/c_n))]dz \tag{A.2}$$

The above equations are in the time domain. Using Fourier transform, both equations are transformed to the frequency domain. Fourier transformation of a time shift a is $F[f(t-a)] = e^{-ia\omega}\tilde{f}(\omega)$. Then equation (A.1) becomes

$$\tilde{\varphi}_{fiber}(\omega) = \int_0^L e^{-i\omega(\tau - z/c_n)}\delta\tilde{\varphi}(z,\omega))dz \tag{A.3}$$

The Fourier transformation of equation (A.2) is

$$\tilde{\varphi}_{fiber,RT}(\omega) = \int_0^L [e^{-i\omega(z/c_n)} + e^{-i\omega(2\tau - z/c_n)}]\delta\tilde{\varphi}(z,\omega))dz$$

$$\tilde{\varphi}_{fiber,RT}(\omega) = \int_0^L e^{-i\omega\tau}[e^{i\omega(\tau - z/c_n)} + e^{-i\omega(\tau - z/c_n)}]\delta\tilde{\varphi}(z,\omega))dz$$

Since $e^{ix} + e^{-ix} = 2cosx$

$$\tilde{\varphi}_{fiber,RT}(\omega) = 2\int_0^L e^{-i\omega\tau}cos(\omega(\tau - z/c_n))\delta\tilde{\varphi}(z,\omega)dz \tag{A.4}$$

The phase noise spectral density is defined to be $S(\omega) = \left\langle|\tilde{\varphi}(\omega)|^2\right\rangle$. The fiber lies in different locations and thus is affected by independent noise sources. Hence , the phase noise of the light inside the fiber is uncorrelated in position. Accordingly, we have to get the phase spectral density for one element in the fiber then integrate it for all the fiber length. From equation (A.3) and since ($|e^{ix}|^2 = e^{ix}e^{-ix}$) the phase noise spectral density of one element $dS_{fiber}(\omega, z)$ in the one-way light is

$$dS_{fiber}(\omega, z) = \left\langle|\delta\tilde{\varphi}(\omega, z)|^2\right\rangle$$

by integrating the above equation for the whole fiber:

$$S_{fiber}(\omega) = \int_0^L \left\langle|\delta\tilde{\varphi}(\omega, z)|^2\right\rangle dz = L \times dS_{fiber}(\omega, z) \tag{A.5}$$

By the same way, for an element the phase noise spectral density $dS_{fiber,RT}(\omega, z)$ in the round-trip light is

$$dS_{fiber,RT}(\omega, z) = 4 \left\langle |cos(\omega(\tau - z/c_n))|^2 \right\rangle \left\langle |\delta\tilde{\varphi}(z,\omega)|^2 \right\rangle$$

since

$$\left\langle |\delta\tilde{\varphi}(\omega, z)|^2 \right\rangle = dS_{fiber}(\omega, z) = \frac{S_{fiber}(\omega)}{L}$$

then

$$S_{fiber,RT}(\omega) = 4\frac{S_{fiber}(\omega)}{L} \int_0^L \left\langle |cos(\omega(\tau - z/c_n))|^2 \right\rangle dz$$

since $cos^2 x = \frac{1}{2}(1 + cos2x)$

$$S_{fiber,RT}(\omega) = 2\frac{S_{fiber}(\omega)}{L} \left\langle \int_0^L [1 + cos(2\omega(\tau - z/c_n))] dz \right\rangle$$

by solving the integration

$$S_{fiber,RT}(\omega) = 2\frac{S_{fiber}(\omega)}{L}[L + \frac{L}{2\omega\tau} sin(2\omega\tau)]$$

since $sinc(x) = sin(x)/x$

$$S_{fiber,RT}(\omega) = 2S_{fiber}(\omega)[1 + sinc(\frac{2\omega L}{c_n})] \tag{A.6}$$

At low frequencies ($sinc(0) \approx 1$) the round-trip phase noise is four times larger than the one-way phase noise, and only two times larger at higher frequencies.

We used a phase-locked-loop (PLL) to compensate the phase noise induced by the fiber on the one way light. The phase noise of the round-trip light is detected after beating with a reference light with negligible phase noise, converted to voltage with a gain G_o , filtered with a transfer function $F(\omega)$, converted to frequency using voltage to frequency converter (VCO) with transfer function $(K/i\omega)$, and then sent to VCO to control an Acousto-optic modulator(AOM) which compensates the phase changes in the transfered frequency. Light passes the compensation system (through AOM) two times, forward and return. The system transfer function for the forward light is $H(\omega)$ and for the return light after round-trip time of 2τ is $H(\omega)e^{-2i\omega\tau}$, where $H(\omega) = G_o F(\omega)K/(i\omega)$, see fig. (A.2). Therefore, the transfer function of the compensation system (open loop gain) [55] is

$$G(\omega) = G_o F(\omega)(i\omega)^{-1} K(1 + e^{-2i\omega\tau}) \tag{A.7}$$

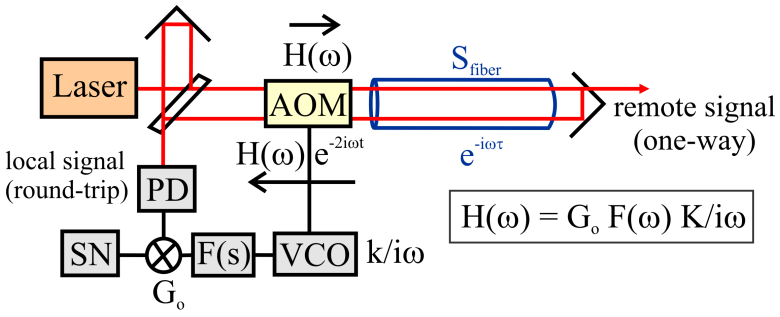

Figure A.2: Phase noise compensation scheme transfer function, SN: frequency synthesizer, PD: photodetector.

The compensated round-trip signal is obtained by applying the error transfer function $1/(1+G(\omega))$ to the round-trip phase noise:

$$\tilde{\varphi}_{local}(\omega) = \frac{1}{1+G(\omega)}\tilde{\varphi}_{fiber,RT}(\omega) \tag{A.8}$$

The phase noise spectral density of equation (A.8) is

$$S_{local}(\omega) = \left|\frac{1}{1+G(\omega)}\right|^2 S_{fiber,RT}(\omega) \tag{A.9}$$

The phase and magnitude of the PLL can be obtained from equation (A.7) as following

$$G(\omega) = G_o F(\omega)\frac{K}{i\omega}(1+e^{-2i\omega\tau})$$

since $e^{-ix} = cosx - isinx$

$$G(\omega) = G_o F(\omega) K(\frac{1}{i\omega} + \frac{cos(2\omega\tau) - isin(2\omega\tau)}{i\omega})$$

$$= \frac{G_o F(\omega) K}{\omega}[-i(1+cos(2\omega\tau)) - sin(2\omega\tau)]$$

Then magnitude of the gain $A^2 = Re^2 + Im^2$ is

$$A^2(\omega) = (\frac{G_o F(\omega) K}{\omega})^2[(1+cos(2\omega\tau))^2 + sin^2(2\omega\tau)]$$

$$= (\frac{G_o K}{\omega})^2[1 + 2cos(2\omega\tau) + cos^2(2\omega\tau) + sin^2(2\omega\tau)]F^2(\omega)$$

$(sin^2 x + cos^2 x = 1)$

$$= (\frac{G_o F(\omega) K}{\omega})^2 [2 + 2cos(2\omega\tau)]$$

since $1 + cos(2\omega\tau) = 2cos^2(\omega\tau)$ then

$$A(\omega) = \frac{2G_o F(\omega) K}{\omega} cos(\omega\tau) \tag{A.10}$$

The phase of the gain transfer function $\phi = tan^{-1}(\frac{Im}{Re})$ is

$$\phi = tan^{-1}(\frac{1 + cos(2\omega\tau)}{sin(2\omega\tau)})$$

since $(sin2x = 2sinx\ cosx)$ and $(cos2x = 2cos^2 x - 1)$ then

$$\phi = tan^{-1}(\frac{cos(\omega\tau)}{sin(\omega\tau)}) = tan^{-1}(cot(\omega\tau)) = tan^{-1}(-tan(\omega\tau + \pi/2))$$

$$\phi = -(\omega\tau + \pi/2) \tag{A.11}$$

The magnitude of the gain becomes zero and the phase becomes $-\pi$ when $f = 1/4\tau$. However, we can compensate for phase noise when $\phi \leq \pi/2$, and hence for frequencies below $f = 1/2\tau$. Oscillations in the compensated phase noise occur if we try to compensate noises at Fourier frequencies $f > 1/4\tau$.

When the error signal is applied to the round-trip signal, the phase noise of the round-trip and the one-way will be compensated. Due to the delay of light into the long fiber, not all the phase noise can be compensated. The remaining noise in the one-way light (remote-signal) can be obtained if we consider a double pass through the AOM for the one-way light, see fig. (A.2). The compensated one-way signal is obtained by applying the one-way transfer function H(ω) $e^{-i\omega\tau}$ to the compensated round-trip phase noise in eq. (A.8). The remaining phase noise in the one-way signal can be obtained by subtracting the compensated one-way phase noise from the uncompensated one:

$$\tilde{\varphi}_{remote}(\omega) = \tilde{\varphi}_{fiber}(\omega) - G_o F(\omega) i\omega^{-1} K e^{-i\omega\tau} \tilde{\varphi}_{local}(\omega)$$

From equation (A.8)

$$= \tilde{\varphi}_{fiber}(\omega) - \frac{G_o F(\omega) i\omega^{-1} K e^{-i\omega\tau}}{1+G(\omega)} \tilde{\varphi}_{fiber,RT}(\omega)$$

$$= \tilde{\varphi}_{fiber}(\omega) - \frac{G_o F(\omega) i\omega^{-1} K e^{-i\omega\tau}}{1+G(\omega)} \tilde{\varphi}_{fiber,RT}(\omega) \frac{G(\omega)}{G(\omega)}$$

using equation (A.7)

$$= \tilde{\varphi}_{fiber}(\omega) - \frac{G(\omega)}{1+G(\omega)} \frac{e^{-i\omega\tau}}{1+e^{-2i\omega\tau}} \tilde{\varphi}_{fiber,RT}(\omega)$$

$$= \tilde{\varphi}_{fiber}(\omega) - \frac{G(\omega)}{1+G(\omega)} \frac{1}{e^{i\omega\tau}+e^{-i\omega\tau}} \tilde{\varphi}_{fiber,RT}(\omega)$$

$$\tilde{\varphi}_{remote}(\omega) = \tilde{\varphi}_{fiber}(\omega) - \frac{G(\omega)}{1+G(\omega)} \frac{1}{2cos(\omega\tau)} \tilde{\varphi}_{fiber,RT}(\omega) \tag{A.12}$$

If we consider frequencies below the PLL bandwidth, where the gain $G(\omega) \to \infty$ then $[G(\omega)/(1+G(\omega))] \to 1$ and using the equations (A.3, A.4) then equation (A.12) becomes

$$\tilde{\varphi}_{remote}(\omega) = \int_0^L e^{-i\omega\tau - \omega z/c_n} \delta\tilde{\varphi}(z,\omega) dz -$$

$$\frac{1}{2cos(\omega\tau)} \int_0^L e^{-i\omega\tau} cos(\omega\tau - \omega z/c_n) \delta\tilde{\varphi}(z,\omega) dz$$

$$= e^{-i\omega\tau} \int_0^L \delta\tilde{\varphi}(z,\omega) [e^{-i\omega(z/c_n)} - \frac{cos(\omega\tau - \omega z/c_n))}{cos(\omega\tau)}] dz$$

$$= e^{-i\omega\tau} \int_0^L \delta\tilde{\varphi}(z,\omega) [cos(\omega z/c_n) + isin(\omega z/c_n) - \frac{cos(\omega\tau)cos(\omega z/c_n)}{cos(\omega\tau)} + \frac{sin(\omega\tau)sin(\omega z/c_n)}{cos(\omega\tau)}] dz$$

$$\tilde{\varphi}_{remote}(\omega) = e^{-i\omega\tau} \int_0^L \delta\tilde{\varphi}(z,\omega) [i - tan(\omega\tau)] sin(\omega z/c_n) dz$$

The phase noise spectral density is then

$$S_{remote}(\omega) = \left\langle \left| \int_0^L \delta\tilde{\varphi}(z,\omega) [i - tan(\omega\tau)] sin(\omega z/c_n) dz \right|^2 \right\rangle \tag{A.13}$$

since at low frequencies, inside the unity gain bandwidth, $tan(\omega\tau) \to \omega\tau$ and $sin(\omega z/c_n) \to \omega z/c_n$ then

$$S_{remote}(\omega) = \left\langle \left| \int_0^L \delta\tilde{\varphi}(z,\omega)[i-\omega\tau](\omega z/c_n)dz \right|^2 \right\rangle$$

$$= (1+\omega^2\tau^2)(\omega^2/c_n^2)\int_0^L z^2 \left\langle |\delta\tilde{\varphi}(z,\omega)|^2 \right\rangle dz$$

since at low frequencies ($\omega^2\tau^2 << 1$) and since $c_n = L/\tau$ then

$$= \frac{\omega^2\tau^2}{L^2}\int_0^L z^2 \left\langle |\delta\tilde{\varphi}(z,\omega)|^2 \right\rangle dz$$

from eq. (A.5), since

$$\left\langle |\delta\tilde{\varphi}(\omega,z)|^2 \right\rangle = dS_{fiber}(\omega,z) = \frac{S_{fiber}(\omega)}{L}$$

then

$$S_{remote}(\omega) = \frac{\omega^2\tau^2}{L^3} S_{fiber}(\omega)\int_0^L z^2 dz$$

again since the noise in the fiber is uncorrelated in position, we have to get the phase spectral density for one element in the fiber then integrate it for all the fiber length. We also assume that the phase noise uniform ally distributed along the fiber.

$$= \frac{\omega^2\tau^2}{L^2}(\frac{L^3}{3})\int_0^L \left\langle |\delta\tilde{\varphi}(z,\omega)|^2 \right\rangle dz$$

$$S_{remote}(\omega) = \frac{\omega^2\tau^2}{3} S_{fiber}(\omega) \tag{A.14}$$

Appendix B

Phase noise and modulation

An ideal oscillator can be described by the ideal harmonic oscillator equation

$$A(t) = A_o cos(\omega_o t + \phi(t)) \tag{B.1}$$

where A_o is the maximum amplitude of the oscillator, $A(t)$ is the amplitude of the oscillator at any time t, $\omega_o = 2\pi\nu_o$ is the angular oscillation frequency, and $\phi(t)$ is the phase at any time t.

Phase noise describes random fluctuations of the phase of an ideal oscillator. Although the random nature of the phase noise, it can be treated as a phase modulation of an ideal oscillator. The phase modulation occurs by applying a wave with frequency ω_m and amplitude δ to the phase of the ideal harmonic oscillator in equ. (B.1)

$$\phi(t) = \phi_o + \delta cos(\omega_m t)$$

therefore if we consider zero intail phase $\phi_o = 0$, eq. (B.1) becomes

$$A(t) = A_o cos(\omega_o t + \delta cos(\omega_m t)) \tag{B.2}$$

δ is called the modulation index and it is a measure of the modulation amplitude $\Delta\omega$ independent of the modulation frequency ω_m or $\delta = \Delta\omega/\omega_m$.

Equation (B.2) can be described as a complex exponential using Euler's formula $e^{i\phi} = cos(\phi) - isin(\phi)$ as [50]

$$A(t) = A_o \Re e[e^{i\omega_o t}\ e^{i\delta cos(\omega_m t)}]$$

By expanding the second term $e^{i\delta cos(\omega_m t)}$ into a power series,

$$e^{i\delta cos(\omega_m t)} = 1 + i\delta cos(\omega_m t) + ...$$

$$= J_0(\delta) + 2iJ_1(\delta)cos(\omega_m t) + ...$$

where

$$J_0(\delta) = 1 - (\frac{\delta}{2})^2 - ..., \quad J_1(\delta) = (\frac{\delta}{2}) - \frac{1}{2}(\frac{\delta}{2})^3 + ..., \quad J_n(\delta)$$

where $J_n(\delta)$ is the Bessel function of the first order.

$A(t)$ can be written as

$$A(t) = A_o \sum_{n=-\infty}^{\infty} \Re e[(i)^n J_n(\delta) \ e^{i(\omega_o + n\omega_m)t}] \tag{B.3}$$

Oscillators utilized in frequency standards in general are supposed to exhibit only little phase noise so that the modulation index is small $\delta << 1$. In this case it is sufficient to take into account only the carrier J_0 and the first-order side-bands J_1, because the Bessel functions of higher orders become very small. If we consider a small modulation index $\delta << 1$, equation (B.3) reduced to a carrier at angular frequency ω_o and and the first order side-band at a frequency $(\omega_o - \omega_m)$ and $(\omega_o + \omega_o)$

$$A(t) = A_o[J_0(\delta)cos(\omega_o t) - J_1(\delta)sin(\omega_o t + \omega_m t) - J_1(\delta)sin(\omega_o t - \omega_m t)] \tag{B.4}$$

Where $J_0(\delta), J_1(\delta)$ is reduced for small phase modulation to:

$$J_0(\delta) = 1$$

$$J_1(\delta) = (\frac{\delta}{2})$$

It is clear from equation (B.4) that, the modulation index δ can be obtained from the ratio of the carrier to the side-band Amplitudes. The modulation index describes the peak change of the modulated from the unmodulated wave. Therefore, it is equivalent to the peak phase deviation $\Delta\phi_{peak}$ of a phase noise. It is possible

then to obtain the peak phase deviation $\Delta\phi_{peak}$ from the ratio of the carrier to the side-band amplitudes. This holds only at a small phase deviation $\Delta\phi_{peak} << 1$.

$$\delta = \Delta\phi_{peak} = 2J_1(\delta)/J_0(\delta)$$

For random phase fluctuations, $\Delta\phi_{peak}$ is replaced with an equivalent $\sqrt{2}\Delta\phi_{rms}$ for 1 Hz bandwidth [74]

$$\Delta\phi_{rms} = \frac{2}{\sqrt{2}}\frac{J_1(\delta)}{J_0(\delta)} = \frac{2}{\sqrt{2}}\frac{E_1}{E_0} \tag{B.5}$$

where $E_0 = J_0(\delta)A_o$ is the amplitude of the carrier and $E_1 = J_1(\delta)A_o$ is the amplitude of the sideband.

Bibliography

[1] T. W. Hänsch, "Nobel lecture: Passion for precision," *Rev. Mod. Phys.*, vol. 78, pp. 1297–1309, 2006.

[2] T. Rosenband, D. Hume, P. Schmidt, C. Chou, A. Brusch, L. Lorini, W. Oskay, R. Drullinger, T. Fortier, J. Stalnaker, S. Diddams, W. Swann, N. Newbury, W. Itano, D. Wineland, , and J. Bergquist, "Frequency ratio of Al^+ and Hg^+ single-ion optical clocks; metrology at the 17th decimal place," *Science*, vol. 319, pp. 1808–1812, 2008.

[3] S. Diddams, J. Bergquist, S. Jefferts, and C. Oates, "Standards of time and frequency at the outset of the 21st century," *Science*, vol. 306, pp. 1318–1324, 2004.

[4] J. Flowers, "The route to atomic an quantum standards," *Science*, vol. 306, pp. 1324–1330, 2004.

[5] J. Yen, K. Kellermann, B. Rayhrer, N. Broten, D. Fort, S. Knowles, W. Waltman, and G. Swenson, "Real-time, very-long-baseline interferometery based on the use of communications satellite," *Science*, vol. 198, pp. 289–291, 1977.

[6] K. Sato, "Tectonic plate motion and deformation inferred from very long baseline interferometery," *Tectonophysics*, vol. 220, pp. 69–87, 1993.

[7] W. Carter and D. Robertson, "Monitoring earth orientation through the end of the century," *Adv. Space Res.*, vol. 13, p. 197, 1993.

[8] Y. Koyama, N. Kurihara, T. Kondo, M. Sekido, Y. Takahashi, H. Kiuchai, and K. Heki, "Automated very-long baseline interferometery observation and data analysis system," *Earth Planets Space*, vol. 50, p. 709, 1998.

[9] R. Vessot, M. Levine, E. Mattison, E. Blomberg, T. Hoffman, G. Nystrom, B. Farrel, R. Decher, P. Eby, C. Baugher, J. Watts, D. Teuber, and F. Wills, "Test of relativistic gravitation with a space-borne hydrogen maser," *Phys. Rev. Lett.*, vol. 45, pp. 2081–2084, 1980.

[10] J. Turneaure, C. Will, B. Farrell, E. Mattison, and R. Vessot, "Test of the principle of equivalence by a null gravitational red-shift experiment," *Phys. Rev. D*, vol. 27, p. 17051714, 1983.

[11] H. Marion, F. Santos, M. Abgrall, S. Zhang, Y. Sortais, S. Bize, I. Maksimovic, D. Calonico, J. Gruenert, C. Mandache, P. Lemonde, G. Santarelli, P. Laurent, and A. Clairon, "Search for variations of fundamental constants using atomic fountain clocks," *Phys. Rev. Lett.*, vol. 90, p. 150801, 2003.

[12] M. Boyd, A. Ludlow, S. Blatt, S. Foreman, T. Ido, T. Zelevinsky, and J. Ye, "^{87}Sr lattice clock with inaccuracy below 10^{-15}," *Phys. Rev. Lett.*, vol. 98, p. 083002, 2007.

[13] S. Reynaud, C. Salomon, and P. Wolf, "Testing general relativity with atomic clocks," *Space Sci. Rev.*, vol. 148, pp. 233–247, 2009.

[14] J. Levine, "Introduction to time and frequency metrology," *Rev. Sci. Instrum.*, vol. 70, pp. 2567–2569, 1999.

[15] A. Bauch, J. Achkar, S. Bize, D. Calonico, R. Dach, R. Hlavac, L. Lorini, T. Parker, G. Petit, D. Prester, and P. Uhrich, "Comparison between frequency standards in Europe and the USA at the 10^{-15} uncertainty level," *Metrologia*, vol. 43, pp. 109–120, 2006.

[16] L.-S. Ma, P. Jungner, J. Ye, and J. L. Hall, "Delivering the same optical frequency at two places: accurate cancellation of phase noise introduced by an optical fiber or other time-varying path," *Opt. Lett.*, vol. 19, p. 1777, 1994.

[17] C. Daussy, O. Lopez, A. Amy-Klein, A. Goncharov, M. Guinet, C. Chardonnet, F. Narbonneau, M. Lours, D. Chambon, S. Bize, A. Clairon, and G. Santarelli, "Long-distance frequency dissmination with a resolution of 10^{-17}," *Phys. Rev. Lett.*, vol. 94, p. 203904, 2005.

[18] G. Grosche, B. Lipphardt, H. Schnatz, G. Santarelli, P. Lemonde, S. Bize, M. Lours, F. Narbonneau, A. Clairon, O. Lopez, A. Amy-Klein, and C. Chardonnet, "Transmission of an optical carrier frequency over a telecommunication fiber link," in *Conference on lasers and electro-optics/quantum electronics, OSA technical digest series (CD) (optical society of america, 2007), paper CMKK1*, 2007.

[19] O. Terra, G. Grosche, K. Predehl, R. Holzwarth, T. Legero, U. Sterr, B. Lipphardt, and H. Schnatz, "Phase-coherent comparison of two optical frequency standards over 146 km using a telecommunication fiber link," *Applied Physics B*, vol. 97, pp. 541–551, 2009.

[20] O. Terra, G. Grosche, W. Ertmer, T. Feldmann, J. Friebe, T. Legero, B. Lipphardt, A. Pape, K. Predehl, E. M. Rasel, M. Riedmann, U. Sterr, T. Wübbena, and H. Schnatz, "Telecommunication fiber link for the remote characterization of a magnesium optical frequency standard," *Proc. SPIE*, vol. 7431, p. 74310B, 2009.

[21] O. Terra, G. Grosche, and H. Schnatz, "Brillouin amplification in phase coherent transfer of optical frequencies over 480 km fiber," *Opt. Express*, vol. 18, p. 16102, 2010.

[22] S. Foreman, K. Holman, D. Hudson, D. Jones, and J. Ye, "Remote transfer of ultrastable frequency references via fiber networks," *Rev. Sci. Instrum.*, vol. 78, p. 021101, 2007.

[23] F. Narbonneau, M. Lours, S. Bize, A. Clairon, G. Santarelli, O. Lopez, C. Daussy, A. Amy-Klein, and C. Chardonnet, "High resolution frequency standard dissmination via optical fiber metroplitan network," *Rev. Sci. Instrum.*, vol. 77, p. 64701, 2006.

[24] P. A. Williams, W. C. Swann, and N. R. Newbury, "High-stability transfer of an optical frequency long fiber-optic links," *J. Opt. Soc. Am. B.*, vol. 25, p. 1284, 2008.

[25] O. Lopez, A. Amy-Klein, C. Daussy, C. Chardonnet, F. Narbonneau, M. Lours, and G. Santarelli, "86 km optical link with a resolution of $2\text{x}10^{-18}$ for rf frequency transfer," *Eur. Phys. J. D*, vol. 48, p. 35, 2008.

[26] E. D. Black, "An introduction to pound drever hall laser frequency stabilization," *Am. J. Phys.*, vol. 69, p. 79, 2001.

[27] H. Stoehr, F. Mensing, J. Helmcke, and U. Sterr, "Diode laser with 1 Hz linewidth," *Optics Letters*, vol. 31, p. 736, 2006.

[28] S. Webster, M. Oxborrow, and P. Gill, "Vibration insensitive optical cavity," *Phys. Rev. A*, vol. 75, p. 011801, 2007.

[29] J. Friebe, A. Pape, M. Riedmann, K. Moldenhauer, T. Mehlstubler, N. Rehbein, C. Lisdat, E. M. Rasel, W. Ertmer, H. Schnatz, B. Lipphardt, and G. Grosche, "Absolute frequency measurement of the magnesium intercombination transition $^1S_0 \rightarrow ^3 P_1$," *Phys. Rev. A*, vol. 78, p. 033830, 2008.

[30] V. Gerginov, N. Nemitz, S. Weyers, R. Schroeder, D. Griebsch, and R. Wynands, "Uncertainty evaluation of the caesium fountain clock PTB-CSF2," *Metrologia*, vol. 47, pp. 65–79, 2010.

[31] H. Schnatz, B. Lipphardt, J. Helmcke, F. Riehle, and G. Zinner, "First phase-coherent frequency measurement of visible radiation," *Phys. Rev. Lett.*, vol. 76, pp. 18–21, 1996.

[32] J. Ye and S. Cundiff, *Femtosecond optical frequency comb technology: principle, operation and applications*. Springer, 2005.

[33] T. Udem, R. Holzwarth, and T. W. Hänsch, "Optical frequency metrology," *Nature*, vol. 416, pp. 233–237, 2002.

[34] P. Kubina, P. Adel, F. Adler, G. Grosche, T. Hänsch, R. Holzwarth, A. Leitenstorfer, B. Lipphardt, and H. Schnatz, "Long term comparison of two fiber based frequency comb systems," *Opt. Express*, vol. 13, pp. 904–909, 2005.

[35] F. Adler, K. Moutzouris, A. Leitenstorfer, H. Schnatz, B. Lipphardt, G. Grosche, and F. Tauser, "Phase-locked two-branch erbium-doped fiber laser system for long-term precision measurements of optical frequencies," *Opt. Express*, vol. 12, p. 5872, 2004.

[36] L. Nelson, D. Jones, K. Tamura, H. Haus, and E. Ippen, "Ultrashort-pulse fiber ring lasers," *Applied Physics B*, vol. 65, pp. 277–294, 1997.

[37] N. Newbury and W. Swann, "Low-noise fiber laser frequency combs," *J. Opt. Soc. Am. B*, vol. 24, p. 1756, 2007.

[38] G. Grosche, B. Lipphardt, and H. Schnatz, "Optical frequency synthesis and measurement using fibre-based femtosecond lasers," *Eur. Phys. J. D*, vol. 48, pp. 27–33, 2008.

[39] A. Bauch, "The ptb primary clocks Cs1 and Cs2," *Metrologia*, vol. 42, pp. S43–S54, 2005.

[40] T. Rosenband, P. Schmidt, D. Hume, W. Itano, T. Fortier, J. Stalnker, K.kim, S. Diddams, J. Koelemeij, J. Bergquist, and D. Wineland, "Observation of the $^1S_0 \rightarrow ^3 P_0$ clock transition in $^{27}Al^+$," *Phys. Rev. Lett.*, vol. 98, p. 220801, 2007.

[41] H. Telle, B. Lipphardt, and J. Stenger, "Kerr-lens, mode-locked lasers as transfer oscillators for optical frequency measurements," *Appl. Phys. B*, vol. 74, pp. 1–6, 2002.

[42] J. Stenger, H. Schnatz, C. Tamm, and H. Telle, "Ultraprecise measurement of optical frequency ratios," *Phys. Rev. lett.*, vol. 88, p. 073601, 2002.

[43] L. Ma, M. Zucco, S. Picard, L. Robertsson, and R. Windeler, "A new method to determine the absolute mode number of a mode-locked femtosecond-laser comb used for absolute optical frequency measurements," *IEEE Quantum electronics*, vol. 9, pp. 1066–1071, 2003.

[44] D. Derickson, *Fiber optic test and measurement.* Prentice hall, 1998.

[45] L. Brillouin, "Diffusion de la lumiere et des rayonnes xpar un corps transparent homogene; influence del agitation thermique," *Annales des Physique*, vol. 17, p. 88, 1922.

[46] R. Smith, "Optical power handling capacity of low loss optical fibers as determined by stimulated Raman and Brillouin scattering," *Appl. Opt.*, vol. 11, pp. 2489–2494, 1972.

[47] Y. Koyamada, "Simulating and designing Brillouin gain spectrum in single mode fibers," *Lightwave Technol.*, vol. 22, p. 631, 2004.

[48] Y. Imai and N. Shimada, "Dependence of stimulated brillouin scattering on temperature distribution in polarization-maintaining fibers," *IEEE Photon. Technol. Lett.*, vol. 5, p. 1335, 1993.

[49] S. Chang, C. Hsu, T. Huang, W. Chuang, Y. Tsai, J. Shieh, and C. Leung, "Heterodyne interferometric measurement of the thermo-optic coefficient of single mode fiber," *Chinese journal of physics*, vol. 38, p. 437, 2000.

[50] F. Riehle, *Frequency Standards.* Wiley- VCH, 2004.

[51] G. Kramer and W. Klische, "Multi-channel synchronous digital phase recorder," *Frequency Control Symposium and PDA Exhibition*, pp. 144 – 151, 2001.

[52] E. Rubiola, "On the measurement of frequency and of its sample variance with high-resolution counters," *Rev. Sci. Instrum.*, vol. 76, p. 054703, 2005.

[53] S. Dawkins, J. Mcferran, and A. Luiten, "Considerations on the measurement of the stability of oscillators with frequency counters," *Ultrasonics, Ferroelectrics and Frequency Control, IEEE Transactions on*, vol. 54, pp. 918 – 925, 2007.

[54] A. Kersey, M. Marrone, and M. Davis, "Polarization-insensitive fibre optic michelson interferometer," *Electron. Lett.*, vol. 27, pp. 518–520, 1991.

[55] F. Gardner, *Phaselock techniques.* Wiley,New York, 1979.

[56] Agilent, "Lightwave signal analyzers measure relative intensity noise," tech. rep., Agilent, 2000.

[57] K. J. Weingarten, B. Braun, , and U. Keller, "In situ small-signal gain of solid-state lasers determined from relaxation oscillation frequency measurements," *Optics Letters*, vol. 19, pp. 1140–1142, 1994.

[58] H. Jiang, F. Kflian, S. Crane, O. Lopez, M. Lours, J. Millo, D. Holleville, P. Lemonde, C. Chardonnet, A. Amy-Klein, and G. Santarelli, "Long-distance frequency transfer over an urban fiber link using optical phase stabilization," *J. Opt. Soc. Am. B.*, vol. 25, pp. 2029–2035, 2008.

[59] K. Predehl, R. Holzwarth, T. Udem, T. Hänsch, O. Terra, G. Grosche, B. Lipphardt, and H. Schnatz, "Ultra precise frequency dissemination across germany towards a 900 km optical fiber link from PTB to MPQ," in *OSA/CLEO/IQEC*, 2009.

[60] E. Desurvire, *Erbium-doped fiber amplifiers-principles and applications.* Wiley, New York, 1994.

[61] G. P. Agrawal, *Fiber-optic communication systems.* Wiley,New York, 2002.

[62] N. Olsson and J. V. der Ziel, "Cancellation of fiber loss by semi-conductor laser pumped brillouin amplification at 1.5 μm," *Appl. Phys. Lett.*, vol. 48, p. 1329, 1986.

[63] R. Tkach and A. Chraplyvy, "Fibre Brillouin amplifiers," *Optical and Quantum Electronics*, vol. 21, p. S105, 1989.

[64] M. Ferreira, J. Rocha, and J. Pinto, "Analysis of the gain and noise characteristics of fibre brillouin amplifiers," *Optical and Quantum Electronics*, vol. 26, p. 35, 1994.

[65] J. Geng, S. Staines, M. Blake, and S. Jiang, "Distributed fiber temperature and strain sensor using coherent radio-frequency detection of spontaneous brillouin scattering," *Appl. Opt.*, vol. 46, p. 5928, 2007.

[66] W. Lee, D. Yu, C. Park, and J. Mun, "The uncertainty associated with the weigted mean frequency of a phase-stabilized signal with white phase noise," *Metrologia 47*, vol. 47, p. 24, 2010.

[67] A. Pape, O. Terra, J. Friebe, M. Riedmann, T. Wübbena, E. M. Rasel, K. Predehl, T. Legero, B. Lipphardt, H. Schnatz, and G. Grosche, "Long-distance remote comparison of ultrastable optical frequencies with 1 $\times 10^{-15}$ instability in a fractions of a second," *Opt. Express*, vol. 18, pp. 21477–21483, 2010.

[68] J. Friebe, *Ein optische Frequenzstandard mit lasergekülten Magnesiumatomen.* PhD thesis, Leibniz University of Hannover, 2010.

[69] F. Walls, A. Clements, C. Felton, M. Lombardi, and M. Vanek, "Extending the range and accuracy of phase noise measurements," tech. rep., National Institute of Standards and Technology (NIST), 1990.

[70] T. Hänsch, J. Alnis, P. Fendel, M. Fischer, G. Gohle, M. Herrmann, R. Holzwarth, N. Kolachevsky, T. Udem, and M. Zimmermann, "Precision spectroscopy of hydrogen and femtosecond laser frequency combs," *Phil. Trans. R. Soc. A*, vol. 363, p. 2155, 2005.

[71] H. Schnatz, O. Terra, K. Predehl, T. Feldmann, T. Legero, B. Lipphardt, U. Sterr, G. Grosche, R. Holzwarth, T. W. Hänsch, T. Udem, Z. H. Lu, L. J. Wang, W. Ertmer, J. Friebe, A. Pape, E. M. Rasel, M. Riedmann, and T. Wübbena, "Phase-coherent frequency comparison of optical clocks using a telecommunication fiber link," *IEEE Transactions on Ultrasonics, Ferroelectrics, and Frequency Control*, vol. 57, p. 175, 2010.

[72] G. Grosche, O. Terra, K. Predehl, R. Holzwarth, B. Lipphardt, F. Vogt, U. Sterr, and H. Schnatz, "Optical frequency transfer via 146 km fiber link with 10^{-19} relative accuracy.," *Opt. Lett.*, vol. 34, p. 2270, 2009.

[73] K. H. Wanser, "Theory of thermal phase noise in Michelson and Sagnac fiber interferometers," *Tenth International Conference on Optical Fibre Sensors*, vol. 2360, pp. 584–587, 1994.

[74] D. Schere, "Design principle and test methods for low phase noise rf and microwave sources," tech. rep., Agilent, 1981.

List of abbreviations

- **PTB**: Die Physikalisch-Technische Bundesanstalt in Braunschweig
- **LUH**: Leibniz Universitt Hannover
- **IQ**: Institute of Quantum optics in Hanover
- **MPQ**: Max-Planck Institute of Quantum optics in Garching
- **SNR**: Signal to noise ratio
- **EDFA**: Erbium doped fiber amplifier
- **BEDFA**: Bi-directional Erbium doped fiber amplifier
- **WDM**: Wavelength division multiplexer
- **FBA**: Fiber Brillioun amplifier
- **ASE**: Amplifier spontaneous emission
- **AVAR**: Allan variance
- **ADEV**: Allan Deviation (square root of AVAR)
- **ModADEV**: Modified Allan Deviation
- **PNSD**: Phase noise spectral density
- **RFSA**: Radio-frequency spectrum analyzer
- **CSL-PTB, CSLYb-PTB**: Cavity stabilized lasers at PTB
- **CSL1-IQ, CSL2-IQ**: Cavity stabilized lasers at IQ
- **NIR-laser**: Near-infrared laser at PTB (fiber laser)

- **CSF1**: Cesium fountain at PTB
- **H5**: Hydrogen maser at PTB
- **H7**: Hydrogen maser at IQ
- **FFCS**: Femtosecond frequency comb systems
- **VCO**: Voltage controlled oscillator
- **DDS**: Direct digital synthesis
- **RBS**: Rayleigh back scattering
- **SBS**: Stimulated Brillouin scattering
- **IL**: Insertion loss
- **RL**: Return loss
- **OTDR**: Optical time domain reflectometer
- **SMF**: single mode fiber
- **CD**: Chromatic dispersion
- **PMD**: Polarization mode dispersion
- **FM**: Faraday mirror
- **DFCS**: Digital phase-frequency comparator
- **TOS**: Tracking oscillator
- **OC**: Optical circulator
- **PD**: Photo detector
- **AOM**: Acousto-optic modulator
- **RIN**: Relative intensity noise
- **BW**: Measurement bandwidth
- **OSA**: Optical spectrum analyzer
- **VA**: Optical variable attenuator

Acknowledgment

Thank you my God for letting me compelete this work.

I would like to dedicate this work to my wife (Rofida) who not only dedicated her efforts to our home and to our children but also helped me to solve some scientific problems, my children (Yomna and Ziad) who without them I wouldn't understand the meaning of noise, and my father and mother who without their every week advice and encouragement I wouldn't complete this work.

I would like to acknowledge my colleagues in Physikalisch-Technischen Bundesanstalt in Braunschweig, Max-Planck Institute for Quantum Optics in Garching, and Institute of Quantum Optics in Hanover, without whom this work wouldn't see the light. I would like to thank particularly:

- Dr. Harald Schnatz: who helped me with patience from the beginning until the end of the work. I cant't count how many things he explained to me.
- Dr. Gesine Grosche: for her useful criticism, useful comments and corrections.
- Prof. Dr. Wolfgang Ertmer: for the supervision on my work, support and suggestions.
- Dr. Uwe Sterr: who explains me with very kind manner many useful concepts at the beginning of my work.
- Dr. Thomas Legero: for maintaining the frequency standards in PTB, and for the useful explanations.
- Mrs. Dipl.-Phys. Katharina Predehl: for our cooperational work.
- Mr. Dipl.-Phys. Andre Pape: for our cooperational work.

- Mr. Dipl.-Ing. Burghardt lipphardt: for the useful discussion.
- Mr. Dipl.-Ing. Mattias Misera: for the magical electronics which in my point of view are the hands and legs of our work.
- Dr. Felix Vogt: for the useful suggestions.
- Mr. Paul Williams (NIST): for the useful discussion.
- Mrs Birgit Voss, Mrs. Elke Hünitzsch, Mrs. Katrin Pfennig und Mrs. Gunhild Faber for there friendly support in all administrative work.

I want to thank also my institute (National Institute of Standards) (NIS) in my home country Egypt for the financial support during my PhD work and giving me the chance to study abroad in such a nice place. I would like to thank The Braunschweig International School of Metrology (IGSM) for the useful lectures and nice scientific field trips and the summer school which was totally free of charge. I would like to thank also SFB 407 (Sonderforschungsbereich) and QUEST (Centre for Quantum Engineering and Space-Time Research) for the financial support of the project material.

Lebenslauf (Curriculum Vitae)

- Name: Osama Terra.
- Date of birth: 27 - 11 - 1975.
- Place of birth: Cairo - Egypt.
- Nationality: Egyptian.
- E-mail:
  osama.terra@ptb.de
  osama.terra@nis.sci.eg
  osama.terra@gmail.com

Scientific Carrier

- 09/1993 - 11/1997 Physics and computer studies Ain-Shams University Cairo-Egypt, Graduation grade (very good).
- 12/1999 - now: Permanent position in the Egyptian National Institute of Standards (NIS).
- 19 Oct 200:, Master degree on "Frequency Stabilization System For He- Ne Lasers", Ain-shams University.
- 02/2005 - 08/2005: Guest research visit in the Physikalisch-Technische Bundesanstalt (PTB) (Multiwavelength interferometry).
- 01/2006 - 04/2006: Guest research visit in the Physikalisch-Technische Bundesanstalt (PTB) (Length primary standard).
- 09/2006 - now: PhD studies in Physikalisch-Technische Bundesanstalt (PTB) (Length primary standard), subject "Long distance frequency comparisons via optical fibers".

Publications

- O. Terra, G. Grosche and H. Schnatz, "*Brillouin amplification in phase-coherent transfer of optical frequencies over 480 km fiber*", Optics Express, 18, 16102-16111 (2010).

- O.Terra, G. Grosche, R. Holzwarth, T. Legero, B. Lipphardt, K. Predehl, U. Sterr, and H. Schnatz, "*Phase- coherent comparison of two optical frequency standards over 146 km using a commercial telecommunication fiber*", Applied Physics B, 97 541-551 (2009).

- O. Terra, G. Grosche, W. Ertmer, J. Friebe, T. Legero, B. Lipphardt, A. Pape, K.Predehl, E. Rasel, M. Riedmann, U. Sterr, T. Wübbena und H. Schnatz "*Frequency measurement of a magnesium frequency standard using a commercial telecommunication fiber link*", Proc. SPIE, Vol. 7431, 74310B (2009);

- G. Grosche, O. Terra, K. Predehl, R. Holzwarth, B. Lipphardt, F. Vogt, U. Sterr, and H. Schnatz, "*Optical frequency transfer via 146 km fiber link with 10^{-19} relative accuracy*", Optics Letters 34, 2270-2272 (2009).

- H. Schnatz, O. Terra, K. Predehl, T. Feldmann, T. Legero, B. Lipphardt, U. Sterr, G. Grosche, R. Holzwarth, T. W. Hänsch, T. Udem, Z. H. Lu, L. J. Wang, W. Ertmer, J. Friebe, A. Pape, E.M. Rasel, M. Riedmann, and T. Wübbena, "*Phase-Coherent Frequency Comparison of Optical Clocks Using a Telecommunication Fiber Link*", IEEE Transactions on Ultrasonics, Ferroelectrics, and Frequency Control, vol. 57, no. 1, (2010) 175-181.

- A. Pape, O. Terra, J. Friebe, M. Riedmann, T. Wübbena, E. M. Rasel, K. Predehl, T. Legero, B. Lipphardt, H. Schnatz, and G. Grosche, "*Long-distance remote comparison of ultrastable optical frequencies with 10^{-15} instability in fractions of a second*", Opt. Express 18, 21477-21483 (2010) .

- G. Grosche, O. Terra, K. Predehl, T. Hänsch, R. Holzwarth, B. Lipphardt, F. Vogt, U. Sterr, H. Schnatz, "*Measurement noise floor for a long-distance optical carrier transmission via fiber*", Frequency Standards and Metrology, Proceedings of the 7th Symposium 2008.

- U. Sterr, T. Legero, T. Kessler, H. Schnatz, G. Grosche, O. Terra, and F. Riehle, "*Ultrastable lasers: new developments and applications*", Proc. SPIE Vol. 7431, 74310A (2009).

- K. Predehl, R. Holzwarth, T. Udem, T. Hänsch, O. Terra, G. Grosche, B. Lipphardt and H. Schnatz, "*Ultra precise frequency dissemination across Germany-towards a 900 km optical fiber link from PTB to MPQ*", CLEO/QELS, Baltimore, 02-04, June, 2009.

- J. Friebe, M. Riedmann, A. Pape, T. Wubbena, E.M. Rasel, W. Ertmer, O. Terra, G. Grosche, B. Lipphardt, K. Predehl, T. Feldmann, and H. Schnatz, "*Characterization of an optical Mg frequency standard via a dark telecommunication fiber*", CLEO Europe - EQEC 2009.

- L. Robertsson, M. Zucco, L-S. Ma, O. Terra, F. Saraiva, S. Gentil, C. Chekirda, Yu Zakharenko, V. Fedorin and L. Mostert, "*Results from the CI-2004 campaign at the BIPM of the BIPM.L-K11 ongoing key comparison*", 2005 Metrologia 42.

- K. Meiners-Hagen, O. Terra, A. Abou-Zeid, "*Two colour interferometry*", Sensoren und Messsysteme 2006, ISBN 978-3-8007-2939-5, p. 249 - 252.

- H. Henawy, M. Sobee, O. Terra, "*Two-Mode frequency stabilization of an internal mirror 633 nm He-Ne laser*", 10th IMEKO TC7 international symposium on advances of measurement science, july 2004, Russia.

Awards

EFTF Best Student paper award, in the area of "Timekeeping, time and frequency transfer, GNSS and Applications". 13-16 April 2010, European Space Agency (ESA).